APERTURE ANTENNAS

A thesis presented for the degree of
Doctor of Philosophy in Electrical Engineering
in the University of Canterbury,
Christchurch, New Zealand

by

A.R. Jamieson, B.E.(Hons.)

1970

Ars longa, vita brevis

Hippocrates

Abstract

Computational and experimental methods for evaluating the radiation and coupling characteristics of wide-beam antennas are presented. The application of these methods to a practical antenna is illustrated by a combined theoretical and experimental investigation of a circular waveguide aperture antenna flush mounted in a large metallic ground plane.

The design and development of the coaxial antenna, a wide-beam radiator suitable for incorporation into a wide scanning array antenna, is also presented. This antenna is the aperture equivalent of three mutually perpendicular dipoles, and has the capability of transmitting or receiving signals of arbitrary polarization over wide scan angles.

Acknowledgements

I am especially appreciative of the guidance and help proffered by my supervisor Mr R.H.T. Bates. His assistance over the duration of the project has been invaluable.

To the workshop staff of the Electrical Engineering Department I wish to express my gratitude for the workmanlike manner in which they constructed the coaxial and circular waveguide antennas.

The financial assistance of the University Grants Committee and the New Zealand Post Office is gratefully acknowledged.

CONTENTS

Page

P A R T 1

FORMULATION OF ANALYTICAL TECHNIQUES

Chapter 1 : Introduction

This thesis discusses computational and experimental methods for evaluating the performances of antennas characterised by wide beam radiation patterns. The design and development of a specific wide beam antenna suitable for inclusion in a radar or communication array antenna is also presented.

In applications employing a wide beam antenna as an isolated radiator, the impedance match and the far-field radiation pattern are the properties of most interest. The impedance can always be determined simply. Although the far-field radiation pattern may be determined experimentally by performing measurements in the far-field, under certain conditions it is preferable to infer the far-field pattern from near-field measurements. A computational procedure is developed which permits the complete three-dimensional far-field radiation pattern of a wide beam antenna to be inferred from limited near-field measurements. This technique is essentially an extension of methods previously applied by Brown and Jull[1], Blakey[2], and Jensen[3] to two-dimensional narrow beam antennas. As an experimental verification, the far-field pattern of a cylindrical waveguide aperture antenna is obtained by applying this technique.

The behaviour of an antenna in an array environment differs from its behaviour as an isolated radiator, because of the effects of mutual coupling between the elements of the array. In view of the current interest in array antennas[4-6] the development of new methods for estimating mutual coupling effects is of practical interest. A technique is presented for computing coupling effects from experimentally derived scattering and radiation characteristics of individual array elements. This element-by-element approach is useful, since it enables a complete array to be designed from measurements performed on a single array element. A simplified, approximate approach is also developed and this is applied to the cylindrical aperture antenna, and the estimate of the coupling effects is compared with the corresponding measured effects.

The development of the coaxial antenna for use in a wide scanning array is also discussed. A feature of this antenna, which is the aperture equivalent of three mutually perpendicular dipoles, is its capability of transmitting or receiving signals of arbitrary polarization.

The thesis is divided into two parts, the formulation of analytical techniques to evaluate the performances of an antenna, and the design of the coaxial antenna. Thus, Part 1 is a contribution to the general theory and, in particular, measurement theory of three-dimensional antennas, while Part 2 contributes to antenna design.

New material is included in Chapters 2-4 and 6-9, with Chapters 1 and 5 being introductory.

Part 1 includes Chapters 1-4, and contains the description of the analytical techniques. A method for inferring the complete far-field radiation pattern of a wide beam antenna from limited near-field measurements called the near-field technique is introduced in Chapter 2. Two formulations are presented: one expressed in terms of waveguide modes of propagation, and the other based upon a spherical vector mode field representation. The waveguide mode formulation is shown to be suitable for inferring the field patterns of aperture antennas mounted in ground planes, while the spherical mode formulation is applicable to any three-dimensional antenna, but is best suited to wide beam antennas. An estimate of the aperture field distribution of an aperture antenna is shown to be possible by applying an extension of this technique. The near-field technique is an improvement to existing methods for inferring antenna patterns, and is new in its application to wide beam antennas mounted above ground planes. Furthermore, the presented technique is complementary to the methods formulated by Jensen[3] for narrow beam antennas, and in conjunction with these methods completes the three-dimensional extension of the method of Brown and Jull[1].

A scattering matrix approach to the problem of determining mutual coupling effects in finite arrays is discussed in Chapter 3. The estimation of the total coupling effects requires a knowledge of the full scattering properties of the array elements, and the range of measurements necessary to determine the scattering properties of a representative element is derived. An approximate coupling description based upon direct path coupling effects is also formulated. This approximate approach represents a new technique for the design of array antennas. In Chapter 4, the performance of a circular cylindrical waveguide antenna is evaluated by applying the techniques presented in the previous chapters. A new formulation of the variational expression for the aperture admittance of this antenna is also included. Chapter 4 concludes with suggestions for further study.

Part 2 contains Chapters 5-9, and outlines the design of the coaxial antenna. This new, wide beam, aperture antenna supports three orthogonal modes of propagation, whereas previously designed coaxial aperture antennas generally support only one mode. Thus, the presented design is entirely new. Chapter 5 introduces the coaxial antenna and specifies the constraints on the element and system designs of the antenna. A review of the relevant literature is also included. In Chapter 6 the radiation patterns of the antenna are derived from the modal fields present in the

aperture. Since these modal patterns are only first order approximations to the actual patterns of the antenna, the application of the near-field technique to the coaxial antenna is also formulated. The system design is presented in Chapter 7. This describes the polarization structure and the circuitry required to provide control over the mode of operation of the antenna. Two system designs are given, with each considered as the optimum system for different applications. The element design based on an experimental study performed at L-band is discussed in Chapter 8. The designs of the waveguide sections of the antenna, the excitation probes, and the necessary matching networks are included. The mutual coupling effects between probes are studied with particular emphasis placed on the compensation of these detrimental effects. Although designed explicitly for an array application, the radiation properties of the coaxial antenna render it useful as an isolated radiator, and two such uses are suggested in Chapter 9. Modifications to the antenna parameters which will improve the performance of the antenna are also discussed. Finally, Chapter 9 concludes with a suggested experimental study that would lead to a more comprehensive understanding of the operation of the antenna.

The numerical computations recorded in Chapter 4 were performed on the IBM 360/44 computer of the University of Canterbury Computer Centre, while the designs of the matching networks outlined in Chapters 8 were evaluated on the EAI 640 computer of the Electrical Engineering Department. With the exception of the standard IBM sub-routines BESJ for cylindrical Bessel functions and MINV for matrix inversion, all computer programs used were written by the author in FORTRAN IV.

Publications to date on topics relevant to the thesis are:

(i) R.H.T. Bates and A.R. Jamieson: "Towards measuring Faraday Rotation by radar with minimum error", paper presented at ANZAAS Conference, Christchurch, N.Z., January 1968.

(ii) R.H.T. Bates and A.R. Jamieson: "Towards reducing errors in radar measurements of Faraday Rotation", Electronics Letters, 4, n8, 19th April 1968, pp 155-156.

(iii) A.R. Jamieson and R.H.T. Bates: "An aerial capable of radiating any polarization", paper presented at Nelcon II conference, Auckland, N.Z., August 1968.

(iv) A.R. Jamieson and R.H.T. Bates: "On the accurate estimation of wide beam antenna radiation patterns", paper presented at Nelcon 70 conference, Auckland, N.Z., August 1970.

Additional papers in preparation include:

(v) A.R. Jamieson and R.H.T. Bates: "Triple polarized coaxial aerial", to be submitted to IERE Journal.

(vi) A.R. Jamieson and R.H.T. Bates: "Antenna radiation pattern inferred from near-field measurements", to be submitted to Proc. IEE.

(vii) A.R. Jamieson and R.H.T. Bates: "Determining array performance from measurements performed on a single radiating element", to be submitted to Proc. IEE.

Chapter 2 : The Near-Field Technique

2.1 Introduction.

In common with classical nomenclature in optics, the electromagnetic field radiated by an antenna has been tradionally divided into the induction field, the Fresnel region, and the Fraunhofer or far-field region. The induction field and the Fresnel region are frequently considered, collectively, as the near-field region. Although the transition from the near-field to the far-field is gradual with no abrupt changes, the accepted on-axis minimum range for the far-field region may be defined as the range allowing a maximum phase difference of $\pi/8$ radians between the radiation fields emitting from various parts of the antenna[7]. For an antenna whose aperture has a maximum dimension D, and is operating at a wavelength λ, this far-field range is $2D^2/\lambda$. Radiation patterns measured within this range are classified as near-field patterns, while those measured at greater ranges are far-field patterns.

The evaluation of the performance of an antenna in a system environment often requires a detailed knowledge of the radiation pattern of the antenna. In the study of array antennas, for example, both the mutual coupling between elements in the array and the overall radiation pattern of the array are dependent upon the radiation

pattern of the isolated individual elements. To be accurate, radiation pattern measurements must be performed within the far-field region[8] of the antenna. For electrically large antennas, such as used in communication and satellite receiving stations, this range may be of the order of many miles, making accurate far-field measurements difficult. Various techniques have been developed involving extra-terrestial ranges[9,10] and the use of aircraft and satellites as both signal sources and passive scatterers, but their usefulness remains limited by cost and accuracy considerations. Electrically small antennas of the type commonly used in wide angle array applications, are characterised by wide beam radiation patterns. Accurate pattern measurements performed solely in the far-field of these antennas are often difficult, especially when the antenna is mounted above a ground plane, since the radiation effects resulting from the edge currents of the finite ground plane, and the effects of spurious reflections from the surroundings, may constitute a significant portion of the total radiation in the far-field. In the near-field the actual radiation from the antenna predominates over these secondary effects. Since, by performing measurements with a small probe penetrating the ground plane, the near-field can be sampled accurately and with a minimum of disturbance to the actual field, it is valuable to have a

technique for inferring the far-field radiation pattern of wide beam antennas from near-field measurements.

Although a comprehensive review of existing methods for inferring antenna patterns has recently been published by Jensen[3], it is nevertheless appropriate to include a short literature review to complete the background of the technique which is presented in this thesis.

The approach to this problem introduced by Bates and Elliot[11] was based upon the development of an asymptotic series representing the near-field pattern in terms of the far-field pattern and correction terms. Since derivatives of the field pattern are included with the correction terms, these methods are sensitive to errors in the measured values of the near-field pattern. Thus, experimental difficulties emerge in measuring the near-field pattern to sufficient accuracy. To measure the fields at a point in space an infinitesimal Hertzian dipole (magnetic or electric) is usually assumed in theory, but in practice, to provide adequate signal strength for the detector, an antenna with a finite sized aperture is required. Using the plane wave spectrum concept[12], Brown[13], investigated the effects of the aperture size of the measuring antenna on gain and, in particular, pattern measurements, and demonstrated that the procedure of Bates and Elliot yields accurate predictions of the field patterns only when small aperture receiving antennas are used to measure the near-field pattern. The defocussing technique

for aperture antennas described by Bickmore[14], involves the readjustment of the aperture phase distribution to produce the far-field pattern as closely as possible in the near-field region. This method has been considered by several authors (for a review see Soejima[15]), and good agreement between the near-field patterns of focused antennas and the corresponding far-field patterns has been reported[15]. But since the necessary phase adjustment is practicable on only certain classes of antenna, notably reflector antennas, the technique is of limited usefulness.

In the method presented by Brown and Jull[1], the total radiation field from the antenna is represented by a complete set of orthogonal cylindrical wave functions, or harmonics, and complex modal amplitudes. By measuring the near-field pattern around a cylindrical surface enclosing the antenna, the measured field is expressed as a Fourier series in the wave functions. The unknown amplitudes are then determined by Fourier analysis of the measured field. Since a complete knowledge of the modal amplitudes at a point in the region exterior to the surface which circumscribes the antenna, serves to define the fields everywhere in that region, these amplitudes specify the total far-field radiation pattern. Although originally suggested for two-dimensional problems, the method can be extended, in principle, to three dimensions by representing the fields in terms of spherical harmonics. This formulation, however, has the

inherent disadvantage of requiring measurements of the near-field pattern, in both modulus and phase, to be performed over a spherical surface enclosing the antenna. Furthermore, the amount of computational effort involved in the term-by-term modal analysis requiring numerical integration of such a three-dimensional field is considerable. The effects of the aperture size of the measuring antenna were also considered by Brown and Jull. By inverting the first few terms of the asymptotic expansion for the near-field pattern measured by a directive antenna[16], Jull[17] developed an equivalent, but approximate, asymptotic series expressing the far-field pattern of a two-dimensional transmitting antenna in terms of the measured near-field pattern and its derivatives. The derivatives are calculated from the measured near-field pattern. This must be measured accurately, since the calculated values of the derivatives are sensitive to even small errors in the measured data. Using this technique, the main beam and major side lobes of the radiation pattern of a narrow beam antenna have been inferred, to a reasonable accuracy, from near-field measurements performed solely within the principal angular range of the pattern[17]. In comparison, the more exact Fourier series method of Brown and Jull requires measurement of the field all around the antenna. Moreover, for a narrow beam pattern, a large number of

wave functions are necessary to represent the field accurately, which generally increases the computational effort involved in determining the modal amplitudes.

Others to apply the Fourier series method include Blakey[2,18] and Martin[19]. Blakey developed an on-line system for processing the near-field measurements of a two-dimensional antenna, while Martin applied high speed digital computer techniques to infer the far-field pattern of a line source antenna. The sensitivity of the method to random errors in the near-field measurements was also investigated by Martin[19]. The three-dimensional extension of Brown and Jull's method was used by James and Longdon[20] to infer the far-field pattern from measurements of the radial component of the near-field. They also applied a matrix method to solve for the unknown modal amplitudes when the near-field pattern is known only at discrete points. Jensen[3], when reviewing these methods, completed the formulation of the three-dimensional method to account for all field components and the effect of the receiving or measuring antenna. The effects of inferring the patterns of two-dimensional antennas from discrete near-field data were also investigated.

It is well known that the aperture field distribution and the far-field radiation pattern of an aperture antenna form a Fourier transform pair[21]. Thus, provided the aperture field is known completely the far-field can be uniquely determined. For large apertures the aperture field distribution can be sampled directly using an electrically small probe, but in general, such a measurement is difficult to accomplish without the physical discontinuity of the probe disturbing the actual field. An alternative approach for planar aperture antennas[22] is based upon the Fourier transform relationship between the power spectrum and the auto-correlation function of the source distribution. This method lends itself to automatic processing and offers an improvement in accuracy over the asymptotic series method. However, in common with the Fourier series method, this technique requires near-field measurements to be performed over a surface effectively enclosing the antenna. The amount of computation is also increased, since, in addition to the evaluation of the Fourier transform relationship, the auto-correlation functions of the near-field patterns must be computed for each field measurement.

To summarize, the Fourier series method is highly practicable for two-dimensional problems, but is of limited usefulness in three-dimensional applications. Many large three-dimensional antennas possess narrow beams in the vertical plane, for example, and wide beams in the horizontal plane. The Fourier

series method may then be used by measuring at field points corresponding to the near-field of the vertical plane pattern and to the far-field of the horizontal plane pattern. The auto-correlation technique can be used, in principle, to infer the radiation pattern of any planar aperture antenna, but is more appropriate for narrow beam antennas.

A new method, similar to the procedure outlined by James and Longdon[20], and called the Near-Field Technique (N.F.T.), is presented whereby the complete radiation pattern of a general, three-dimensional, wide beam antenna can be inferred from limited near-field measurements performed in one plane. The measurement and computational procedure is formulated for an arbitrarily shaped antenna with the class of waveguide aperture antennas being given special attention. It is demonstrated that a consequence of applying the N.F.T. to an aperture antenna is that an estimate can be made of the higher order modes excited at the aperture discontinuity. The accuracy of the method is discussed with particular regard to the sampling of the near-field pattern. The design of the sampling probes is outlined, and finally, an appraisal of the N.F.T. is given. The experimental and computational results of an application of the N.F.T. to a waveguide aperture antenna are presented in Chapter 4.

2.2 Formulation of the N.F.T.

2.21 Field representations.

Consider an arbitrary antenna centred at the origin and totally enclosed by a surface S such that the region exterior to S is source free, as in Figure 2.1. The total field at any point in a region can be expressed in terms of the sources within the region and the values of the tangential components of the fields over the boundaries of the volume[23]. Since the region exterior to S is source free, the total field from the antenna can be completely specified in terms of the tangential components of the field on S. The field on S, being piecewise continuous, may be represented exactly by a complete, denumerably infinite, set of orthogonal vector eigenfunctions[24]. Because of the infinite order of this field representation, solutions to problems involving its use are not generally amenable to purely analytical techniques. Such problems, however, can be solved by applying approximation methods on high speed digital computers. The set representing the field is truncated to approximate the true field on S, to within a prescribed error bound, by

$$\underline{U}(r,x,\psi) = \sum_{n}^{N} A_n \underline{\Phi}_n(r,x,\psi) \qquad (2.1)$$

where $\underline{U}(r,x,\psi)$ is the approximation to the true field on S, A_n are the complex amplitude constants, $\underline{\Phi}_n(r,x,\psi)$ are orthogonal vector eigenfunctions, and the coordinates (r,x,ψ) describe S.

Two representations having the form of (2.1) will be considered: one in terms of spherical vector modes for arbitrarily shaped antennas, and the other in terms of waveguide modes of propagation for the particular class of aperture antennas.

(a) Arbitrary antennas.

For an arbitrarily shaped antenna the most convenient form for the enclosing surface S is a sphere, with the fields on S represented, via (2.1), as a set of spherical vector modes[25]. These vector modes represent all waves crossing S, whether inward or outward travelling with respect to the antenna. In the present case the region exterior to S is source free implying that only those modes corresponding to outward travelling waves need to be considered. Therefore, the electric and magnetic fields at any point P, coordinates (ρ,θ,ϕ), on S are given by

$$\underline{E}_n(\rho,\theta,\phi) = \sum_{\substack{emn \\ o}}^{N} \left[a_{emn} \underline{m}_{emn}(\rho,\theta,\phi) + b_{emn} \underline{n}_{emn}(\rho,\theta,\phi) \right] \quad (2.2)$$

$$\underline{H}_n(\rho,\theta,\phi) = \frac{jk}{\omega\mu} \sum_{\substack{emn \\ o}}^{N} \left[a_{emn} \underline{n}_{emn}(\rho,\theta,\phi) + b_{emn} \underline{m}_{emn}(\rho,\theta,\phi) \right] \quad (2.3)$$

where the $a_{\substack{e\\o}mn}$ and $b_{\substack{e\\o}mn}$ are the suitably ordered complex modal amplitudes of the transverse electric (TE) and transverse magnetic (TM) spherical vector modes $\underline{m}_{\substack{e\\o}mn}$ and $\underline{n}_{\substack{e\\o}mn}$, respectively, given in Appendix I. The radial functions included in this representation are spherical Hanekl functions of the second kind which satisfy the radiation condition at infinity. A complete knowledge of the modal strengths at one point in a region is sufficient to specify uniquely the fields everywhere in the regibn. Consequently, the modal amplitudes in (2.2) and (2.3) specify the fields everywhere exterior to S to the same accuracy as the field representation on S. Estimates of the fields interior to S are liable to be less accurate since the effects of the neglected higher order modes become increasingly more significant as the antenna is approached. Equations (2.2) and (2.3) may now be considered as the electric and magnetic field representations at any field point $P(\rho,\theta,\phi)$ on or exterior to S.

The fields $\underline{E}_n$ and $\underline{H}_n$ are dependent upon the 2N complex coefficients $a_{\substack{e\\o}mn}$ and $b_{\substack{e\\o}mn}$. For a practical antenna, although the functional forms of the vector modes will be known, their relative strengths are likely to be unknown. By performing independent field measurements of both magnitude and phase of $\underline{E}_n$ or $\underline{H}_n$, a set of linear independent, algebraic equations is obtained in the unknowns $a_{\substack{e\\o}mn}$ and $b_{\substack{e\\o}mn}$. These unknowns may be conveniently solved for by arranging the set of simultaneous equations in matrix form. Thus,

$$U_i = \sum_j H_{ij} A_j \qquad (2.4)$$

where U_i is the i^{th} element of the column matrix [U] and corresponds to the field measurement performed at the i^{th} field point, and H_{ij} is the $(i,j)^{th}$ element of the square matrix [H] which gives the functional variation at the i^{th} field point of the j^{th} mode, whose amplitude is given by A_j, the j^{th} element of the column matrix [A]. Implicit in (2.4) are three scalar matrix equations corresponding to the three spherical components of the measured field. From a computational point of view, it is desirable to achieve such separation by considering the field component-by-component. Standard numerical methods, either matrix inversion or iterative techniques[26], permit a unique solution for the A_j in (2.4) provided [H] is non-singular. Once these coefficients have been determined, the total radiation pattern of the antenna can be predicted. In particular, measurements performed in the near-field can be operated on computationally to infer the total radiation from the antenna.

(b) Aperture antennas.

A general electromagnetic field can be completely expressed in terms of an electric vector potential and a magnetic vector potential[27]. For the special class of aperture antennas it is convenient to consider the surface S as part of the aperture plane. Considering the field on S and applying the equivalence principle[28], the field radiated

by the aperture antenna is found to be the same as that produced by the equivalent magnetic current sources in the aperture plane, alone. If the tangential electric field in the aperture plane, external to the aperture, is zero as is the case for aperture antennas mounted in infinite, perfectly conducting ground planes, then the equivalent magnetic current sources exist only over the aperture region. Thus the radiated field can be fully specified by an electric vector potential expressed in terms of the tangential electric field in the aperture.

The aperture fields of an aperture antenna mounted in a ground plane can be represented by a complete set of wave-guide modes of propagation suitable to the geometry. In general, this set must include both TE and TM modes to express the field fully. From (2.1) and applying the boundary conditions on the electric fields, the tangential electric field on S for such an antenna is given by

$$\underline{E}_t(r,\psi) = \sum_n [A_n \hat{\underline{Z}} \times \underline{E}_{TE_n}(r,\psi) + B_n \hat{\underline{Z}} \times \underline{E}_{TM_n}(r,\psi)], \qquad (2.5)$$

where (r,ψ) are cylindrical coordinates in the aperture, $\hat{\underline{Z}}$ is the z direction unit vector normal to the aperture plane, the A_n and B_n are the ordered complex modal amplitudes representing the relative strengths of the waveguide modes, and $\underline{E}_{TE_n}(r,\psi)$ and $\underline{E}_{TM_n}(r,\psi)$ are the aperture electric field components of the n^{th} TE and TM modes respectively.

Introduce an electric vector potential $\underline{F}$, such that scalar Helmholtz equation is satisfied by the rectangular components of $\underline{F}$ given by

$$F_x = -\frac{1}{2\pi}\iint_{S'} P(x,y)\,\frac{e^{-jkR}}{R}\,dS', \tag{2.6}$$

$$F_y = \frac{1}{2\pi}\iint_{S'} Q(x,y)\,\frac{e^{-jkR}}{R}\,dS', \tag{2.7}$$

where $P(x,y)$ and $Q(x,y)$, respectively, are the $\hat{x}$ and $\hat{y}$ direction components of the tangential electric field in the aperture, $\frac{e^{-jkR}}{R}$ is the scalar Green's function for unbounded space with the source and observational coordinates defined in Figure 2.1, and S' is the aperture domain, a sub-domain of S. By substituting the rectangular components of (2.5) into (2.6) and (2.7) and transforming $\underline{F}$ into spherical components, the fields radiated by the antenna can be determined in spherical components, via

$$\underline{E} = \underline{\nabla} \times \underline{F} \tag{2.8}$$

and

$$\underline{H} = \frac{j}{\omega\mu}\left[\underline{\nabla}\,\underline{\nabla}\cdot\underline{F} + k^2\underline{F}\right], \tag{2.9}$$

where $\underline{\nabla}$ is the vector differential operator. Separation of the functional dependence of the source coordinates from that of the observational coordinates in the Green's function facilitates the evaluation of the integrals in (2.6) and (2.7). This is achieved by expanding the

Green's function in terms of scalar spherical harmonics,

$$\frac{e^{-jkR}}{R} = -jk \sum_{\ell=0}^{\infty} (2\ell+1) P_\ell(\cos\gamma) \begin{cases} j_\ell(kr) h_\ell^{(2)}(k\rho) & \text{for } r \leq \rho \\ j_\ell(k\rho) h_\ell^{(2)}(kr) & \text{for } r > \rho \end{cases} \tag{2.10}$$

where $\gamma, r, \rho,$ and R are defined in Figure 2.1, $j_\ell(kr)$ and $h_\ell^{(2)}(k\rho)$ are spherical Bessel and Hankel functions, respectively, and $P_\ell(\cos\gamma)$ are Legendre polynomials representing zonal harmonics. This expansion separates the radial coordinate variations of the source point and the observation point. An application of the Legendre polynomial addition theorem[29], which is equivalent to expressing the zonal harmonics in terms of tesseral harmonics, transforms the field expressions (from (2.8) and (2.9)) into forms more suitable for the analytical integration over the azimuthal coordinate. Considering the field components individually and imposing the appropriate boundary conditions on the ground plane, the field variations of the remaining components (normal electric and tangential magnetic field components) are of the form

$$U(\rho,\phi) = \sum_{\ell=0}^{\infty} a_\ell V_\ell(\rho,\phi) \tag{2.11}$$

where $U(\rho,\phi)$ is the field component, the $V_\ell(\rho,\phi)$ are the functional variations or modes of the field component in the exterior region described by the coordinates (ρ,ϕ), and the a_ℓ are coefficients independent of the field variat-

ions but characteristic of the exterior modes. Furthermore, the a_ℓ are known functions of the modal amplitudes in (2.5). As before, performing a series of independent field measurements on the field components enables a matrix equation similar to that implicit in (2.4) to be derived from a suitably truncated form of (2.11). The matrix [H] now contains the functional forms of the exterior modes from (2.11), and the column matrix [A] contains the a_ℓ coefficients as elements. Once these coefficients have been determined by numerical solution of the matrix equation, the total radiation pattern of the aperture antenna may be deduced.

2.22 Separability of field values.

A unique solution for the modal coefficients in (2.4) or (2.11) is possible if and only if the matrix [H] is non-singular. This implies that not only must the near-field measurements of the electric or magnetic field component be linearly independent, but also the effects of all the modes in the exterior region must be separable. To satisfy these requirements it is sufficient to perform the measurements along constant coordinate curves in one plane. Thus, separation of the azimuthal angular variations of the modes is ensured by performing the measurements at field points with a constant radial coordinate, since for different mode indices the azimuthal modes are mutually orthogonal. Similarly, measuring at field points with constant azimuthal angular coordinate permits separation of the radial

variations of the field expressions, due to the orthogonality conditions on the radial modes.

Consideration must also be given to the separability of the TE modes from the TM modes in the spherical vector mode field representation. When performing the measurements as outlined above, two of the three orthogonal curvilinear coordinates (ρ, θ, ϕ), necessarily assume constant values. From the forms for the TE and TM vector modes, given in Appendix I, the modal variations in the remaining coordinate for modes of one type (TE or TM), become linearly dependent upon similar index modes of the other type. For example, a consideration of $\underline{\hat{\theta}}$ components of TE and TM modes for constant ϕ and θ values (that is, measurements performed to separate radial variations), shows that the radial variation of the TM mode of radial mode index n, is a linear combination of TE modes of radial mode indices (n-1) and (n+1). Consequently, (2.2) and (2.3) are rearranged so that all modes with the same functional dependence on the field variation coordinate for each particular set of measurements are grouped together, leading to the re-defining of all the modal coefficients in (2.4). As a result of the measurement pattern, these derived coefficients are independent of the field variation coordinate but are functions of the remaining two field coordinates as well as

the modal amplitudes. *Therefore, the field of the antenna can not be inferred simply from a knowledge of these coefficients derived from near-field measurements performed on a single field component.* Since for different field components the derived coefficients have different functional dependences on the modal amplitudes, the unknown amplitudes can be determined by measuring two field components and solving the double set of simultaneous equations. The tangential components of the electric and magnetic fields are dependent upon both TE and TM modes, whereas the radial components are functions of the TM modes only. Measurements performed on the electric or magnetic radial component can be used, therefore, to determine the sub-set of the b_{emn}^{o} or a_{emn}^{o} modal amplitudes, respectively. This sub-set together with computations on measurements of any other field component yields the complete set of modal amplitudes. Although these amplitudes may be derived from measurements performed on the two radial field components, it is more convenient in practice, and more accurate (since then there is no need to calibrate the sampling probes as only relative measurements are required), to measure a radial and a tangential component of the same field.

Separability of the mode effects causes similar problems in the waveguide mode field representation for aperture antennas. It might be thought that (2.11) could be rearranged into the form

$$U(\rho,\phi) = \sum_{n}^{N} [A_n S_n(\rho,\phi) + B_n T_n(\rho,\phi)] \qquad (2.12)$$

where the A_n and B_n are as in (2.5), and the $S_n(\rho,\phi)$ and $T_n(\rho,\phi)$ are the functional variations of the TE_n and TM_n waveguide modes in the exterior region. Determination of the modal amplitudes would then follow directly from the numerical solution of a matrix equation as above. Further investigation reveals, however, that the matrix containing the $S_n(\rho,\phi)$ and $T_n(\rho,\phi)$ as elements, is either analytically singular or numerically so ill-conditioned that a reliable, accurate solution for the modal amplitudes is not possible. As in the case of the vector mode representation, it is more accurate to solve for derived coefficients, which are functions of the modal amplitudes.

2.23 Field measurements.

From (2.4), to solve for N complex modal coefficients, N complex independent field measurements are required, where a complex field measurement is defined as the measurement of both the magnitude and the phase of the field at a point.

Truncation of the set of eigenfunctions representing the field to an upper mode index N as in (2.2), (2.3) and (2.5) results in 2N functions being included in the representation, implying that the matrix equation derived from (2.4) is of order 2N. Combining the similar index modes of each type (TE and TM) with the same functional variations in the exterior region, and defining new coefficients which are known functions of the respective modal amplitudes, reduces the matrix equation to order N for all field components. Hence, numerical solution of an N order matrix equation derived from N complex independent measurements of a field component, yields a set of N complex coefficients, which in conjunction with the set of N coefficients computed from measurements performed on another field component, permits the required 2N modal amplitudes to be determined.

To summarize, determination of the 2N complex modal amplitudes appearing in the modal field representations (2.2), (2.3), and (2.5), requires a total of 2N complex independent field measurements, that is N complex measurements for each of the two field components. Since these modal amplitudes completely specify the field radiated by the antenna to within the accuracy limits imposed by the truncation of the field representation, 2N complex measurements of the near-field pattern are sufficient to infer the total radiation pattern of the antenna.

2.3 Source field distributions.

It is well known that the aperture field distribution and the far-field radiation pattern of a planar aperture antenna form a Fourier transform pair[21]. A complete knowledge of one in both magnitude and phase over all regions of space, therefore, uniquely defines the other. Estimating the aperture field distribution requires a complete knowledge of the radiation pattern, but in practice this information is likely to be incomplete, since the radiation pattern will be known or measured only over the visible region of space[30]. A meaningful approximation to the aperture field of an antenna with a narrow beam radiation pattern, can be inferred by assuming the pattern function to be negligible in the invisible region. However, for a wide beam antenna or an array antenna, the pattern function is not negligible in the invisible region, in which the square of the magnitude of the pattern function is a measure of the reactive energy stored in the near-field of the antenna[31]. It has been shown[21] that the radiation pattern of a planar aperture antenna is an analytic function, and can be analytically continued from the visible region into the invisible region. Therefore, provided the radiation pattern is accurately known within the visible region, analytic continuation can be used to specify completely the pattern function over both visible and invisible regions. The aperture field distribution can be determined by Fourier transforming the pattern function.

By applying the N.F.T., the complete far-field pattern of an antenna can be inferred to within the accuracy limit imposed by the field representation (2.1). Fourier transforming the field pattern in both visible and invisible regions of space then gives an estimate of the equivalent aperture source distribution. However, this estimate is likely to be error sensitive, because the higher order modes, which are neglected in (2.1), contribute mainly to the reactive energy stored about the antenna, and they have a greater effect on the pattern function in the invisible region than in the visible region. Even when a pattern function is known accurately in the visible region, its analytic continuation into the invisible region will in general be very difficult to compute accurately[30], because such a computation is equivalent to extrapolation outside the measurement interval. The Fourier transform method is useful in that the equivalent aperture sources so determined (effective current line sources) are the sources whose effects in the far-field are of the most importance.

An alternative approach for aperture antennas is to solve for the modal amplitudes in the waveguide mode field representation (2.5) using the modal coefficients in (2.11), which have been determined by applying the N.F.T. The two sets of coefficients are related by a matrix equation

$$[a] = [G][A] \tag{2.13}$$

where the column matrices [A] and [a] contain as elements the modal coefficients in (2.5) and (2.11), respectively. The elements of the square matrix [G] are the functions describing the dependence of the field on the modal indices in (2.5) and (2.11). Provided the matrix [G] is non-singular the amplitudes of the waveguide modes can be determined from the numerical solution of (2.13). As with the Fourier transform method, this technique can give an estimate only of the strengths of the modes whose effects are significant in the exterior field region.

2.4 Error analysis.

The accuracy of the N.F.T. is limited by two factors: the approximation that the piecewise continuous electromagnetic fields can be represented by a finite set of eigenfunctions, and the accuracy to which the near-field of the antenna can be sampled.

2.41 Truncation error.

The truncation of the set of eigenfunctions is justified since the field representation is uniformly convergent except at physical discontinuities on the antenna. Increasing the order of the approximation, N, in (2.1) improves the accuracy of the representation, but also increases the computational effort and time required to determine the modal amplitudes. The computation

associated with the solution of the matrix equation, in particular, is greatly increased, because the number of numerical operations necessary to invert a matrix is proportional to the cube of the order of the matrix. However, in practice the choice of N is govenred almost entirely by consideration of the accuracy of the field representation. An electrically small antenna radiates most strongly in the lower order modes, with the higher order modes contributing significantly to the total field only at points very close to the antenna. For wide beam antennas of this type, only a limited number of modes are necessary to represent the far-field accurately, and the order of the matrix equation is restricted accordingly. Due to the efficiency of standard numerical techniques for solving matrix equations and the restricted order of the equations encountered in the analysis of these antennas, the computational effort required by the N.F.T. is considerably less than for a complete mode-by-mode analysis of the three-dimensional near-field as would be necessary in the three-dimensional method of Brown and Jull[1] as formulated by Jensen[3].

2.42 Field sampling error.

Ideally, the electric and magnetic field components should be measured with an infinitesimally small Hertzian dipole (electric or magnetic) to satisfy the requirements that the sampling probe cause no disturbance to the field, and that the field be sampled at a point in space.

To ensure adequate signal strength and sensitivity for the detector, a practical probe must have a finite size. It has been shown for electric probes[32] that provided the probe is electrically small (that is, the probe length is much less than a quarter of a wavelength), the scattering of the sampled field by the probe will be negligible. Similarly, the perturbation of the field caused by a magnetic probe will be small provided the loop diameter is well below a quarter of a wavelength. A small magnetic probe responds to the electric field component that is parallel to the plane of the loop as well as to the magnetic field component linking with the loop. To sample the magnetic field only, the loop must be either extremely small (diameter less than a hundredth of a wavelength) or shielded[33]. It has been shown[34] that due to the "antenna effect" an unshielded probe a tenth of a wavelength in diameter responds equally to the electric field component as to the magnetic field component.

Radiation and scattering effects caused by the physical connections to the sampling probe can be totally eliminated in the important category of antennas mounted on or above metallic ground planes. For these antennas the near-field components are sampled close to the surface

of the ground plane by a small probe penetrating the ground plane. Consequently, by placing all the detection equipment beneath the ground plane, the only disturbance to the field is caused by the measuring probe itself.

The field component being measured varies across the finite extent of the probe, with the result that the probe, rather than sampling the field at a point, averages the field value over a small but finite region of space. This causes a small error in the field values assumed in (2.4) or (2.11). The order of magnitude of these errors can be estimated by integrating the field component across the effective aperture of the probe and comparing with the actual field value at the field point. For example, consider an electric probe sampling the E_θ field component on the ground plane. The sampling error results from the variation of the E_θ component with elevation angle θ, and from the vector and scalar spherical mode representations for E_θ, the θ dependence resides entirely in the Legendre functions. In fact, because of the boundary conditions on the fields on the surface of the ground plane, E_θ depends only on the Legendre functions of the form $P^m_{m+2\ell}(\cos\theta)$. Since

$$\left[\frac{\partial P^{m}_{m+2\ell}(\cos\theta)}{\partial\theta}\right]_{\theta=\frac{\pi}{2}} = 0, \qquad (2.14)$$

the functions of low order and degree are slowly varying as θ approaches $\pi/2$. Moreover, the uniformly convergent forms of the field representations mean that for a wide beam antenna only these lower index functions contribute significantly to the sampling error. Assuming that the modal amplitudes determined by the N.F.T. are accurate, the magnitude of the percentage error is estimated from the scalar mode representation for E_θ, by summing the integrations of the $P^{m}_{m+2\ell}(\cos\theta)$ functions over the effective length of the sampling probe, and comparing with the value of E_θ at $\theta = \pi/2$. The sampling error introduced by an electric probe a thirtieth of a wavelength long, operating at a frequency of $2GH_z$, and located at a field point on the ground plane a quarter of a wavelength distant from the aperture rim of a circular waveguide aperture antenna (the near-field sampling point closest to the antenna in the measurements reported in Chapter 4), has been estimated by this method as less than 1% of the actual field.

In a similar manner a loop probe measuring the magnetic field components on the ground plane introduces sampling errors which can also be estimated by integrating the appropriate field variations over the aperture of

the probe. The error introduced by a shielded loop probe sampling the H_ρ component is caused by the variation of H_ρ across the aperture of the probe. This variation is given by the dependence of H_ρ on the angular field coordinates θ and ϕ. In common with the E_θ component discussed above, the θ dependence of H_ρ is given by Legendre functions of the form $P^m_{m+2\ell}(\cos\theta)$, whereas the ϕ dependence is determined by the form of the source field. For the previously quoted example of the circular aperture antenna, the radial magnetic field component in the aperture varies as $\cos\phi$, since the antenna is excited in the dominant waveguide mode. Therefore, by symmetry, H_ρ in the region external to the aperture also varies as $\cos\phi$, and from the vector mode field representation, the θ dependence is of the form $P'_{2n-1}(\cos\theta)$. Integrating these functions over the probe aperture A and summing the modes included in the field representation gives

$$I = \int_A \int \cos\phi \sum_n^N C_{2n-1} P'_{2n-1}(\cos\theta)\, dA \qquad (2.15)$$

where the C_{2n-1} are coefficients from the H_ρ field representation derived from the N.F.T. By expressing $\cos\phi$ and $\cos\theta$ as functions of (r,ψ) the coordinates of A (that is,

$$\cos\phi = \frac{d}{\sqrt{r^2\cos^2\psi+d^2}}, \text{ and } \cos\theta = \frac{d}{\sqrt{r^2\sin^2\psi+d^2}}, \qquad (2.16)$$

where $d = \lambda/4$ = the radius of the field point), applying the binomial theorem, and neglecting terms in small quantities raised to powers higher than the second, the magnitude of the difference between (2.15) and the value of H_ρ at the field point is found to be less than 0.5%.

The same method can be applied to determine the sampling error caused by a finite sized shielded loop probe measuring the H_ϕ component on the ground plane. However, a more serious source of measurement error results from the response of the probe to the electric field. The shielded probe considered is shown in Figure 2.2. This probe is of standard design[33] with a single turn (or inner conductor) and an unbalanced shield to match the unbalanced coaxial feed line of 50 ohms nominal characteristic impedance. A probe of this type with a mean radius of 5mm and an outer conductor diameter of 1mm was constructed and found to have adequate sensitivity. Although the shield of this probe eliminates any coupling with the electric field component perpendicular to the ground plane, the probe may respond to the tangential electric field component parallel to both the plane of the loop and the ground plane. This tangential component necessarily must be zero on the ground plane, but may increase rapidly at points away from the surface. Hence, measurements of the magnetic

field components are affected by spurious responses due to tangential components of the electric field. In the measurement of the H_ρ component of the circular aperture antenna discussed above, the only electric field component present at the field points where H_ρ is sampled, is the E_ϕ component. Since E_ϕ is normal to the plane of the loop, the measurement of H_ρ for this particular antenna is not affected by the presence of the electric field. Conversely, the measurement of H_ϕ on the ground plane is sensitive to the electric field, as both the E_θ and E_ρ components are present at the field points where H_ϕ is sampled, and are aligned parallel to the plane of the loop. The shielding of the probe eliminates the response due to the E_θ component, so that only the E_ρ component causes the measurement error in the sampling of H_ϕ. The magnitude of this error can be estimated by integrating the E_ρ component around the perimeter of the loop. A simpler but more approximate approach is to consider the section of the loop that is substantially parallel to E_ρ as acting like an electric dipole[34]. The magnitude of the voltage induced in the probe by H_ϕ is given by[35]

$$V_H = \tfrac{1}{2}\omega\mu H.A \qquad (2.17)$$

where A is the area of the loop. The voltage generated in the probe by the electric field is

$$V_E = E_\rho h_e, \qquad (2.18)$$

where h_e is the effective length of the probe parallel to E_ρ and is assumed to be 0.707 x loop diameter as a first approximation. An estimate of the significance of the V_E signal is given by comparing (2.18) with (2.17). For the circular aperture antenna the ratio of E_ρ to H_ϕ was evaluated at the field sampling point closest to the antenna by assuming that the modal amplitudes in the vector mode representations for these components, determined by the N.F.T. were correct. Thus, V_E was found to be less than 3% of V_H which is the signal it is desired to measure.

2.5 Critique of the N.F.T.

The N.F.T. may be summarized as follows. The fields of the antenna are expressed as a set of orthogonal, vector wave functions, or modes, whose relative amplitudes are derived from a limited number of near-field measurements. Provided these field measurements are linearly independent the matrix equation relating the set of measurements to the field representation can be solved by numerical methods for the unknown relative amplitudes of the modes. Once determined, these amplitudes together with the asymptotic expansions of the modes are used to infer the complete radiation pattern of the antenna.

In common with the Fourier series method of Brown and Jull[1] and the matrix formulations of the three-dimensional extension of this method[3], the desired accuracy of the field representation governs the number of near-field measurements required, since the determination of N complex modal amplitudes requires a set of N independent complex equations derived from N complex field measurements. Because a knowledge of the relative amplitudes of the modes in the field representation is sufficient to specify the radiation pattern of the antenna, only relative measurements of the near-field pattern are necessary. Thus, accurate calibration of the sampling probes is not necessary unless measurements are required of both an electric and a magnetic field component. In this case, the two sets of field measurements must be related to each other, implying the need for calibration of each probe. The determination of N modal amplitudes, in general, requires the numerical solution of two matrix equations of order N/2, since field measurements must be performed on two field components as a consequence of the inclusion of the TE and TM subsets of modes in the field representations. When compared with the solution of a matrix equation of order N, numerical solution of these two equations results in a net reduction of the total

computational effort and time involved (see Section 2.43). Furthermore, upon comparison with the Fourier series method and more especially the auto-correlation method of Hamid[22], the N.F.T. requires less computation. A further advantage of the N.F.T. is that the complete three-dimensional radiation pattern is inferred from limited near-field measurements performed in one plane only, as compared with the measurement of the near-field pattern over a three-dimensional surface enclosing the antenna in the previous three-dimensional methods[3,20]. This is of practical importance for antennas mounted above ground planes, since their radiation patterns can be inferred from near-field measurements performed by a small probe penetrating the ground plane. With the detection equipment placed below the ground plane the disturbance of the field is minimised. For the special class of aperture antennas, whose aperture fields may be represented in terms of a set of waveguide modes of propagation suitable to the particular geometry of the antenna, the N.F.T. enables an estimate to be made of the higher order modes present in the aperture. Finally, the N.F.T. is more suitable for inferring the far-field patterns of a wide beam antenna than for an antenna with a narrow beam radiation pattern. The latter requires a greater number of modal functions to represent the fields of the antenna accurately, and subsequently, the number of measurements and the computational effort required are significantly increased.

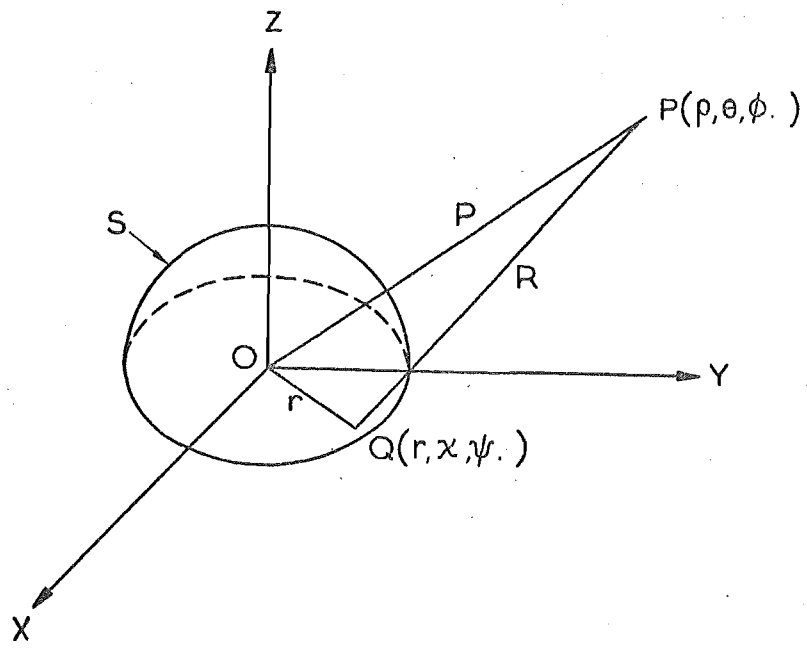

FIGURE 2·1 : ANTENNA COORDINATE SYSTEM

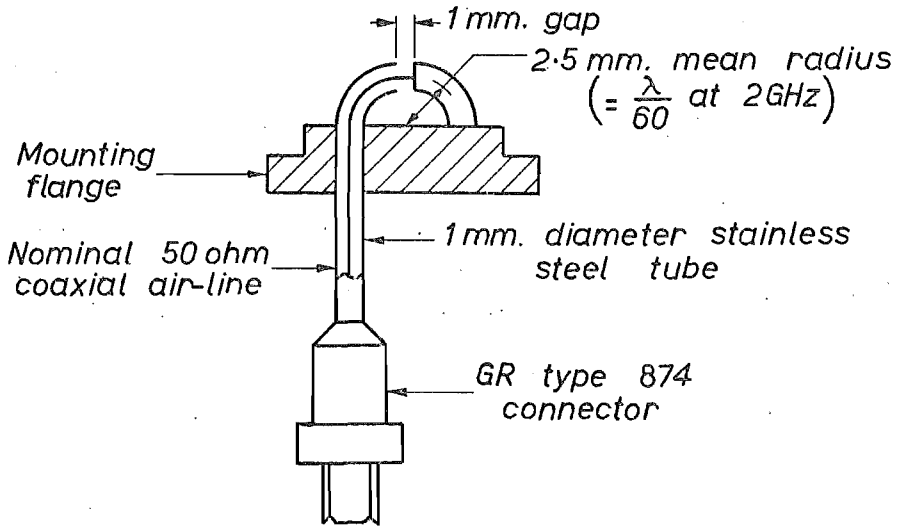

FIGURE 2·2 : SCHEMATIC OF SHIELDED LOOP PROBE

Chapter 3 : Scattering matrix approach to the study of mutual coupling.

3.1 Introduction.

In recent years considerable attention has been directed at the design and analysis of array type antennas[4-6]. The performance of an array is determined partly by the array geometry and partly by the characteristics of the individual radiating elements. Because of the mutual coupling effects of the surrounding elements the behaviour of a particular element in an array environment may be markedly different from its behaviour as an isolated antenna. Moreover, in an electronically scanned array, since the coupling effects vary with the phasings of the element excitations as the radiation beam of the array is steered over the scan volume, the element and array characteristics vary with scanning. Before an accurate description of the performance of an array can be developed, therefore, it is necessary to evaluate the effects of mutual coupling in the array.

The earliest mutual coupling studies were concerned with pairs of dipole antennas. Carter[36] formulated the induced emf method to derive the self and mutual impedances of two identical parallel dipoles in broadside, collinear, and echelon configurations. The radiation resistance of a dipole in an infinite array was calculated by Wheeler[37],

who first introduced the unit cell concept. The driving point and mutual impedances of two similar thin wire dipoles were determined by King[38] using a current integral equation technique. By this technique King was also able to compute the current distributions and radiation patterns of the dipoles. Allen et.al.[39], in a series of studies, investigated the coupling effects in large dipole arrays mounted over ground planes. The method used to calculate the coupling effects was based upon the impedance formulae originally developed by Carter. By applying a bidimensional Fourier series for the fields in terms of plane waves, Stark[40] derived expressions for the radiation resistance and reactance of a dipole in an infinite array backed by a ground plane. This approach extended the results of Wheeler by including the reactance of the array and allowing for arbitrary scan angles. The short dipole form of Carter's formulae was used by Allen[41] to estimate the coupling effects in unequally spaced dipole arrays. The importance of including mutual coupling effects in the calculations of array patterns was especially emphasised in this study. Chang[42] extended the integral equation approach followed by King to derive an accurate solution for the infinite dipole array, and calculated the current distributions and the admittances of typical array elements.

Because of the periodicity of equally spaced arrays, the unit cell or periodic structure approach has been used extensively in the analysis of infinite planar arrays of waveguide elements. Since coupling between elements decays rapidly with increasing distance, these infinite arrays closely approximate the behaviour of large but finite arrays. Wheeler's unit cell concept was extended by Edelberg and Oliner[43] who incorporated susceptance effects and the variation of the element admittance with the scanning of the array, in the study of an array of slot antennas. Using a similar technique Galindo and Wu[44,45] investigated restricted scan planes of infinite planar arrays of thin and thick walled waveguides. The thin wall problem was solved exactly while an approximate numerical solution was derived for the thick wall array. The results of these studies were presented in the form of the element reflection coefficients as functions of the array scanning angle. A method for pictorially representing the variation of the element impedance with the scanning angle was presented by Wheeler[46]. This method, known as the grating-lobe series, combines the effects of the array periodicity with the impedance characteristics of the element, such as described by the impedance crater concept[47]. The unit cell technique was applied by Farrell and Kuhn[48] to determine the coupling in an infinite array of rectangular

waveguides. Borgiotti[49] followed a similar approach but increased the generality of the analysis to include rectangular or circular radiators in arbitrary array lattices. Based upon the analytic continuation arguments of Rhodes[47] and Borgiotti[50] for the complex power of a planar aperture antenna, Diamond[51] formulated a generalized analysis of infinite planar arrays, applicable to all array problems where the fields can be specified over the complete aperture plane. In particular, the grating-lobe series for the admittance of a narrow slot array and the impedance of a dipole array both with and without a ground plane were derived by this method, and were shown to agree exactly with the previously published results of Edelberg and Oliner and Stark.

Purely analytical investigations of mutual coupling effects between complicated elements are generally not feasible, so that experimental methods must be employed to determine the properties of an array. From the unit cell technique and image theory, an infinite array can be simulated by surrounding a single element with perfect electric or magnetic walls in the form of a waveguide[52]. This waveguide simulator concept was developed by Hannan et.al.[53] and Hannan and Balfour[54] into a practical method for experimentally analysing large arrays.

The geometrical theory of diffraction as formulated by Keller[55] has been applied to determine the coupling in simple arrays of similar elements. By using wedge diffraction techniques, Dybdal et.al.[56] computed the coupling between two parallel plate waveguides for various modes of excitation. Although the results they presented apply to identical elements, the formulation is not so restricted and can be used to obtain the coupling between elements with different geometries. Hamid[57] calculated the coupling between two identical sectoral horns by using an approach based on the geometrical theory of diffraction.

A feature of array behaviour caused by mutual coupling effects that has generated considerable interest recently is the appearance of nulls in element patterns at scan angles somewhat less than the scan angles associated with the incidence of grating lobes. Several authors have reported pattern measurements exhibiting these nulls. Bates[58] measured the element pattern of an open ended waveguide in a small linear array, covered by a dielectric slab. Lechtreck[59] obtained the element pattern of an array of coaxial horns fitted with radomes, while Hannan[60] detected a pattern null for a simulated array of dielectric-loaded circular apertures.

From the initial discovery of these nulls, they have been explained in terms of a surface-wave supported by the array structure[58,61]. Thus, pattern nulls occur in arrays whose structures contain dielectric material or another form of slow-wave loading such as corrugations or waveguides projecting above a ground plane. Wu and Galindo[62] studied the effects of dielectric slabs on the radiation properties of an infinite rectangular waveguide array, using an integral formulation. This study showed that forced surface-wave resonances occur at certain scan angles, when a higher order mode associated with the slab causes a complete reflection of the incident power in each element, resulting in a null in the element pattern. Furthermore, this surface-wavelike mode was shown to be characteristic of a modified form of the array and not of the array itself. In a similar investigation of an infinite array of parallel plate waveguides covered by a dielectric sheet Knittel et.al.[63] invoked the unit cell concept and also showed that the surface-wave is supported by the modified array structure, and is present only when the array is scanned to the angle corresponding to the element pattern null. Moreover, it was demonstrated that although the actual array structure could not support true surface-waves it could support leaky waves. The presence of such leaky waves would then account for the width of the pattern null. A study of the effects of dielectric loading, plugging, and covering on the

performance of an infinite array of circular waveguides arranged in a hexagonal grid was presented by Amitay and Galindo[64]. The three dielectric configurations considered were shown to correspond to three different cases of forced surface-wave resonances, and it was further observed that these occurred at isolated scan angles. Wu[65] applied the integral equation approach to analyse the coupling effects in dielectric loaded infinite arrays of TE mode excited parallel plate waveguides, and demonstrated the existence of surface-wave resonances for this type of excitation. The conditions for resonance were shown to be identical with those for resonances in infinite arrays of the same elements. Extending this analysis, Wu[66] also calculated the edge effects in finite parallel plate waveguide arrays by comparing the computed element patterns and array reflection coefficients as functions of array scan angle, with the equivalent results for infinite arrays. With the occurrence of surface-wave resonances, Wu found that the coupling effects had a strong dependence on the number of elements in the array. Thus, when the waveguides were loaded with dielectric plugs more elements were required to simulate an infinite array environment than when the elements were not loaded.

Several authors have analysed coupling in arrays from an equivalent circuit viewpoint based upon the scattering matrix representation for antennas introduced by Dicke[67]. The power transfer between closely spaced antennas in a complex environment were calculated by Raschke and Heidrich[68]. The group of antennas, not necessarily considered as an array, was represented by a multi-port network, so that the self and mutual coupling effects between the antennas were described by the scattering matrix of the network. Applying a similar method, Dufort[69] determined the reflection coefficient of an array of rectangular waveguides as a function of scan angle, from the equivalent circuit of the array. Mailloux[70] represented the coupling between two closely spaced rectangular waveguides, each capable of supporting two orthogonally polarized modes, by a four-port network. The scattering matrix describing the coupling effects was computed from the admittance matrix of the network. Although only two modes in each waveguide were taken into account in the analysis, the computed coupling values were shown to be in close agreement with experimentally derived values. However, Mailloux noted that this formulation was of insufficient accuracy to describe the element pattern nulls associated with large arrays. Wasylkiwskyj and Kahn[71] formulated element efficiency and coupling coefficients of an

infinite linear array in terms of the impedance matrix of the array, and showed the relationship between the scattering matrix and the reflection coefficient of the array. The coupling effects between minimum scattering antennas[67] have also been studied by these authors[72]. In particular, by employing the full scattering matrix formalism, as compared with the application of the input scattering matrix corresponding to a multi-port network representation as in the previous studies, they formulated the self and mutual impedances of two minimum scattering antennas radiating into either a two or three-dimensional space. Gately et.al.[73] formulated a network representation for an array of minimum scattering antennas and showed that a physical antenna can be represented in terms of these canonical antennas. The performance of a Yagi-Uda antenna was analysed using this technique.

The possibility of compensating for the effects of mutual coupling by interconnecting the elements of the array with networks whose effects are dependent upon the scan angle was proposed by Hannan[74]. In an analysis of coupling in finite arrays he demonstrated that it is theoretically possible to achieve an impedance match for the array over all scan angles by directly coupling the elements to each other. Hannan et.al.[75] suggested

that by interconnecting adjacent array elements with reactive circuit elements the array match could be improved over a wide range of scan angles. A systematic approach to the design of practical compensation networks for matching an array over a prescribed scanning range was presented by Amitay[76]. The networks considered introduced a reactive network between each array element and a step change in the characteristic impedance of the transmission line feeding each element. Hannan[77] showed that an array can be matched over all real scan angles by incorporating shunt susceptance circuits between all elements. Since this requires N^2 compensation circuits for an N element array, the procedure is clearly impracticable. Varon and Zysman[78] considered the problem of matching an infinite phased array and demonstrated that, although the array match can be substantially improved by the use of compensation networks, in general a perfect match over a continuous scanning range can not be realized.

Various elemental radiators other than dipoles, slots, and waveguides have been suggested as elements for particular array applications, but because of their geometrical complexity very few attempts have been made to analyse their coupling behaviour. King and Peters[79] followed an equivalent circuit approach to describe the coupling effects in an array of polyrod elements. This study was significant since the experimental results obtained showed the effects of mutual

coupling in an array of directive elements. More recently, Kyle[80] has computed the self and mutual impedances and the element patterns of log-periodic dipole elements in small arrays. Numerical techniques were applied to determine the solution of the equations describing the array, which was represented by a multi-port network.

The coupling behaviour of arrays of complicated elements can be evaluated by measuring the impedance and radiation characteristics of representative elements in the complete array system. For all but the simplest arrays involving only a few elements, such measurements will be impracticable, particularly during the element design stage of development when a number of adjustments to each element are likely to be necessary to achieve the optimum design. Large arrays, which for the majority of elements can be considered as infinite arrays, can be studied using Hannan's waveguide simulator technique. However, this technique predicts array performance for only a limited number of scan angles, whereas the procedure presented below permits the array performance to be evaluated for all scan angles.

The theoretical basis of the procedure is the scattering matrix representation for antennas, originally introduced by Dicke[67] and extensively applied recently in connection with the analysis of arrays of minimum scattering antennas[81,72]. For many practical antennas the minimum scattering concept

can not be applied, and it is necessary to perform measurements on the antenna to determine its properties. In the presented procedure, the response of an antenna when it is irradiated by a second antenna having identical properties is evaluated with special emphasis on the range of measurements required to specify the response accurately. Although applicable, in principle, to arrays of arbitrary three-dimensional antennas, the method is formulated in terms of arrays of wide beam antennas mounted above perfectly conducting ground planes.

The general scattering matrix formalism for an arbitrary three-dimensional radiating system is introduced and the important features of this representation for both individual antennas and array antennas are summarized. The calibration of an antenna, in order to determine its scattering properties, is discussed with special emphasis on the experimental effort involved. An alternative measurement procedure, that requires significantly less experimentation, for estimating mutual coupling between identical antennas is presented. This modified technique accounts for only first order coupling effects and it is demonstrated that the assumption of neglecting second and higher order effects is equivalent to a special case of the minimum scattering condition. It is also shown that the

modified technique contains a built-in experimental check on its accuracy. Finally, methods incorporating waveguide simulator techniques for experimentally verifying the accuracy of the presented procedure are described. Results of an experimental application of the procedure to a waveguide aperture antenna are reported in Chapter 4.

3.2 Network description of antennas.

An arbitrary antenna radiating into free space can be considered as a general multi-port network as indicated in Figure 3.1. At the N excitation ports denoted by the subscript α and which correspond to the input ports of the antenna, the incident and reflected waves are defined and suitably ordered to form the N dimensional column matrices $\underset{\sim}{a}_\alpha$ and $\underset{\sim}{b}_\alpha$, respectively. From Section 2.2, by enclosing the antenna with a surface S of constant radial-type coordinate, the electromagnetic fields on and exterior to S can be represented by a complete, denumerably infinite set of orthogonal vector wave functions. These vector modes represent all the waves crossing S, whether inward or outward travelling with respect to the antenna, and consequently, the associated modal amplitudes completely specify the fields everywhere exterior to S. The radiation ports denoted by the subscript β, correspond to each of the vector modes at the antenna. The amplitudes of the waves incident from space and reflected back into space at these ports are ordered to form the infinite dimensional

column matrices $\underset{\sim}{a}_\beta$ and $\underset{\sim}{b}_\beta$, respectively. The complete radiation and scattering properties of the antenna can now be expressed in the form

$$\underset{\sim}{b} = \underset{\sim}{S}\,\underset{\sim}{a} \tag{3.1}$$

where $\underset{\sim}{a}$ and $\underset{\sim}{b}$, respectively, are column matrices containing the matrix pairs $\underset{\sim}{a}_\alpha$ and $\underset{\sim}{a}_\beta$, and $\underset{\sim}{b}_\alpha$ and $\underset{\sim}{b}_\beta$ as elements, and $\underset{\sim}{S}$ is the scattering matrix of the antenna. The total input power to the antenna is $\underset{\sim}{a}^+\underset{\sim}{a}$ (where the superscript + indicates the complex conjugate transpose), and the output power is $\underset{\sim}{b}^+\underset{\sim}{b}$. For a lossless antenna, power is conserved and $\underset{\sim}{a}^+\underset{\sim}{a} = \underset{\sim}{b}^+\underset{\sim}{b}$, which implies that $\underset{\sim}{S}$ is a unitary matrix. That is,

$$\underset{\sim}{S}^+\underset{\sim}{S} = \underset{\sim}{I} \tag{3.2}$$

where $\underset{\sim}{I}$ is the identity matrix.

Equation (3.1) can be considered more conveniently in partitioned form, thus,

$$\begin{bmatrix} \underset{\sim}{b}_\alpha \\ \underset{\sim}{b}_\beta \end{bmatrix} = \begin{bmatrix} \underset{\sim}{S}_{\alpha\alpha} & \underset{\sim}{S}_{\alpha\beta} \\ \underset{\sim}{S}_{\beta\alpha} & \underset{\sim}{S}_{\beta\beta} \end{bmatrix} \begin{bmatrix} \underset{\sim}{a}_\alpha \\ \underset{\sim}{a}_\beta \end{bmatrix} \tag{3.3}$$

where $\underset{\sim}{S}_{\alpha\alpha}$ is an N x N square matrix, $\underset{\sim}{S}_{\beta\alpha}$ is an infinite row and N column matrix, $\underset{\sim}{S}_{\alpha\beta}$ is an N row and infinite column matrix, and $\underset{\sim}{S}_{\beta\beta}$ is an infinite dimensional square

matrix. The significance of the submatrices in the proportional form of $\underset{\sim}{S}$ is as follows:

$\underset{\sim}{S}_{\alpha\alpha}$: describes the mutual and self coupling between the N excitation ports of the antenna, and hence, represents the matching of the individual antenna ports when the antenna is isolated.

$\underset{\sim}{S}_{\beta\alpha}$: describes the complete radiation pattern, both near and far-fields, of the antenna. Thus, each column of this matrix represents the radiation due to the excitation of a particular input port.

$\underset{\sim}{S}_{\alpha\beta}$: describes the receiving pattern of the antenna with each row corresponding to the signals appearing at each input port due to the waves impinging on the radiation ports. For a reciprocal antenna $\underset{\sim}{S}_{\alpha\beta} = \underset{\sim}{S}^{T}_{\beta\alpha}$, where the superscript T denotes the transpose.

$\underset{\sim}{S}_{\beta\beta}$: describes the scattering properties of the antenna, relating the relative complex amplitudes of the radiation modes that are scattered from the antenna, to the equivalent amplitudes of the waves incident from the exterior region.

The network representation for an array antenna of N elements can be formulated in precisely the same manner as for an isolated antenna with N input ports. For the array antenna, the scattering matrix is of the

same form as $\underset{\sim}{S}$ in (3.1) - (3.3), with $\underset{\sim}{S}_{\alpha\alpha}$ describing the mutual and self coupling between the array elements. Thus, $\underset{\sim}{S}_{\alpha\alpha}$ is equivalent to the scattering matrix of the corresponding N-port network, and furthermore, may also be expressed in terms of the impedance or admittance of the network. The $\underset{\sim}{S}_{\beta\alpha}$, $\underset{\sim}{S}_{\alpha\beta}$ and $\underset{\sim}{S}_{\beta\beta}$ submatrices, as before, describe the radiation, receiving, and scattering characteristics of the array, respectively.

The radiation modes can be considered individually provided that they are orthogonal wave functions corresponding to a separable coordinate system. For most applications involving three-dimensional antennas it will be convenient to enclose the antenna by a spherical surface and express the fields of the antenna in terms of the wave functions associated with spherical polar coordinates. The techniques to be discussed in the following sections will be based upon these spherical modes. It is expected that similar procedures using spheroidal or hyperboloidal wave functions could be formulated. However difficulties might arise owing to the differences between scalar and vector separability[83].

3.3 Calibration of the scattering properties of an arbitrary antenna.

The electromagnetic properties of a radiating system are completely specified by its scattering matrix. Therefore, the mutual interaction effects between systems can be evaluated in full from a knowledge of the scattering

matrices of the individual systems. In an array composed of similar antennas an estimate of the mutual coupling between the array elements requires the determination of the scattering matrix of the element antenna. This determination is often difficult, since the $\underset{\sim}{S}_{\beta\beta}$ submatrix is difficult to measure or to compute. For the special class of canonical minimum scattering antennas[81] $\underset{\sim}{S}_{\beta\beta}$ can be found analytically, and provided an antenna can be resolved meaningfully into sections which behave in a minimum scattering manner[73,82], accurate practical results can be obtained from calculation alone. However, for many practical antennas, the minimum scattering concept cannot be applied and it is necessary to perform a series of measurements to determine the scattering properties of the antenna.

The experimental determination of $\underset{\sim}{S}_{\beta\beta}$ for an antenna whose properties are described by (3.3), requires the antenna to be irradiated by an accurately known field. It will be shown that, by expressing this calibration field with respect to the phase centre of the antenna and in terms of the radiation modes implicit in (3.3), there is a series of measurements, performed both with and without the antenna present, which is sufficient to determine the elements of $\underset{\sim}{S}_{\beta\beta}$.

3.31 Calibration field representation.

The necessary calibration field can be obtained from a small electric dipole sufficiently far removed so that it illuminates the antenna under test with an essentially plane wave. If the antenna is mounted above a perfectly conducting ground plane, however, it is more convenient to use a small monopole penetrating the ground plane. Consider such an antenna and refer to Figure 3.2. Assume that the ground plane is infinite in extent and that its surface lies in the X_1Y_1 plane. A small monopole is introduced with its feed point at the origin O_1. The exact field radiated by a small monopole is well known and can be expressed simply in terms of spherical vector wave functions[83]. At the field point P, the fields with respect to O_1, and which are independent of azimuthal variation are,

$$\underline{E}(\rho_1,\theta_1,\phi_1) = \sum_n^{\infty} b_{2n-1}\, \underline{n}_{2n-1}(\rho_1,\theta_1,\phi_1) \tag{3.4}$$

and

$$\underline{H}(\rho_1,\theta_1,\phi_1) = \frac{jk}{\omega\mu} \sum_n^{\infty} b_{2n-1}\, \underline{m}_{2n-1}(\rho_1,\theta_1,\phi_1) \tag{3.5}$$

where the vector modes are given in Appendix I. The radial variations of the modes are chosen to represent outward travelling waves referred to O_1; that is, spherical Hankel functions of the second kind, $h^{(2)}_{2n-1}(k\rho_1)$. By introducing a small sampling probe at P (preferably arranged to be on the ground plane), the unknown modal amplitudes in (3.4) and (3.5) are determined by applying the N.F.T. presented in Chapter 2. Once evaluated these modal amplitudes completely specify

the radiation field of the monopole with respect to O_1.

The above field representations are expressed in terms of the radiation modes implicit in (3.3) by utilizing the addition theorems for spherical modes developed by Stein[84] and Cruzan[85]. Thus, the field of the monopole at P which is entirely outgoing with respect to O_1 is expressed in terms of incoming and outgoing modes with respect to a new origin O_2 (see Figure 3.2). From (3.4) and (3.5), and changing the mode index to ν,

$$\underline{E}(\rho_2,\theta_2,\phi_2) = \sum_{\nu}^{\infty} \sum_{mn} b_{2\nu-1}\left[A_{mn}^{0,2\nu-1}\, \underline{n}_{mn}(\rho_2,\theta_2,\phi_2) + B_{mn}^{0,2\nu-1}\, \underline{m}_{mn}(\rho_2,\theta_2,\phi_2)\right] \tag{3.6}$$

and

$$\underline{H}(\rho_2,\theta_2,\phi_2) = \frac{jk}{\omega\mu} \sum_{\nu}^{\infty} \sum_{mn} b_{2\nu-1}\left[A_{mn}^{0,2\nu-1}\, \underline{m}_{mn}(\rho_2,\theta_2,\phi_2) + B_{mn}^{0,2\nu-1}\, \underline{n}_{mn}(\rho_2,\theta_2,\phi_2)\right] \tag{3.7}$$

where $\underline{m}_{mn}$ and $\underline{n}_{mn}$, respectively, are the TE and TM spherical modes referred to O_2.

The $A_{mn}^{0,2\nu-1}$ and $B_{mn}^{0,2\nu-1}$ are coefficients dependent upon the coordinates of O_2 with respect to O_1, and their known forms are given in Appendix III. Since O_2 corresponds to a point in space, the fields at O_2 must be finite. Hence, for $\rho_2 < \rho_o$ the radial dependence of the vector modes in (3.6) and (3.7) is of the form of spherical Bessel functions of the first kind, $j_n(k\rho_2)$, while for $\rho_2 \geq \rho_o$ the functions assume the form $h_n^{(2)}(k\rho_2)$. From Appendix III the radial dependences of the addition theorem coefficients are of the forms $h_n^{(2)}(k\rho_o)$ and $j_n(k\rho_o)$, respectively, for the two cases.

It is convenient to express the fields at P directly in terms of the vector modes referred to O_2 in the alternative standard form,

$$\underline{E}(\rho_2,\theta_2,\phi_2) = \sum_{mn} [a_{mn}\underline{m}_{mn}(\rho_2,\theta_2,\phi_2) + b_{mn}\underline{n}_{mn}(\rho_2,\theta_2,\phi_2)] \quad (3.8)$$

and

$$\underline{H}(\rho_2,\theta_2,\phi_2) = \frac{jk}{\omega\mu} \sum_{mn} [a_{mn}\underline{n}_{mn}(\rho_2,\theta_2,\phi_2) + b_{mn}\underline{m}_{mn}(\rho_2,\theta_2,\phi_2)] \quad (3.9)$$

where to comply with the condition requiring finite fields at O_2 the radial functions incorporated into the modes are of the form $j_n(k\rho_2)$. Together with the relationship

$$j_n(k\rho_2) = \tfrac{1}{2}[h_n^{(1)}(k\rho_2) + h_n^{(2)}(k\rho_2)] \quad (3.10)$$

this implies that the modal amplitudes in (3.6),(3.7),(3.8), and (3.9) can be interpreted as the complex amplitudes of the incoming and outgoing spherical vector modes with respect to O_2. Furthermore by comparing (3.8) and (3.9) with (3.6) and (3.7) the modal amplitudes in the former are identified as

$$a_{mn} = \sum_{\nu}^{\infty} b_{2\nu-1} B_{mn}^{0,2\nu-1} \tag{3.11}$$

and

$$b_{mn} = \sum_{\nu}^{\infty} b_{2\nu-1} A_{mn}^{0,2\nu-1} \tag{3.12}$$

Consequently, provided the $b_{2\nu-1}$ amplitudes are accurately known, the radiation field of the monopole can be evaluated with respect to any new origin O_2. In virtue of (3.10), the a_{mn} and b_{mn} modal amplitudes are combined to represent the strengths of the subsets of incoming and outgoing waves referred to O_2. Following the notation of Section 3.2, these combined amplitudes form the elements of the column matrices $\underset{\sim}{a}_\beta$ and $\underset{\sim}{b}_\beta$. Moreover, since O_2 is a point in space, a consideration of the scattering matrix of free space[67] shows that

$$\underset{\sim}{a}_\beta = \underset{\sim}{b}_\beta. \tag{3.13}$$

3.32 Scattered field of the test antenna.

The test antenna assumed to be lossless, passive, and terminated in its match impedance, is now placed at O_2. The field at P then consists of the incident field radiated by the calibration monopole, and the field scattered from

the test antenna. Therefore, at P the total field referred to O_2 is

$$\underline{E}(\rho_2,\theta_2,\phi_2) = \sum_{mn} [a'_{mn}\underline{m}^{(3)}_{mn}(\rho_2,\theta_2,\phi_2) + b'_{mn}\underline{n}^{(3)}_{mn}(\rho_2,\theta_2,\phi_2)$$

$$+ a''_{mn}\underline{m}^{(4)}_{mn}(\rho_2,\theta_2,\phi_2) + b''_{mn}\underline{n}^{(4)}_{mn}(\rho_2,\theta_2,\phi_2)] \qquad (3.14)$$

and

$$\underline{H}(\rho_2,\theta_2,\phi_2) = \frac{jk}{\omega\mu}\sum_{mn} [a'_{mn}\underline{n}^{(3)}_{mn}(\rho_2,\theta_2,\phi_2) + b'_{mn}\underline{m}^{(3)}_{mn}(\rho_2,\theta_2,\phi_2)$$

$$+ a''_{mn}\underline{n}^{(4)}_{mn}(\rho_2,\theta_2,\phi_2) + b''_{mn}\underline{m}^{(4)}_{mn}(\rho_2,\theta_2,\phi_2)] \qquad (3.15)$$

where the superscripts (3) and (4) indicate spherical Hankel functions of the first and second kinds, respectively. The modal amplitudes a'_{mn} and b'_{mn} represent the strengths of the incoming modes, and in the scattering matrix notation of Section 3.2, they form the elements of the column matrix $\underset{\sim}{a}'_\beta$. Similarly, the modal amplitudes a''_{mn} and b''_{mn} correspond to the outgoing modes and constitute the column matrix $\underset{\sim}{b}'_\beta$. (Note that the primes are included to distinguish the modal amplitudes in (3.14) and (3.15) from those used previously). Provided that mutual coupling effects between the monopole and the test antenna are negligible, then

$$\underset{\sim}{a}'_\beta = \underset{\sim}{a}_\beta. \qquad (3.16)$$

From (3.3) and (3.16), since the antenna is passive the incoming and outgoing modes in (3.14) and (3.15) are related by

$$\underset{\sim}{b}^{\prime}_{\beta} = \underset{\sim}{S}_{\beta\beta}\underset{\sim}{a}_{\beta}. \qquad (3.17)$$

The field scattered by the antenna, $\underset{\sim}{f}_{\beta}$, is defined as the difference in $\underset{\sim}{b}_{\beta}$ with and without the antenna present. Thus,

$$\underset{\sim}{f}_{\beta} = \underset{\sim}{b}_{\beta} - \underset{\sim}{b}^{\prime}_{\beta} = \underset{\sim}{a}_{\beta} - \underset{\sim}{b}^{\prime}_{\beta} \qquad (3.18)$$

using (3.13). From (3.17) and (3.18) the field scattered by the antenna is related to the incident field by

$$\underset{\sim}{f}_{\beta} = (\underset{\sim}{I}_{\beta\beta} - \underset{\sim}{S}_{\beta\beta})\underset{\sim}{a}_{\beta} \qquad (3.19)$$

where $\underset{\sim}{I}_{\beta\beta}$ is the infinite dimensional identity matrix.

The modal amplitudes in (3.14) and (3.15) corresponding to $\underset{\sim}{a}^{\prime}_{\beta}$ are given by the elements of $\underset{\sim}{a}_{\beta}$ determined by applying the N.F.T. to a set of field measurements performed without the test antenna present. With the antenna located at O_2, introducing the field sampling probe at P, performing the necessary set of electric or magnetic field measurements, and following the same computational procedure, permits the evaluation of the remaining modal amplitudes in (3.14) and (3.15). These amplitudes correspond to the elements of $\underset{\sim}{b}^{\prime}_{\beta}$, so that from a set of equations similar to (3.17) or (3.19) the elements of $\underset{\sim}{S}_{\beta\beta}$ can be computed.

3.33 Determination of the $\underset{\sim}{S}_{\beta\beta}$ submatrix.

To describe exactly the scattering properties of the antenna the $\underset{\sim}{S}_{\beta\beta}$ submatrix must be of infinite order. For many practical antennas, especially if characterised by the wide beam radiation patterns, the contributions to the radiation field from the lower order vector modes in the field representation are much stronger than those from the higher order modes (see Section 2.4). Consequently, the scattering properties of the antenna are adequately described by a consideration of the lower order modes only. The truncation of $\underset{\sim}{S}_{\beta\beta}$ to an N x N matrix, so that the scattering description is limited to N incident modes and their intermode couplings, permits an approximate representation of the scattering effects, with the accuracy being governed by the choice of N.

Because of the symmetry of the full scattering matrix of a lossless reciprocal antenna[82], the N order $\underset{\sim}{S}_{\beta\beta}$ submatrix has N(N+1)/2 unknown complex elements. These elements are determined from the numerical solution of a matrix equation derived from (3.17). (Alternatively (3.19) could be used as the basis for solution but would be less direct). Since (3.17) is an N order matrix equation, a set of (N+1)/2 independent matrix equations of similar form is necessary to solve for the unknowns. Thus, (N+1)/2 independent values of the $\underset{\sim}{a}_{\beta}$ and $\underset{\sim}{b}^{0}_{\beta}$ matrices are also required. From (3.11), (3.12), and Appendix III, independent sets of the modal amplitudes associated with the incoming waves are obtained

by varying the relative position of O_1 with respect to O_2. For each independent set of these amplitudes, that is each $\underset{\sim}{a}_\beta$, there corresponds a particular set of the outgoing modal amplitudes $\underset{\sim}{b}'_\beta$. Hence, variation of the calibration monopole coordinates allows as many independent values of both $\underset{\sim}{a}_\beta$ and $\underset{\sim}{b}'_\beta$ as are necessary. In effect, this variation of the geometry is equivalent to the separation of the azimuthal and radial modes incident upon the antenna, in a similar manner to the separation of the radiation modes in the N.F.T. measurement procedure (see Section 2.2). Combining the (N+1)/2 matrix equations similar to (3.17) and rearranging, the elements of $\underset{\sim}{S}_{\beta\beta}$ are given by the solution of the matrix equation

$$[b] = [A][s] \tag{3.20}$$

where [b] is an N(N+1)/2 order column matrix whose elements are the members of the (N+1)/2 values of the N order b'_β matrix, [A] is an N(N+1)/2 order square matrix derived from the (N+1)/2 values of the $\underset{\sim}{a}_\beta$ matrix, and [s] is an N(N+1)/2 order column matrix containing the N(N+1)/2 unknown elements of $\underset{\sim}{S}_{\beta\beta}$. Provided [A] is non-singular (3.20) can be solved numerically for [s]. From (3.8), (3.9), (3.14), and (3.15), in order to maintain the prescribed accuracy of the scattering representation, the amplitudes of the incoming and outgoing waves must be determined in groups of N. If N is even, therefore, (N+2)/2 values of the N order $\underset{\sim}{a}_\beta$ and $\underset{\sim}{b}_\beta$ matrices must be evaluated, so that

$N(N+2)/2$ elements of $\underset{\sim}{S}_{\beta\beta}$ are computed from the solution of (3.20).

By utilizing the N.F.T. the N complex unknowns, contained as the elements of $\underset{\sim}{a}_{\beta}$ and representing the strengths of the incoming modes, are computed from a set of N independent complex field measurements related to (3.9) and (3.10). A complex field measurement is defined as a measurement of both magnitude and phase at a particular field point. Following the same procedure, the N modal amplitudes of the outgoing modes contained in $\underset{\sim}{b}^{\prime}_{\beta}$ are evaluated from (3.14) and (3.15) and a further set of N field measurements, assuming that $\underset{\sim}{a}_{\beta}$ has been determined previously. A considerable reduction in the experimental effort is possible if the modal amplitudes in (3.4) and (3.5) are determined. The elements of $\underset{\sim}{a}_{\beta}$ are computed from (3.11) and (3.12) for each position of the calibration monopole, rather than repeating the set of N field measurements each time. However, the elements of $\underset{\sim}{b}^{\prime}_{\beta}$ must be computed from sets of measurements corresponding to each calibration position. To summarize, the minimum number of field measurements required to enable the elements of the $\underset{\sim}{S}_{\beta\beta}$ submatrix to be determined are

(i)	For N odd	$N(N+3)/2$	
(ii)	For N even	$N(N+4)/2$	(3.21)

3.4 Measurement procedure for mutual coupling estimation.

A knowledge of the full scattering matrix of an antenna enables an estimate to be made of the mutual coupling effects present in an array composed of these antennas. For most antennas this knowledge can be derived only from measurements. However, the determination of the scattering properties of an antenna represented by the $\underset{\sim}{S}_{\beta\beta}$ submatrix, in particular requires a considerable experimental effort, as demonstrated in the preceding section. The measurements correspond to the separation of the effects of each vector mode incident upon the antenna, and its mutual interactions with all the remaining modes. Even if only a moderate number of vector modes are sufficient to describe the scattering properties of the antenna the associated field measurements virtually render the determination of $\underset{\sim}{S}_{\beta\beta}$ by experiment impracticable. The contributions of $\underset{\sim}{S}_{\beta\beta}$ to the mutual coupling effects will be shown to be second or higher order effects, so that it is sometimes possible to compute a meaningful estimate of mutual coupling upon the basis of the remainder of the scattering matrix, namely the $\underset{\sim}{S}_{\alpha\alpha}$, $\underset{\sim}{S}_{\beta\alpha}$, and $\underset{\sim}{S}_{\alpha\beta}$ submatrices.

3.41 Direct path coupling.

Assume a lossless reciprocal antenna whose input, radiation, receiving, and scattering properties are described by (3.3). Further assume that the N input ports of the antenna are matched and decoupled from each other,

that is $\underset{\sim}{S}_{\alpha\alpha} = \underset{\sim}{O}$ where $\underset{\sim}{O}$ is the null matrix. The mutual coupling between this antenna and another antenna having similar characteristics, mounted in an otherwise source free region, can be considered as the reflected waves appearing at the input ports due to the waves incident upon the radiation ports. Thus from (3.3) and referring to Figure 3.3, the coupling signal appearing at the input ports of antenna 1 is

$$\underset{\sim}{b}_{\alpha} = \underset{\sim}{S}_{\alpha\beta}\ \underset{\sim}{a}_{\beta} \tag{3.22}$$

where $\underset{\sim}{a}_{\beta}$ is determined by the coupling effects between the two antennas. A similar expression gives the coupling signal appearing at the input ports of antenna 2. The coupling signal $\underset{\sim}{b}_{\alpha}$ consists of two parts; the direct path radiation from antenna 2, and the energy back-scattered between the two antennas. Hence, considering the wave scattered by antenna 2 ,

$$\underset{\sim}{b}'_{\beta} = \underset{\sim}{S}_{\beta\alpha}\underset{\sim}{a}'_{\alpha} + \underset{\sim}{S}_{\beta\beta}\underset{\sim}{a}'_{\beta} \tag{3.23}$$

the first term represents direct radiation, part of which illuminates antenna 1. Of this incident wave a portion is received by the antenna appearing at the input ports as part of $\underset{\sim}{b}_{\alpha}$, and the remainder is back-scattered, being contained in b_{β} together with a direct radiation term $\underset{\sim}{S}_{\beta\alpha}\ \underset{\sim}{a}_{\alpha}$ from antenna 1. A part of $\underset{\sim}{b}_{\beta}$ illuminates antenna 2 giving rise to $\underset{\sim}{a}'_{\beta}$. Consequently, the second term in (3.23) represents the

scattering by antenna 2 of a portion of the direct radiation from antenna 1, and also further scattering of some of the energy already back-scattered by antenna 1. This back-scattering process described by $\underset{\sim}{S}_{\beta\beta}$ repeats ad infinitum. Therefore, the mutual coupling contributions due to the terms involving $\underset{\sim}{S}_{\beta\beta}$ are second or higher order effects. The primary coupling effects are described by $\underset{\sim}{S}_{\alpha\beta}$ as in (3.22), with $\underset{\sim}{a}_{\beta}$ determined by the radiation characteristics of antenna 2.

By expressing the field of the antenna in terms of spherical vector modes and applying the N.F.T., the radiation pattern is found in terms of these modes, giving $\underset{\sim}{S}_{\beta\alpha}$ directly. Since the antenna is lossless and reciprocal, $\underset{\sim}{S}_{\alpha\beta} = \underset{\sim}{S}^{T}_{\beta\alpha}$, and the receiving pattern is evaluated to the same accuracy as the radiation pattern. Provided the contributions of $\underset{\sim}{S}_{\beta\beta}$ to $\underset{\sim}{a}_{\beta}$ are small, it is possible to make a meaningful estimate of mutual coupling effects upon the basis of this knowledge of $\underset{\sim}{S}_{\alpha\beta}$ alone. A prediction of the behaviour of an individual antenna in an array system follows in a relatively simple manner. Furthermore, a built-in experimental check on the significance of the $\underset{\sim}{S}_{\beta\beta}$ contributions, and hence the accuracy of this method, is provided by comparing the computed impedance of an array element with the measured impedance determined by applying the waveguide simulator technique.

3.42 Field representation.

As an example of the estimation of mutual coupling effects by the application of (3.22) consider an arbitrary antenna mounted above an infinite, perfectly conducting ground plane such that the region exterior to a surface enclosing the antenna is source free. The properties of the antenna are described by (3.3) and the antenna is positioned so that its phase centre is located at O_1 in Figure 3.2. The field of the antenna is represented by a set of spherical vector modes in a similar manner to the field representation of the calibration monopole in Section 3.3. Hence, the electric field at the field point P is

$$\underline{E}(\rho_1,\theta_1,\phi_1) = \sum_{mn} [a_{mn}\underline{m}_{mn}(\rho_1,\theta_1,\phi_1) + b_{mn}\underline{n}_{mn}(\rho_1,\theta_1,\phi_1)] \qquad (3.24)$$

A corresponding expression represents the magnetic field at P, but, for the present case, it is sufficient to consider the electric field alone. Since the field is entirely outgoing with respect to O_1 the radial functions included in the vector modes are of the form $h_n^{(2)}(k\rho_1)$. The modal amplitudes a_{mn} and b_{mn} are determined by applying the N.F.T. The field radiated by the antenna forms a space wave, part of which irradiates any other antennas within the same region. In particular a second antenna is to be

positioned at O_2. To determine the wave that will be incident upon this second antenna the field at P which in (3.24) is solely outgoing with respect to O_1, must be referred to O_2 in the form of both incoming and outgoing modes. This translation of the field reference is achieved by applying the addition theorems for spherical vector modes[84,85]. Changing the modal indices in (3.24) from m and n to μ and ν, respectively, and applying the appropriate addition theorems, the electric field at P referred to O_2 is

$$\underline{E}(\rho_2,\theta_2,\phi_2) = \sum_{\mu\nu}\sum_{mn} a_{\mu\nu}[A_{mn}^{\mu\nu}\,\underline{m}_{mn}(\rho_2,\theta_2,\phi_2) + B_{mn}^{\mu\nu}\,\underline{n}_{mn}(\rho_2,\theta_2,\phi_2)] + b_{\mu\nu}[A_{mn}^{\mu\nu}\,\underline{n}_{mn}(\rho_2,\theta_2,\phi_2) + B_{mn}^{\mu\nu}\,\underline{m}_{mn}(\rho_2,\theta_2,\phi_2)] \tag{3.25}$$

The coefficients $A_{mn}^{\mu\nu}$ and $B_{mn}^{\mu\nu}$, whose forms are given in Appendix III, are dependent upon the coordinates of O_2, (ρ_o,θ_o,ϕ_o), with respect to O_1, and must be computed for each position of O_2. The radial functions incorporated into (3.25) are generally different from those in (3.24), being determined by the relationship between ρ_2 and ρ_o. As for the field representations of the calibration monopole (3.6) and (3.7), the radial functions included for $\rho_2 < \rho_o$ are of the form $j_n(k\rho_2)$ to satisfy the condition that the fields be finite at $\rho_2 = 0$. For $\rho_2 \geq \rho_o$ the radial functions are of the form $h_n^{(2)}(k\rho_2)$.

Once again it is convenient to express the electric field at P directly in terms of the spherical modes referred to O_2 as in (3.8). The radial functions, chosen to satisfy the field condition at the origin, are of the form $j_n(k\rho_2)$, and subsequent to (3.10) the modal amplitudes in this representation and in (3.25) are interpreted as representing the strengths of the incoming and outgoing modes with respect to O_2. Comparing (3.8) with (3.25) the modal amplitudes in the former representation (which is considered as representing the field of the arbitrary antenna) are identified as

$$a_{mn} = \sum_{\mu\nu} [a_{\mu\nu} A_{mn}^{\mu\nu} + b_{\mu\nu} B_{mn}^{\mu\nu}] \qquad (3.26)$$

$$b_{mn} = \sum_{\mu\nu} [a_{\mu\nu} B_{mn}^{\mu\nu} + b_{\mu\nu} A_{mn}^{\mu\nu}] \qquad (3.27)$$

As before, the a_{mn} and b_{mn} are combined to form the elements of the $\underset{\sim}{a}_{\alpha}$ and $\underset{\sim}{b}_{\beta}$ matrices which also satisfy (3.13).

3.43 Mutual impedance of arbitrary antennas.

A second antenna with identical electrical properties as antenna 1 at O_1 is introduced into the region and positioned at O_2. Assume that this antenna is passive with each input port terminated in its match impedance. The signals appearing at the input ports, which are independent of each other, are due to mutual coupling with the radiating antenna 1. These signals are given by

$$\underset{\sim}{b}'_{\alpha} = \underset{\sim}{S}_{\alpha\beta}\ \underset{\sim}{a}'_{\beta} \qquad (3.28)$$

where the prime denotes the waves associated with antenna 2 at O_2, and $\underset{\sim}{a}'_{\beta}$ is determined from the expression for the field at P. With antenna 2 present, the electric field at P referred to O_2 must be represented as incoming and outgoing modes as in (3.14). As in the previous example of the calibration monopole, the modal amplitudes of the TE and TM spherical modes corresponding to incoming waves are grouped together to form the elements of $\underset{\sim}{a}'_{\beta}$, whereas the amplitudes corresponding to the outgoing waves constitute the matrix $\underset{\sim}{b}'_{\beta}$. If the secondary coupling effects associated with the waves back-scattered by the antennas are small, that is $\underset{\sim}{S}_{\beta\beta}$ is assumed to be small, then from (3.3) $\underset{\sim}{b}'_{\beta}$ is small since the antenna is passive. Therefore, the waves irradiating antenna 2 are approximately the same as the waves incident upon O_2 without the antenna present, i.e.

$$\underset{\sim}{a}'_{\beta} \approx \underset{\sim}{a}_{\beta} \qquad (3.29)$$

The signals appearing at the input ports of the antenna 2, from (3.28) and (3.29), are $\underset{\sim}{S}_{\alpha\beta}\ \underset{\sim}{a}_{\beta}$, which then represent the effects of mutual coupling between the two antennas.

The mutual coupling effects can also be expressed in terms of the open circuit impedance matrix associated with the N-port network representation of the particular array. The

elements of this matrix for an array of identical antennas are defined by

$$Z_{nm} = \left.\frac{V_n}{I_m}\right|_{I_n = 0,\ n \neq m} = Z_{mn} \qquad (3.30)$$

where V_n is the voltage at the n^{th} array input port and I_m is the current at the m^{th} port. Assuming that each of the two antennas considered above has a single input port, and noting the relations between the incident and reflected waves at the input ports and the port voltages and currents[67], from (3.30), the mutual impedance of antenna 2 is

$$Z_{21} = \left.\frac{V_2}{I_1}\right|_{I_2 = 0} = \frac{2b_2}{a_1 - b_1} = 2b_2 \qquad (3.31)$$

where b_2 is the complex amplitude of the reflected wave at the port of antenna 2 when open circuited, a_1 is the strength of the input wave to antenna 1 and is normalized to unity, and b_1, the reflected wave at the input port of antenna 1, is zero since the antenna is matched. With antenna 2 open circuited the incident and reflected waves at the input ports are equal. From (3.3) the reflected waves at the radiation ports are consequently,

$$\underset{\sim}{b}'_\beta = \underset{\sim}{S}_{\beta\alpha}\ \underset{\sim}{a}'_\alpha = \underset{\sim}{S}_{\beta\alpha}\ \underset{\sim}{S}_{\alpha\beta}\ \underset{\sim}{a}'_\beta \qquad (3.32)$$

assuming that $\underset{\sim}{S}_{\beta\beta}$ is zero. Applying (3.3) to the lossless condition on the scattering matrix (3.2) and substituting

the null matrix for $\underset{\sim}{S}_{\beta\beta}$ yields

$$\underset{\sim}{S}_{\beta\alpha}\ \underset{\sim}{S}_{\alpha\beta} = \underset{\sim}{I}_{\beta\beta} \qquad (3.33)$$

since the antenna is reciprocal. Combining (3.33) with (3.32) implies that on open circuit antenna 2 re-radiates the incident wave in the same manner as occurs in the absence of the antenna. This means that the antenna with all its input ports open circuited is invisible, in the sense that it behaves as a point in space. Consequently, the assumption that $\underset{\sim}{S}_{\beta\beta}$ is zero is equivalent to a special case of the minimum scattering condition. The waves irradiating antenna 2 are the same as those incident upon O_2, as in (3.29), so that b_2 is given by $\underset{\sim}{S}_{\alpha\beta}\ \underset{\sim}{a}_{\beta}$.

The open circuit mutual impedance of antenna 1, Z_{12} is found in a similar manner with antenna 2 excited. By symmetry, with antenna 2 identically excited to antenna 1, when determining Z_{21}, $Z_{12} = Z_{21}$. Further, from the definitions of the input port waves, voltages, and currents the open circuit input impedance or self impedances are $Z_{11} = Z_{22} = 1$.

3.5 Conclusion.

Although the complete description of mutual coupling in an array requires a knowledge of the full scattering matrix of each individual antenna, for many practical antennas these scattering matrices are likely to be known

only in part. The submatrices describing the input, radiation, and receiving properties of an antenna can be evaluated in relatively simple fashion, but it has been shown that the experimental determination of the submatrix describing the scattering properties is difficult or at best tedious. However, an estimate of mutual coupling that accounts for first order effects is possible when only the input and radiation characteristics are known. (The receiving pattern is determined from the radiation pattern by reciprocity). This estimate which is based on the complete knowledge of the scattering matrix, with the exception that the $\underset{\sim}{S}_{\beta\beta}$ submatrix describing the scattering properties of the antenna is assumed to be zero, and the application of the addition theorems for spherical vector modes, has been formulated to determine the signals appearing at the input ports of a second identical antenna, due to direct path coupling. For a larger array of similar antennas, the direct path coupling is evaluated by summation of the coupling signals at the ports of one antenna corresponding to the radiation from the remaining members of the array.

The validity of the assumption that the performance of an antenna in an array is predicted meaningfully by considering only the first order mutual coupling effects,

can be verified experimentally by applying simulator techniques. A simple two element array is simulated by introducing a large plane reflector alongside the test antenna. By image theory the antenna-image pair constitutes a simple two element array. Provided the input ports of the driven element are matched, implying that the image element is also matched, the direct path coupling signals are given by following the procedure described in Section 3.4. This estimate of mutual coupling effects may be compared with the actual values measured on the text antenna, and the difference between the two indicates the significance of the contributions due to the scattering characteristics of the antenna. An advantage of this simulator is that it enables a study to be made of the effects on mutual coupling of varying the inter-element spacing. In a similar manner, the conditions of element excitation and array geometry corresponding to certain scan angles of an infinite array can be simulated using the waveguide simulator techniques[53,54]. However, for each array configuration the array performance can be predicted in only a limited number of scan angles by using either of the suggested simulator methods, where the procedure described in Section 3.43 can be used to predict array behaviour over all scan angles, in those applications where the $S_{\beta\beta}$ contributions are small.

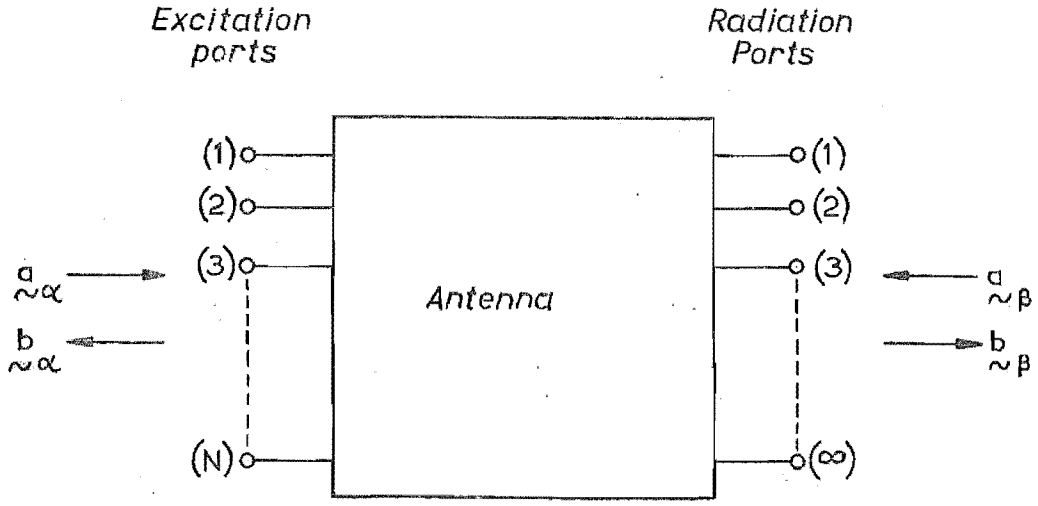

FIGURE 3·1 : NETWORK REPRESENTATION OF ANTENNA

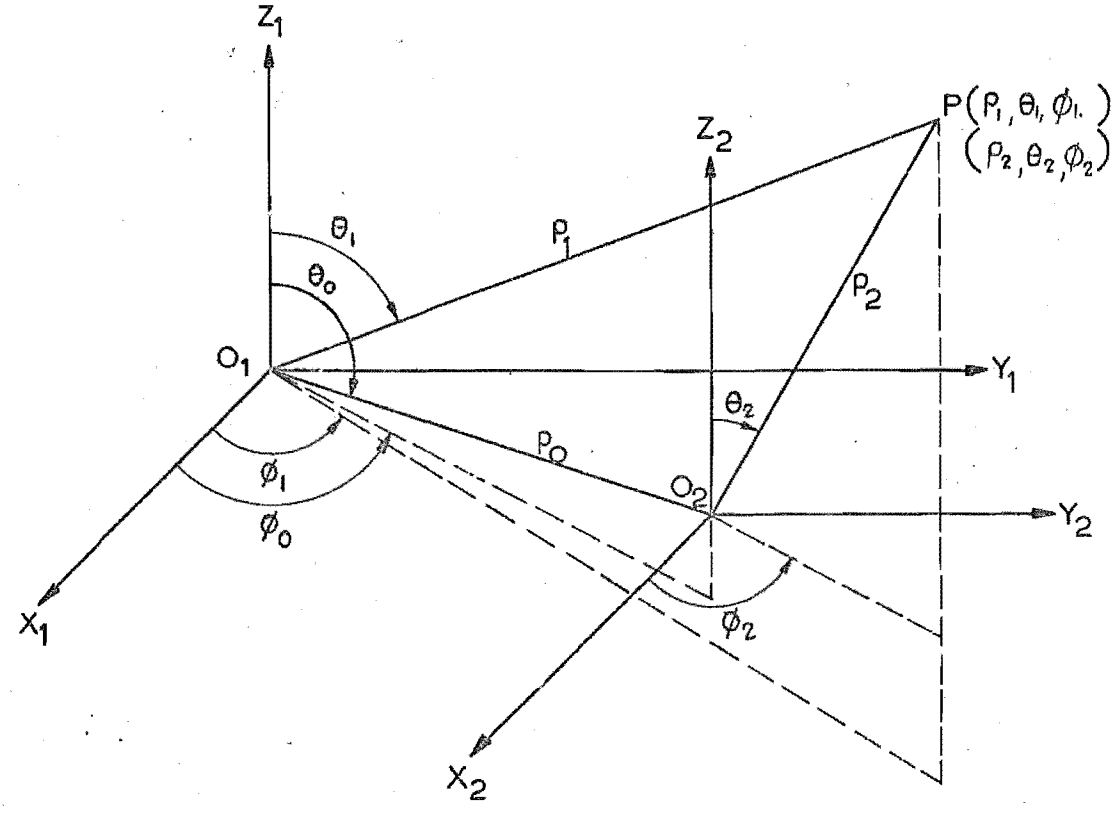

FIGURE 3·2 : COORDINATE SYSTEM FOR TWO ARBITRARY ANTENNAS

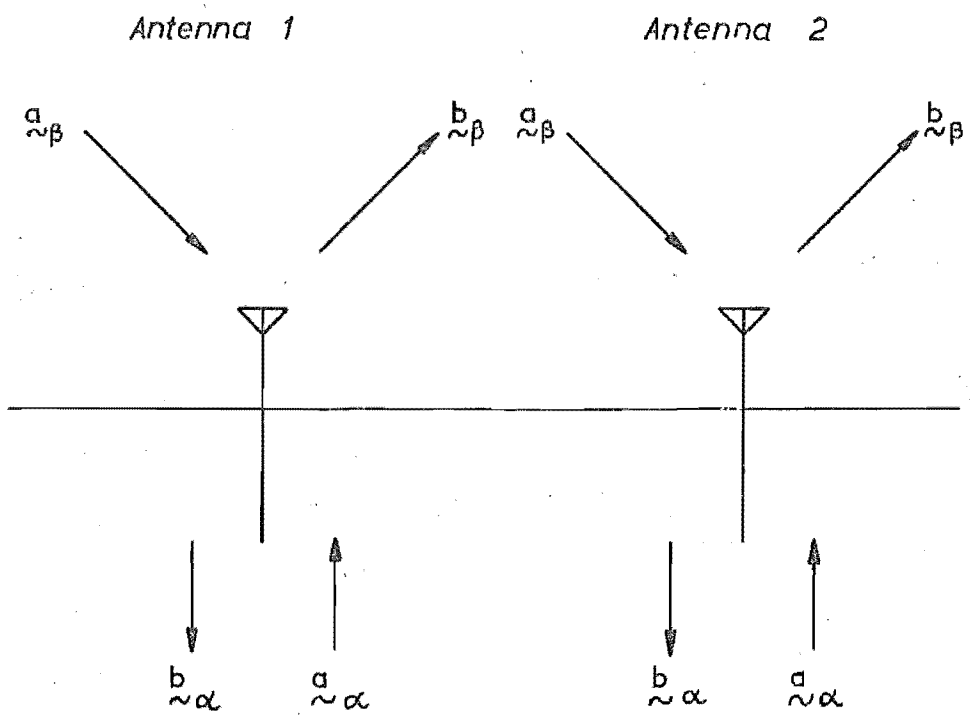

FIGURE 3·3 : INPUT AND RADIATION PORT WAVES

Chapter 4 : The Experimental and Computational Determination of the Performance of a Circular Waveguide Antenna

4.1 Introduction

The application to a practical antenna of the techniques presented in Chapters 2 and 3 is illustrated with a combined theoretical and experimental investigation of a circular waveguide, aperture antenna flush mounted in an infinite, perfectly conducting, ground plane. The aperture diameter is assumed to be less than a wavelength to ensure that the antenna radiates over a wide range of angles, since the presented techniques, although formulated in terms of arbitrary three-dimensional antennas, were shown in Chapters 2 and 3, to be more suitable for determining the characteristics of wide beam antennas. The necessary field measurements were performed at L-band on a circular waveguide antenna with an aperture diameter of two-thirds of a wavelength, flush mounted in a twelve wavelengths square ground plane.

Several authors have determined the exact solution to the problem of the semi-infinite circular waveguide antenna radiating into free space by applying the Wiener-Hopf technique[86-88]. However, almost all other theoretical studies, especially of antennas mounted in ground planes for which the Wiener Hopf technique cannot be applied, have relied

upon the variational technique of Levine and Schwinger[89] to estimate aperture admittances[90-92] and the aperture field method of Silver[93] to determine the radiation fields[94,95]. In both of these methods the accuracy of the solution is dependent upon the accuracy of the aperture field representation. Because of the great theoretical and experimental difficulties involved in obtaining definitive knowledge of the complete aperture field, it has usually been assumed that it can be approximated adequately by the field of the dominant waveguide mode alone. A consideration of the edge conditions at the aperture rim[96] shows this assumption to be in error, since an infinity of higher order modes in addition to the dominant mode must be present to satisfy Maxwell's equations at the discontinuity. This has been emphasised by Cole et. al.[97] who have shown the variational formulation to be unstable for relatively moderate perturbations in the assumed aperture field. Furthermore, the neglect of the higher order modes, which is inherent in the aperture field method, results in the predicted radiation patterns being accurate only over angles close to the direction of maximum radiation.

A more accurate estimation of the aperture field, by direct probing is difficult to achieve without the physical discontinuity of the sampling probe disrupting the actual field. The necessarily finite sized probe acts as a scattering body so that the perturbed field rather than

actual field is measured. However, the actual field can be sampled in the near-field region with a minimum of disturbance by a small measuring probe penetrating the ground plane (see Section 2.4). Applying the near-field technique (N.F.T. of Chapter 2) to a set of these measurements permits the far-field radiation pattern to be inferred and provides an estimate of the aperture field, indicating which higher order modes excited at the aperture rim have significant radiation effects. A first order estimate of mutual coupling effects is also possible by following the scattering matrix procedure outlined in Chapter 3.

The N.F.T. and the scattering matrix coupling technique are formulated for the circular waveguide antenna, and a variational expression for the aperture admittance of the antenna is developed. The aperture field obtained from the N.F.T. is substituted into this variational expression, which is compared with the aperture admittance obtained by direct measurement, thereby contriving an experimental verification of the N.F.T. The results of the various experiments, and the associated computations, are presented in Section 4.5.

4.2 Near-field formulation

The far-field radiation pattern of the circular waveguide aperture is derived by applying the N.F.T. which was developed in Chapter 2. Two series representations of the aperture field of the antenna will be considered: one in terms of circular waveguide modes of propagation and the other in terms of spherical vector modes.

4.21 Waveguide mode aperture field representation

Consider an open-ended circular waveguide flush mounted in an infinite perfectly conducting ground plane as shown in Figure 4.1. The antenna is excited in the basic TE_{11} mode which is incident upon the aperture plane from the negative $\hat{z}$ direction, and the waveguide is dimensioned so that all other modes are evanescent. To satisfy the boundary conditions in the aperture region, in addition to the incident and reflected dominant mode, a denumerable infinity of higher order TE and TM modes are excited at the discontinuity. These modes are both reflected back into the internal waveguide section of the antenna and transmitted across the aperture plane into space. Provided the waveguide has perfectly conducting walls and is regular in shape, the higher order modes have the same azimuthal orientation as the dominant mode, due to the symmetry of the aperture. Extending this symmetry argument, it can be shown that the azimuthal variations of the excited modes are the same as that of the incident mode. (This result

follows in a more rigorous manner from the matching of modal field components across the aperture plane.) Consequently, the modes present in the aperture are the general TE_{1n} and TM_{1n} modes. From Section 2.2 and noting the field expressions for these modes[98], the tangential components of the aperture electric field can be represented as in (2.5) with

$$\hat{z} \times \underline{E}_{TE_n}(r,\psi) = \hat{r} \sin\psi \frac{J_1(h_n' r)}{r} + \hat{\psi} h_n' \cos\psi J_1'(h_n' r) \quad (4.1)$$

and

$$\hat{z} \times \underline{E}_{TM_n}(r,\psi) = \hat{r} h_n \sin\psi J_1'(h_n r) + \hat{\psi} \cos\psi \frac{J_1(h_n r)}{r} \quad (4.2)$$

where

$$J_\nu'(x) = \frac{\partial}{\partial x} J_\nu(x) , \quad (4.3)$$

(r,ψ) are cylindrical coordinates in the aperture, $\hat{r}$ and $\hat{\psi}$ are unit vectors, and $J_1(x)$ is the first order Bessel function of the first kind. The boundary conditions for the TE and TM modes, respectively, reduce to the equations

$$J_1'(h_n' a) = 0, \qquad J_1(h_n a) = 0 \quad (4.4)$$

whose n^{th} roots are h_n' and h_n, with a being the radius of the waveguide.

Following the procedure outlined in Section 2.2, (4.1) and (4.2) are substituted into (2.5) and transformed into rectangular components, from which the rectangular components of the electric vector potential $\underline{F}$ are found as in (2.6) and (2.7). The region of integration for the vector

potential is restricted to the aperture of the antenna, since the equivalent magnetic sources in the aperture plane external to the aperture itself are zero. The spherical components of the radiated fields are determined via (2.8) and (2.9) from the spherical components of $\underline{F}$. By using (2.10) and applying the addition theorem for Legendre polynomials, the azimuthal integration over ψ is performed, but the radial integration over r must be performed numerically. Imposing the appropriate boundary conditions corresponding to the various field components, the non-vanishing components on the ground plane are:

$$E_\theta(\rho,\phi) = \sin\phi \sum_{\ell=1}^{\infty} c_{2\ell}\, h^{(2)}_{2\ell-1}(k\rho), \tag{4.4}$$

where

$$c_{2\ell} = 2\ell\, a_{2\ell}x_{2\ell}+(2\ell+2)b_{2\ell}y_{2\ell}-(2\ell-1)a_{2\ell-2}x_{2\ell-2}-(2\ell-3) \times b_{2\ell-2}y_{2\ell-2},$$

$$a_{2\ell} = \int_0^a j_{2\ell}(kr) \sum_{n=1}^{N} \{A_n h'_n J_0(h'_n r) + B_n h_n J_0(h_n r)\}\, rdr,$$

$$b_{2\ell} = \int_0^a j_{2\ell}(kr) \sum_{n=1}^{N} \{A_n h'_n J_2(h'_n r) - B_n h_n J_2(h_n r)\}\, rdr, \tag{4.5}$$

$$x_{2\ell} = (P_{2\ell}(0))^2$$

and

$$y_{2\ell} = \frac{(2\ell-2)!}{(2\ell+2)!}\,(P^2_{2\ell}(0))^2;$$

$$H_\phi(\rho,\phi) = \frac{jk\sin\phi}{\omega\mu} \sum_{\ell=0}^{\infty} \{a_{2\ell}U_{2\ell}(k\rho) + b_{2\ell}V_{2\ell}(k\rho)\}, \tag{4.6}$$

where

$$U_{2\ell}(k\rho) = x_{2\ell}\left[h^{(2)}_{2\ell-1}(k\rho)\left(k\rho + \frac{2\ell+1}{k\rho}\right) + h^{(2)}_{2\ell+1}(k\rho)\left(k\rho - \frac{2\ell}{k\rho}\right)\right],$$

$$V_{2\ell}(k\rho) = y_{2\ell}\left[h^{(2)}_{2\ell-1}(k\rho)\left(k\rho - \frac{2\ell+3}{k\rho}\right) + h^{(2)}_{2\ell+1}(k\rho)\left(k\rho + \frac{2\ell-2}{k\rho}\right)\right]; \qquad (4.7)$$

and

$$H_\rho(\rho,\phi) = \frac{jk\cos\phi}{\omega\mu}\left\{ja_0 h^{(2)}_1(k\rho) + \sum_{\ell=0}^{\infty} d_{2\ell} h^{(2)}_{2\ell}(k\rho)\right\}, \qquad (4.8)$$

where

$$d_{2\ell} = \frac{2\ell}{4\ell-1}\left[(2\ell-2)a_{2\ell-2}x_{2\ell-2} - (2\ell-4)b_{2\ell-2}y_{2\ell-2}\right] + a_{2\ell}x_{2\ell}\left[4\ell+1 - \frac{8\ell(2\ell+1)(2\ell-1)}{(4\ell-1)(4\ell+3)}\right] + b_{2\ell}y_{2\ell}\left[-(4\ell+1) + \frac{2\ell(2\ell+3)}{4\ell-1} + \frac{(2\ell+1)(2\ell-2)}{4\ell+3}\right] + \frac{2\ell+1}{4\ell+3}\left[(2\ell+3)a_{2\ell+2}x_{2\ell+2} - (2\ell+5)b_{2\ell+2}y_{2\ell+2}\right]. \qquad (4.9)$$

By performing sets of near-field measurements on these field components at field points corresponding to various values of the radial coordinate ρ and with constant angular coordinate ϕ, (4.4), (4.6), and (4.8) can be arranged into matrix equations similar to (2.4), and hence solved numerically for the unknown modal coefficients. From (4.6) and (4.7) it would appear as if measurements of H_ϕ alone are sufficient to infer the radiation pattern. But the square

matrix, containing the functions $U_{2\ell}(k\rho)$ and $V_{2\ell}(k\rho)$ as elements, is numerically ill-conditioned even for relatively small matrix orders, since these functions are so similar in form. Consequently, the numerical solution of the matrix equation derived directly from (4.6) can not be relied upon as being accurate. The $a_{2\ell}$ and $b_{2\ell}$ coefficients are determined by performing measurements on two field components. For example, measurements of the E_θ and H_ρ components and the subsequent computation yield solutions for the $c_{2\ell}$ and $d_{2\ell}$ coefficients, which, being independent functions of $a_{2\ell}$ and $b_{2\ell}$, are solved simultaneously for the required coefficients. The total far-field radiation pattern can be inferred immediately since the $a_{2\ell}$ and $b_{2\ell}$ completely specify the fields radiated by the antenna.

4.22 Vector mode field representation

As before, consider the open-ended circular waveguide antenna shown in Figure 4.1. Completely enclose the antenna with a hemispherical surface, S, bounded by the ground plane, and let the spherical coordinates of a field point, P, lying on S be (ρ,θ,ϕ). Then the vector fields at P are given by (2.2) and (2.3) in terms of spherical-vector modes. Invoking symmetry arguments once again, the azimuthal dependence of the radiated field is the same as that of the dominant mode. Thus,

$$E_\phi \propto \cos\phi,$$
$$\text{and} \quad E_\theta \propto E_\rho \propto \sin\phi. \tag{4.10}$$

Together with the forms of the TE and TM vector modes given in Appendix I, (4.10) implies both that m = 1 in (2.2) and that the TE and TM modes are even and odd functions of ϕ respectively. On the ground plane the boundary conditions require tangential electric field components to be zero. Hence, even index TE modal coefficients and odd index TM modal coefficients are zero for the electric field representation. Similarly, applying the boundary conditions on the ground plane to the magnetic field components, and noting that by the symmetry of the aperture

$$H_\phi \propto \sin\phi,$$
$$\text{and} \quad H_\theta \propto H_\rho \propto \cos\phi, \tag{4.11}$$

the complete representations for the fields radiated by the antenna are

$$\underline{E}_n(\rho,\theta,\phi) = \sum_n^N \left[a_{2n-1}\underline{m}_{e,2n-1}(\rho,\theta,\phi) + b_{2n}\underline{n}_{o,2n}(\rho,\theta,\phi)\right], \tag{4.12}$$

and

$$\underline{H}_n(\rho,\theta,\phi) = \frac{jk}{\omega\mu}\sum_n^N \left[a_{2n-1}\underline{n}_{e,2n-1}(\rho,\theta,\phi) + b_{2n}\underline{m}_{o,2n}(\rho,\theta,\phi)\right], \tag{4.13}$$

where the subscripts e and o denote even and odd functions of ϕ, respectively.

Since the azimuthal variations of the fields are known the near-field measurements are performed on the ground plane along curves of constant ϕ. As discussed in Section 2.2, two field components must be sampled in order to separate the effects of TE and TM modes of similar mode index. From (4.12) and (4.13) it is apparent that of the non-vanishing components on the ground plane, it is most convenient to measure the two tangential magnetic field components. The measurements of H_ρ and H_ϕ are performed along the coordinates $\phi=0$ and $\phi=\pi/2$, respectively. The solution of the matrix equation derived from the set of H_ρ measurements yields the subset of a_{2n-1} modal amplitudes directly, as this component is dependent upon the TM modes only. The representation of the H_ϕ component, however, depends upon both types of modes and must be rearranged into the form

$$H_\phi = \frac{jk \sin\phi}{\omega\mu} \{-a_1 \frac{2}{3} h_0^{(2)}(k\rho) + \sum_n^N c_{2n} h_{2n}^{(2)}(k\rho)\}, \quad (4.14)$$

where

$$c_{2n} = -\frac{2n+2}{4n+3} \frac{P_{2n+1}^1(\cos\theta)}{\sin\theta} \cdot a_{2n+1} + \frac{2n-1}{4n-1} \frac{P_{2n-1}^1(\cos\theta)}{\sin\theta} \cdot a_{2n-1}$$

$$- \tfrac{1}{2}[2n(2n+1)P_{2n}(\cos\theta) - P_{2n}^2(\cos\theta)] \cdot b_{2n}, \quad (4.15)$$

and $P_n^m(\cos\theta)$ is the m^{th} order associated Legendre function of the n^{th} degree. Thus, the computation based on the set of H_ϕ measurements defines the subset of combined coefficients c_{2n}, which in conjunction with the a_{2n-1}

subset is used to compute the unknown b_{2n} modal amplitudes from (4.15).

4.23 Aperture field distribution

To evaluate the impedance properties of the circular waveguide antenna from its aperture admittance (see Section 4.3) it is convenient to express the aperture field distribution in terms of the dominant and higher order waveguide modes present in the aperture. The aperture field and the far-field radiation pattern, or the field pattern over any surface completely enclosing the antenna, form a Fourier transform pair. However, computing the Fourier transform of the far- field pattern as derived from the N.F.T. determines the aperture field distribution in terms of the equivalent current line sources in the aperture which are not simply related to the vector fields of the individual waveguide modes. The strengths of these aperture modes can be estimated by following the alternative procedure outlined in Section 2.3. From (4.5) the unknown amplitudes of the waveguide modes are related to the $a_{2\ell}$ and $b_{2\ell}$ coefficients by two matrix equations similar to (2.13). These are either solved directly or partitioned into the forms

$$[a] = [G_a][A] + [G_b][B], \tag{4.16}$$

and

$$[b] = [F_a][A] - [F_b][B], \tag{4.17}$$

where the column matrices $[a]$, $[b]$, $[A]$, and $[B]$ contain as elements the $a_{2\ell}$, $b_{2\ell}$, A_n, and B_n modal coefficients

respectively. The elements of the square matrices $[G_a]$, $[G_b]$, $[F_a]$, and $[F_b]$ are the integrations over the aperture of the products of the spherical and cylindrical Bessel functions in (4.5). Provided these matrices are well-conditioned, the amplitudes of the waveguide modes are determined by the numerical solution of (4.16) and (4.17). This solution effectively infers the aperture field distribution from the sets of near-field measurements.

As discussed in Section 2.3, the higher order exterior region modes in (4.4), (4.6), and (4.8) contribute mainly to the reactive energy stored in the near-field, so that their effects become increasingly more significant as the antenna is approached, which implies that the near-field modal representations become less accurate. The accuracy of the aperture field distribution derived from the $a_{2\ell}$ and $b_{2\ell}$ coefficients is limited, therefore, by the order of the higher order modes included in these field representations. The aperture field estimate is improved by increasing the number of modes but the maximum order of the modes considered is governed by the experimental accuracy to which the near-field components are sampled. Thus, this technique provides an estimate of the strengths of only those aperture modes which have significant effects in the exterior region.

4.3 Aperture admittance

A variational expression for the aperture admittance of the circular waveguide antenna forms the basis of the experimental verification of the N.F.T. Miles[90] applied the variational technique to determine the characteristics of a circular waveguide antenna excited by a scalar field, while more recently Mishustin[92] and Samaddar[91] formulated the aperture admittance in terms of vector fields. The method presented here follows the approach of Lewin[99] who studied a similar problem involving a rectangular waveguide antenna.

Consider the antenna as shown in Figure 4.1 and denote the region internal to the waveguide as region 1, and the free-space region (that is, the region defined by $z > 0$) external to the waveguide and bounded by the aperture plane as region 2. The antenna is excited in the TE_{11} mode which is incident on the aperture from the negative $\hat{z}$ direction. The fields in region 1 are represented by a set of waveguide modes, which from the previous section, includes the general TE_{1n} and TM_{1n} modes. Hence, noting the expressions for the field components of these modes[98], the tangential field components in region 1 are

$$E_{\rho 1} = A_1(e^{-j\beta_1 z} + \Gamma e^{j\beta_1 z})\sin\phi \frac{J_1(h_1'\rho)}{\rho}$$

$$+ \sin\phi \sum_{n=1}^{\infty}{}' \left[A_n \frac{J_1(h_n'\rho)}{\rho} e^{\gamma_n z} + B_n h_n J_1'(h_n\rho) e^{\kappa_n z}\right],$$

$$E_{\phi 1} = A_1(e^{-j\beta_1 z} + \Gamma e^{j\beta_1 z})\cos\phi\, h_1' J_1'(h_1'\rho) \tag{4.18}$$

$$+ \cos\phi \sum_{n=1}^{\infty}{}' \left[A_n h_n' J_1'(h_n'\rho) e^{\gamma_n z} + B_n \frac{J_1(h_n\rho)}{\rho} e^{\kappa_n z}\right];$$

$$H_{\rho 1} = -A_1(e^{-j\beta_1 z} - \Gamma e^{j\beta_1 z})\cos\phi \frac{\beta_1}{\omega\mu} h_1' J_1'(h_1'\rho)$$

$$+ j\cos\phi \sum_{n=1}^{\infty}{}' \left[A_n \frac{\gamma_n h_n'}{\omega\mu} J_1'(h_n'\rho) e^{\gamma_n z} - B_n \frac{\omega\varepsilon}{\kappa_n} \frac{J_1(h_n\rho)}{\rho} e^{\kappa_n z}\right],$$

and (4.19)

$$H_{\phi 1} = A_1(e^{-j\beta_1 z} - \Gamma e^{j\beta_1 z})\sin\phi \frac{\beta_1}{\omega\mu} \frac{J_1(h_1'\rho)}{\rho}$$

$$- j\sin\phi \sum_{n=1}^{\infty}{}' \left[A_n \frac{\gamma_n}{\omega\mu} \frac{J_1(h_n'\rho)}{\rho} e^{\gamma_n z} - B_n \frac{\omega\varepsilon}{\kappa_n} h_n J_1'(h_n\rho) e^{\kappa_n z}\right],$$

where Γ is the reflection coefficient for the TE_{11} mode, β_1 is the TE_{11} modal phase constant, and γ_n and κ_n are the propagation constants of the TE_{1n} and TM_{1n} modes, respectively. The prime on the summation sign indicates that the TE_{11} mode has been omitted since it is already included in the first term.

As with the fields in region 1, it is appropriate to express the fields in region 2 in terms of cylindrical components. These components are found by introducing an

electric vector potential $\underline{F}$ as in Section 2.2, transforming $\underline{F}$ into cylindrical components, and applying the cylindrical coordinate forms of the vector operators in (2.8) and (2.9). These expressions show that the tangential field components in region 2 tend to the tangential aperture field components as z tends towards zero; that is,

$$E_{\rho 2}\big|_{z\to 0} \to E_{\rho'} \qquad E_{\phi 2}\big|_{z\to 0} \to E_{\phi'} \tag{4.20}$$

$$H_{\rho 2}\big|_{z\to 0} \to H_{\rho'} \qquad H_{\phi 2}\big|_{z\to 0} \to H_{\phi'} \tag{4.21}$$

where $E_{\rho'}$, $E_{\phi'}$, H_{ρ} and H_{ϕ} are the tangential components of the aperture field.

The tangential field components must be continuous across the aperture so that the two field representations must be identical at the aperture plane. Equating the tangential field components at $z = 0$,

$$E_{\rho} = E_{\rho 1}\big|_{z=0'} \qquad E_{\phi} = E_{\phi 1}\big|_{z=0'} \tag{4.22}$$

$$H_{\rho} = H_{\rho 1}\big|_{z=0'} \qquad H_{\phi} = H_{\phi 1}\big|_{z=0'} \tag{4.23}$$

From these continuity equations the unknown modal amplitudes are determined in terms of the aperture fields by applying the orthogonality conditions on the modes in the aperture region. Hence, by combining (4.22) with (4.18), multiplying the resultant expressions for E_{ρ} by $\sin\phi\, J_1(h'_m\rho)$ and E_{ϕ} by $\rho\cos\phi\, h'_m J'_1(h'_m\rho)$, integrating their sum over the

aperture domain and solving for the modal amplitudes of the TE_{11} and TE_{1n} modes gives

$$A_{11}(1+\Gamma) = C_{h1} I_{h1}, \qquad \text{and} \quad A_n = C_{hn} I_{hn}, \tag{4.24}$$

where $$C_{hn} = \frac{2}{\pi J_1^2(h_n' a)(h_n'^2 a^2 - 1)}$$

and $$I_{hn} = \int_0^{2\pi} \int_0^a [E_\rho \sin\phi \frac{J_1(h_n'\rho)}{\rho} + E_\phi \cos\phi \, h_n' J_1'(h_n'\rho)] \rho d\rho d\phi. \tag{4.25}$$

Similarly, multiplying the E_ρ and E_ϕ components by $\rho \sin\phi \, h_m J_1'(h_m\rho)$ and $\cos\phi \, J_1(h_m\rho)$, respectively, integrating over the aperture, and solving for the modal amplitudes of the TM_{1n} modes gives

$$B_n = C_{en} I_{en}, \tag{4.26}$$

where $$C_{en} = \frac{2}{\pi h_n^2 a^2 J_0^2(h_n a)},$$

and $$I_{en} = \int_0^{2\pi} \int_0^a [E_\rho \sin\phi \, h_n J_1'(h_n\rho) + E_\phi \cos\phi \frac{J_1(h_n\rho)}{\rho}] \rho d\rho d\phi. \tag{4.27}$$

Changing the variables of integration in (4.25) and (4.27) to (r,ψ), and substituting (4.24) and (4.26) into the magnetic field continuity equation (4.23) yields two

simultaneous equations relating the H_ρ and H_ϕ components to the normalized aperture admittance Y, defined by

$$Y = \frac{1-\Gamma}{1+\Gamma} . \tag{4.28}$$

From (4.21) and the coordinate transformation of $\underline{F}$ into cylindrical components, the two magnetic field components in the aperture are

$$H_\rho = L_1 . F_x + L_2 . F_y , \tag{4.29}$$

and

$$H_\phi = L_3 . F_x + L_4 . F_y . \tag{4.30}$$

The L_i are operators defined by

$$\begin{aligned}
L_1 . F_x &= \frac{j}{\omega\mu} \left[\cos\phi \frac{\partial^2}{\partial\rho^2} - \frac{\sin\phi}{\rho} \frac{\partial^2}{\partial\phi\partial\rho} \right. \\
&\quad \left. + \frac{\sin\phi}{\rho^2} \frac{\partial}{\partial\phi} + k^2 \cos\phi \right] . F_x \\
L_2 . F_y &= \frac{j}{\omega\mu} \left[\sin\phi \frac{\partial^2}{\partial\rho^2} + \frac{\cos\phi}{\rho} \frac{\partial^2}{\partial\phi\partial\rho} \right. \\
&\quad \left. - \frac{\cos\phi}{\rho^2} \frac{\partial}{\partial\phi} + k^2 \sin\phi \right] . F_y \\
L_3 . F_x &= \frac{j}{\omega\mu} \left[- \frac{\sin\phi}{\rho} \frac{\partial}{\partial\rho} + \frac{\cos\phi}{\rho} \frac{\partial^2}{\partial\phi\partial\rho} - \frac{\cos\phi}{\rho^2} \frac{\partial}{\partial\phi} \right. \\
&\quad \left. - \frac{\sin\phi}{\rho^2} \frac{\partial^2}{\partial\phi^2} - k^2 \sin\phi \right] . F_x \\
L_4 . F_y &= \frac{j}{\omega\mu} \left[\frac{\cos\phi}{\rho} \frac{\partial}{\partial\rho} + \frac{\sin\phi}{\rho} \frac{\partial^2}{\partial\phi\partial\rho} - \frac{\sin\phi}{\rho^2} \frac{\partial}{\partial\phi} \right. \\
&\quad \left. + \frac{\cos\phi}{\rho^2} \frac{\partial^2}{\partial\phi^2} + k^2 \cos\phi \right] . F_y .
\end{aligned} \tag{4.31}$$

A stationary expression for Y, that is stable for small changes in the assumed aperture field, results from substituting (4.29) and (4.30) into the simultaneous equations derived from (4.23). The H_ρ component equation is multiplied by ρE_ϕ, the H_ϕ component equation is multiplied by $-\rho E_\rho$, and their sum is integrated over the aperture domain. Solving for Y and expressing $\underline{F}$ in terms of the aperture field as in (2.6) and (2.7), the variational expression for Y is

$$Y = \left\{\frac{1}{2\pi}\int_0^{2\pi}\int_0^a\int_0^{2\pi}\int_0^a \left[(E_r\sin\psi + E_\psi\cos\psi)(E_\phi L_1 - E_\rho L_3)\right.\right.$$

$$\left. + (-E_r\cos\psi + E_\psi\sin\psi)(E_\phi L_2 - E_\rho L_4)\right] \frac{e^{-jkR}}{R}\, r\rho\, dr\, d\psi\, d\rho\, d\phi$$

$$\left. + j \sum_{n=1}^{\infty}{}' \left[\frac{\gamma_n}{\omega\mu} C_{hn} I_{hn}^2 - \frac{\omega\varepsilon}{\kappa_n} C_{en} I_{en}^2\right]\right\} \Big/ \frac{\beta_1}{\omega\mu} C_{h1} I_{h1}^2, \tag{4.32}$$

where the L_i are understood to operate on the Green's function, and E_r, E_ψ, E_ρ, E_ϕ are the tangential components of the aperture field. The proof of the stationary nature of (4.32) is given in Appendix IV.

The form of Y in (4.32) is simplified by substituting for the aperture field components. Thus, from Appendix V, equations (V-2) and (V-3), the variational expression reduces to

$$Y = \{y_{num} + j\pi \sum_{n=1}^{\infty}{}' \left[\frac{A_n^2 \gamma_n}{2\omega\mu} J_1^2(h_n' a)(h_n'^2 a^2 - 1) - \frac{B_n^2 \omega\varepsilon}{2\kappa_n} h_n^2 a^2 J_0(h_n a)\right]\} / \frac{A_1^2 \beta_1 \pi}{2\omega\mu} J_1^2(h_1' a)(h_1'^2 a^2 - 1), \quad (4.33)$$

where y_{num} is given by (V-11).

4.4 Mutual coupling study

By applying the simulator techniques discussed in Chapter 3, measurements performed on the circular waveguide antenna can be used to determine the significance of the scattering properties of an antenna when evaluating mutual coupling effects in an array. In particular, a large, perfectly conducting, plane reflector, perpendicular to the ground plane, and placed adjacent to the aperture produces an image antenna identical with the driven antenna except that its excitation is such to produce a field which cancels the electric field tangential to the reflector due to the driven antenna, as shown in Figure 4.3. From the figure, for $\phi' = 0$ the excitation of the image antenna lags that of the driven antenna by π radians, while for $\phi' = \pi/2$ the excitations of both antennas are in phase. The direct path mutual coupling between the antenna-image pair can be estimated by following the procedure outlined in Section 3.4.

Initially, consider the antenna excited in the TE_{11} mode, and radiating into free-space. The total fields of the antenna are derived by applying the spherical vector mode form of the N.F.T. These fields, given by (4.12) and (4.13), are entirely outgoing, so that in the notation of Chapter 3 the modal amplitudes in (4.12) and (4.13) form the elements of the matrix $\underset{\sim}{b}_{\beta}$. The antenna has a single input port corresponding to the excitation of the TE_{11} mode, and since the input signal a_1 to this port is known, or can be measured, the modal radiation pattern $\underset{\sim}{S}_{\beta\alpha}$ is determined from

$$\underset{\sim}{b}_{\beta} = \underset{\sim}{S}_{\beta\alpha}\ \underset{\sim}{a}_{\alpha}, \qquad (4.34)$$

where the matrix $\underset{\sim}{a}_{\alpha}$ has a single element, a_1. Assuming that the antenna is reciprocal, the receiving pattern $\underset{\sim}{S}_{\alpha\beta}$ is given by the transpose of $\underset{\sim}{S}_{\beta\alpha}$. Similarly, considering the image antenna as an isolated radiator for $\phi' = 0$ and $\pi/2$, the input signal is $-a_1$ and $+a_1$ respectively, which implies that the matrix representing the outgoing waves is $-\underset{\sim}{b}_{\beta}$ and $+\underset{\sim}{b}_{\beta}$ respectively, since the radiation and receiving patterns of the image antenna are the same as for the driven antenna. (The -ve sign associated with the matrix indicates that all the matrix elements are shifted in phase by π radians.)

Introduce the plane reflector alongside the antenna and consider the driven antenna to be located at an origin O_2 while the image antenna is at an origin O_1. O_2 has spherical coordinates $(\rho_0, \theta_0, \phi_0)$ with respect to O_1. From Section 3.4, the direct path coupling waves, incident upon the driven antenna, are found by applying the appropriate addition theorems to express the field from the image antenna with respect to O_2. For spherical modes the addition theorems require the field to be expressed in terms of the complex forms of the vector modes rather than the odd and even function forms. Hence, expressing the field representation equivalent to (4.12) for the image antenna in terms of the complex modes given in Appendix I, and in view of (3.26), (3.27) and (3.29), the elements of the matrix $\underset{\sim}{a}^{i}_{\beta}$ representing the incoming waves referred to O_2 for $\phi^i = 0$ are found from

$$a_{mn} = -\tfrac{1}{2} \sum_{\nu} \left[a_{2\nu-1} A^{\mu,2\nu-1}_{mn} - j\sigma_{\mu} b_{2\nu} B^{\mu,2\nu}_{mn} \right], \qquad (4.35)$$

and

$$b_{mn} = -\tfrac{1}{2} \sum_{\nu} \left[a_{2\nu-1} B^{\mu,2\nu-1}_{mn} - j\sigma_{\mu} b_{2\nu} A^{\mu,2\nu}_{mn} \right], \qquad (4.36)$$

for $\mu = +1$ and -1,

and where $\sigma_{\mu} = +1$ when $\mu = +1$ and $\sigma_{\mu} = -1$ when $\mu = -1$. The coefficients $a_{2\nu-1}$ and $b_{2\nu}$ are defined in (4.12) and (4.13). For $\phi^i = \pi/2$, the elements of $\underset{\sim}{a}^{i}_{\beta}$ are found in the same manner except that the sign of (4.35) and (4.36) is positive. The

coupling signal appearing at the input port of the driven antenna is then given by $\underset{\sim}{S}_{\alpha\beta}\underset{\sim}{a}^{i}_{\beta}$.

4.5 Results and discussion

The experimental verifications of the techniques formulated in Chapters 2 and 3 were based upon measurements performed on a circular waveguide antenna with an aperture diameter of two-thirds of a wavelength, flush mounted in a twelve wavelengths square ground plane and operating at a frequency of 2 GH_z. The results obtained from these experimental studies are presented in this section.

4.51 Far-field radiation pattern

The far-field pattern of the antenna was derived by applying the spherical vector mode form of the N.F.T. As demonstrated in Section 4.2 near-field measurements of the H_ρ and H_ϕ field components on the ground plane are sufficient to determine the modal amplitudes in (4.12) and (4.13). Using the shielded magnetic loop probe shown in Figure 2.2, these components were sampled at nine equally spaced field points lying on the $\phi = 0$ and $\phi = \pi/2$ coordinate curves. (In practice, the same field points were used for both curves, since it was simpler to rotate the probe exciting the TE_{11} mode in the waveguide through $\pi/2$ radians.) The detection system shown in schematic form in Figure 4.2, was a standard General Radio heterodyne receiver, with the measurements of phase obtained by

incorporating into the received signal or probe line a variable phase shifter and a reference signal line from the generator. A series of measurements in both magnitude and phase of each component was conducted at each field point, and then repeated with the probe rotated through π radians to minimize sampling errors due to any asymmetry in the loop. These readings were then averaged.

Errors in the field measurements resulted from the perturbation of the true field by the sampling probe (which was discussed at length in Section 2.4), instrument reading errors, and the presence of standing waves on the probe line. The reading accuracy of the square law detector used in the experiment was ± 0.05 dB of the indicated value in dB. Since the field values at each point were obtained as relative measurements, the error for each magnitude measurement was ± 0.1 dB. Assuming the errors to be random the standard deviation at the ninth field point was ± 0.49 dB. For the worst case, that is the H_ϕ measurement, the field magnitude at the ninth field point referred to magnitude at the first point was -9.85 dB, so that the cumulative error represented an error of 5%. In the phase measurements the detector was used solely as a null detector, and consequently the reading error did not contribute significantly to the phase error. The variable phase shifter used in the experiment was a variable length line stretcher, which was adjusted in length until the received signal cancelled with

the reference signal to produce a null on the detector. By measuring the changes in line length with a vernier, the phase could be measured to within $\pm 2^{o}$ between two field points, provided no standing waves existed on the probe line. Hence, over the nine field points the r.m.s. phase error was $\pm 9^{o}$ at the ninth point, corresponding to a phase error of $\pm 3.2\%$ for the H_{ρ} measurements and slightly less for the H_{ϕ} measurements. The standing wave caused by the probe mismatch resulted in the point at which the received and reference signals cancelled being shifted with a subsequent error in the phase measurement. But with the loop probe referred to previously, the VSWR on the probe line was reduced to 1.10:1, so that in practice, the phase errors caused by the probe mismatch were small. To summarize, the cumulative experimental error in the relative field measurements of the H_{ρ} and H_{ϕ} components in both magnitude and phase was estimated at 5% over the nine field points.

Following the procedure given in Section 4.2, the modal amplitudes of the spherical vector mode field representation were computed. In each set of near-field measurements of each field component, the data associated with the nine field points were grouped in nine subsets of eight field points, that is, eight field values chosen in C_{8}^{9} ways. The sets of modal amplitudes computed from these subsets were averaged to reduce the effects of errors in the field measurements. The resultant values for the first fifteen

amplitudes computed from the nine subsets are tabulated in Table 4.1 together with their standard deviations expressed as a percentage of the mean magnitude of each amplitude. The first modal amplitude was normalized to unity. From the table, as the modal order increases the accuracy of the amplitude decreases, as shown by the deteriorating correlation between the different subsets. This is attributable to the convergent form of the field representation, in that the higher order modes contribute less significantly to the radiated field than do the lower order modes. Conversely, because of these smaller contributions a large standard deviation in a higher order amplitude is not significant. The change in the total field due to variations in such an amplitude will be very small, even though the proportional change in the amplitude may be very large. For example, the twelfth amplitude has a standard deviation of 52% but a mean magnitude of 0.6376×10^{-6}, so that the effect on the total field of a 52% variation of this amplitude will be negligible.

The electric field radiation patterns for the E-plane and H-plane, corresponding to the E_θ and E_ϕ components, respectively, were evaluated by substituting the tabulated amplitudes into (4.12) and representing the Hankel functions by their asymptotic forms. These patterns are plotted in Figure 4.4 for various numbers of modes to demonstrate the convergence of the patterns with increasing numbers of modes.

	Magnitude	Phase	% Std. Deviation		Magnitude	Phase	% std. Deviation
a_1	1.0	0^o	0	b_2	0.4239	-165^o	1.3
a_3	0.2237	-142^o	3.7	b_4	0.9326×10^{-1}	67^o	4.0
a_5	0.4683×10^{-1}	106^o	7.8	b_6	0.1412×10^{-1}	31^o	9.1
a_7	0.6096×10^{-2}	30^o	10.5	b_8	0.1139×10^{-2}	-98^o	19.8
a_9	0.3660×10^{-3}	-16^o	15.9	b_{10}	0.4177×10^{-4}	-146^o	37.1
a_{11}	0.8967×10^{-5}	-45^o	28.2	b_{12}	0.6376×10^{-6}	175^o	52.0
a_{13}	0.8379×10^{-7}	-62^o	43.6	b_{14}	0.3786×10^{-8}	139^o	47.6
a_{15}	0.2371×10^{-9}	-73^o	60.5				

Table 4.1: Modal amplitudes of the first fifteen spherical vector modes.

The radiation patterns calculated by the aperture field method, assuming the field of the TE_{11} mode to be the total aperture field, are also plotted for comparison.

A direct check on the computed patterns is not possible since there are no recorded measurements of the far-field patterns of a circular waveguide antenna mounted in a ground plane, with the experiment arranged so that the ground plane edge effects are removed. In the present study, the lack of suitable pattern range facilities in conjunction with the practical difficulties associated with performing far-field measurements on a wide beam antenna mounted above a ground plane (see Section 2.1), prevented these patterns from being measured. However, a comparison can be made with the electrically similar circular horn antenna. King[100] has published measured E-plane and H-plane patterns for a circular horn excited in the TE_{11} mode, with an aperture diameter of 1.4λ and a flare angle of approximately 10^{o}. These patterns, which are also plotted in Figure 4.4, confirm the general form of the computed patterns of the circular waveguide antenna. Although the horn is not flanged, the two antennas are expected to have similar aperture field distributions, because of the small flare angle of the horn and the comparable dimensions of the two apertures. The differences between the two antennas are illustrated, in particular, by the E-plane patterns. The incidence of a side lobe structure and the generally narrower pattern of the horn are a

consequence of the wider aperture, while the higher radiation levels of the horn close to the aperture plane result from the absence of a ground plane.

An alternative check on the analysis, based on the aperture field estimated from the near-field measurements and the variational expression for the aperture admittance, is presented in the following section.

4.52 Aperture field

An estimate of the modal amplitudes of the waveguide modes representing the aperture field distribution of the circular waveguide antenna was obtained by following the procedure discussed in Section 4.2. The solution of (4.16) and (4.17) for these amplitudes requires a knowledge of the $a_{2\ell}$ and $b_{2\ell}$ coefficients which can be found most conveniently from the combined coefficients given by (4.5) and (4.9). These combined coefficients were evaluated from the vector mode amplitudes in Table 4.1 by equating equivalent coefficients in the waveguide mode and the spherical vector mode field representations for the E_θ and H_ρ components. This method was preferred to the direct application of the N.F.T. to the waveguide mode field representation, since it did not require the calibration of the sampling probes. To solve for the $a_{2\ell}$ and $b_{2\ell}$ from (4.5) and (4.9), the coefficients in (4.4) and (4.8) must be correctly normalized with respect to each other. But in applying the N.F.T. the E_θ and H_ρ components must be sampled with different probes,

so that to normalize the two sets of measurements, it is necessary to calibrate the probes. The matrix equations relating the $a_{2\ell}$ and $b_{2\ell}$ coefficients to the waveguide mode amplitudes were solved numerically to give an estimate of the aperture field. The restricted accuracy of this estimate, discussed previously in Section 4.2, was reflected in the numerical evaluation of the elements of the $[G_a]$, $[G_b]$, $[F_a]$, and $[F_b]$ matrices in (4.16) and (4.17). Although these matrices were analytically non-singular, they were sufficiently ill-conditioned numerically to require that the individual matrix elements be evaluated to eight or nine significant figures. This was necessary to ensure that the respective inverse matrices could be computed accurately. Moreover, this method is limited to estimating the strengths of the lower order modes only, since if the matrix sizes are increased to take into account more modes, the matrices become increasingly ill-conditioned. The estimated modal amplitudes of the most significant modes in the aperture are tabulated in Table 4.2. By substituting these modal amplitudes into (4.33) the aperture admittance and consequently the voltage reflection coefficient of the antenna can be computed. Thus, an experimental check on the accuracy of the set of estimated modal amplitudes is provided by comparing the computed value of the reflection coefficient with the corresponding measured value. The measured value was obtained by sampling the voltage standing wave in the antenna

with a small electric field probe. The disturbance of the field inside the antenna due to the probe was determined by measuring the change in the antenna input port match as the probe was inserted. By this method it was found that a probe a thirtieth of a wavelength long produced an effect on the field that was not detectable. The probe was matched and connected to a standard heterodyne detector.

Mode	Modal amplitudes	
	Magnitude	Phase
TE_{11}	1.0	0°
TE_{12}	0.2380	0°
TE_{13}	0.01916	0°
TM_{11}	0.4383	180°
TM_{12}	0.08175	180°

Table 4.2: Normalized amplitudes of the lower order aperture modes.

The measured value of reflection coefficient and the values computed for various numbers of lower order modes are summarized in Table 4.3.

Modes included in (4.33)	Reflection coefficient	
	Magnitude	Phase
Measured	0.416	164°
TE_{11}	0.472	-148°
TE_{11}, TM_{11}	0.614	-148°
$TE_{11}, TE_{12}, TM_{11}$	0.360	141°
$TE_{11}, TE_{12}, TM_{11}, TM_{12}$	0.364	135°

Table 4.3: Measured and calculated values of reflection coefficient.

The tabulated values confirm the limited accuracy of the estimated aperture field, but show that a reasonable estimate of the aperture admittance is possible from a knowledge of the strengths of only the lower order modes. The limited accuracy is further emphasised by comparing the far-field radiation patterns of the antenna shown in Figure 4.4 with the corresponding patterns in Figure 4.5, calculated by the vector potential method from the modal amplitudes in Table 4.2. Although the E-plane patterns in the two figures are of the same form, indicating that the lower order modes are sufficient to describe this pattern,

the H-plane patterns are quite different. Hence, the higher order modes necessarily present at the aperture discontinuity, and especially the higher order TE modes (which alone contribute to the H-plane pattern), are significant in determining the radiation properties of the antenna.

An improved estimate of the antenna reflection coefficient is possible by modifying the modal amplitudes to match the two E-plane patterns. Concentrating on the three modes TE_{11}, TE_{12} and TM_{11}, the new modal amplitudes derived by this pattern matching method are given in Table 4.4.

Mode	Modal amplitudes	
	Magnitude	Phase
TE_{11}	1.0	0°
TE_{12}	0.2925	0°
TM_{11}	0.5875	180°

Table 4.4: Modified modal amplitudes

Substitution of these values into (4.33) gives a computed value for the reflection coefficient as $0.416\angle 139^{\circ}$, which compares extremely favourably with the measured value of $0.416\angle 164^{\circ}$. The radiation patterns corresponding to these modified amplitudes are plotted in Figure 4.5. As may be expected, the pattern matching method does not improve the

estimate of the H-plane pattern, since the effects of the higher order TE modes are not included.

Although the aperture field distribution inferred from the near-field measurements is of limited accuracy, it represents a significant improvement over the commonly used assumption that the dominant TE_{11} mode is an accurate representation of the complete aperture field. The method can be used to estimate the strengths of the lower order aperture modes, and hence the aperture admittance. As the results presented in Table 4.1 and Figure 4.4 show, the radiation pattern can be inferred accurately from the near-field measurements, by applying N.F.T.

4.53 Determination of mutual coupling

The effects of mutual coupling between the circular waveguide antenna and its identical image were studied experimentally by introducing a large plane reflector alongside the antenna, monitoring the input impedance of the driven element, and noting the deterioration of the match as the spacing between the antennas was reduced. In the experiment the reflector was first placed transverse to the E-plane of symmetry at various spacings from the antenna, and then the measurements were repeated with the reflector transverse to the H-plane. To ensure good electrical contact with the ground plane the reflector, which measured eight wavelengths by four wavelengths, was bolted to the ground plane for each position. The effects of coupling on

the match condition were also estimated for the two orientations of the elements by applying the direct path coupling method discussed in Section 4.4. The comparisons between the measured and computed values of the antenna match are plotted in Figures 4.6 and 4.7 as functions of the spacing between the aperture rim of the antenna and the reflector. The antenna VSWR was calculated by comparing the coupling signal $\underset{\sim}{S}_{\alpha\beta}\underset{\sim}{a}'_{\beta}$ with the input signal $\underset{\sim}{a}_{\alpha}$, normalised with respect to $\underset{\sim}{b}_{\beta}$ by the lossless condition (3.2).

The divergence between the computed and measured value of the VSWR in the excited antenna for both orientations of the reflector when the spacing is less than a quarter of a wavelength, can be attributed to three factors. The first factor is insufficient accuracy in the numerical evaluation of the addition theorem expansion coefficients. As the spacing approaches zero the higher order Hankel functions contained within the expansion coefficients assume very large values. Hence, the computed value of VSWR, which then depends upon the differences of large quantities, is sensitive to truncation and round-off errors. This effect is minimised by performing all calculations in double-precision arithmetic. The second factor is the neglect of the $\underset{\sim}{S}_{\beta\beta}$ coupling contributions (see Section 3.4). These might be very strong in comparison with the direct path coupling terms for small antenna-image spacings. However, this is not likely since the $\underset{\sim}{S}_{\beta\beta}$ contributions would have to

decay extremely rapidly for spacings greater than a quarter of a wavelength. The third factor is the accuracy of the elements of $S_{\sim\beta\alpha}$ and $S_{\sim\alpha\beta}$. These elements were derived by applying the N.F.T., so that from Section 2.21, $S_{\sim\alpha\beta}$ accurately represents the receiving pattern of the antenna only at field points whose radial coordinates are equal to or greater than the radial coordinate of the near-field sampling point closest to the antenna. Because of the convergent form of the spherical mode field representation, $S_{\sim\alpha\beta}$ is accurate at field points slightly closer to the antenna than the sampling points, but as the antenna is approached even closer the accuracy, to which $S_{\sim\alpha\beta}$ represents the receiving pattern, deteriorates. In the experimental determination of the elements of $S_{\sim\beta\alpha}$ (that is, the inferring of the radiation pattern of the antenna by applying the N.F.T.), the near-field sampling point closest to the antenna was a quarter of a wavelength from the aperture. Consequently, the computation of the antenna VSWR for spacings less than a quarter of a wavelength is equivalent to extrapolation beyond the measurement interval, in a similar manner to the inferring of the aperture field distribution from the near-field measurements discussed in the previous section. It is this third factor, apparently, which limits the application of the direct path coupling method.

The correlation between the computed and measured values over the remaining regions of Figures 4.6 and 4.7 verifies that a meaningful estimate of mutual coupling effects is possible for the circular waveguide antenna by neglecting the $S_{\beta\beta}$ contributions, for spacings greater than a quarter of a wavelength.

4.54 Suggested topics for further study

The techniques developed in this thesis have been experimentally verified for wide-beam antennas as shown by the results reported in this section. These techniques are applicable in principle to arbitrary three-dimensional antennas. It is suggested that their practical limitations be determined by applying them to a number of antennas with successively narrower radiation patterns.

The accuracy of the estimated aperture field distribution could be improved by performing the necessary near-field measurements closer to the antenna. These measurements will also give a more accurate estimation of the mutual coupling effects between closely spaced antennas. But by using measurement points nearer to the antenna the sampling error of the measurements will be increased, since the interaction between the field probe and the antenna increases as their separation decreases. Hence, an experimental study on methods to improve the accuracy of measuring the field immediately surrounding the antenna is desirable.

Finally it is suggested that a further study be conducted on the significance of the $S_{\beta\beta}$ coupling contributions, on an antenna exhibiting strong coupling effects. This is recommended since the circular waveguide antenna produced only low level coupling signals which made it difficult to determine the true significance of the $S_{\beta\beta}$ contributions.

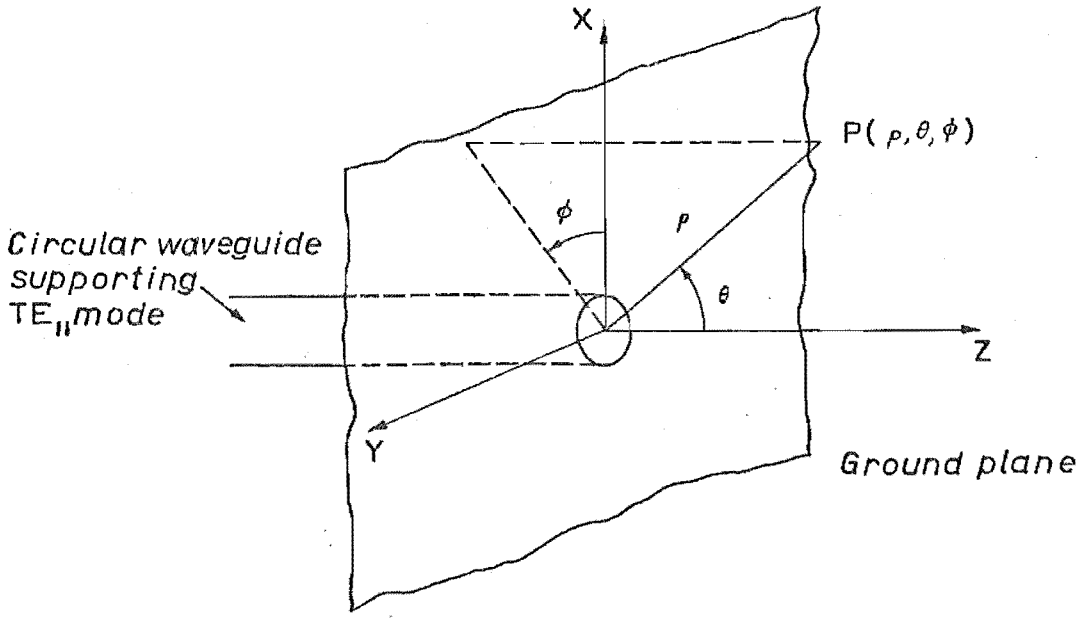

FIGURE 4·1 : CIRCULAR WAVEGUIDE APERTURE ANTENNA

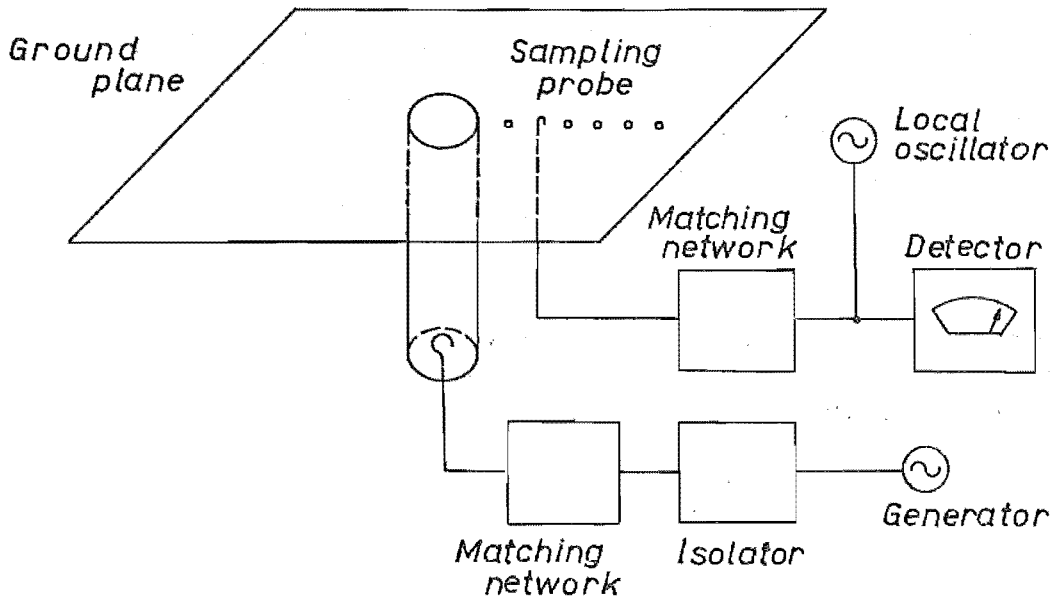

FIGURE 4·2 : SCHEMATIC OF NEAR-FIELD MEASUREMENT

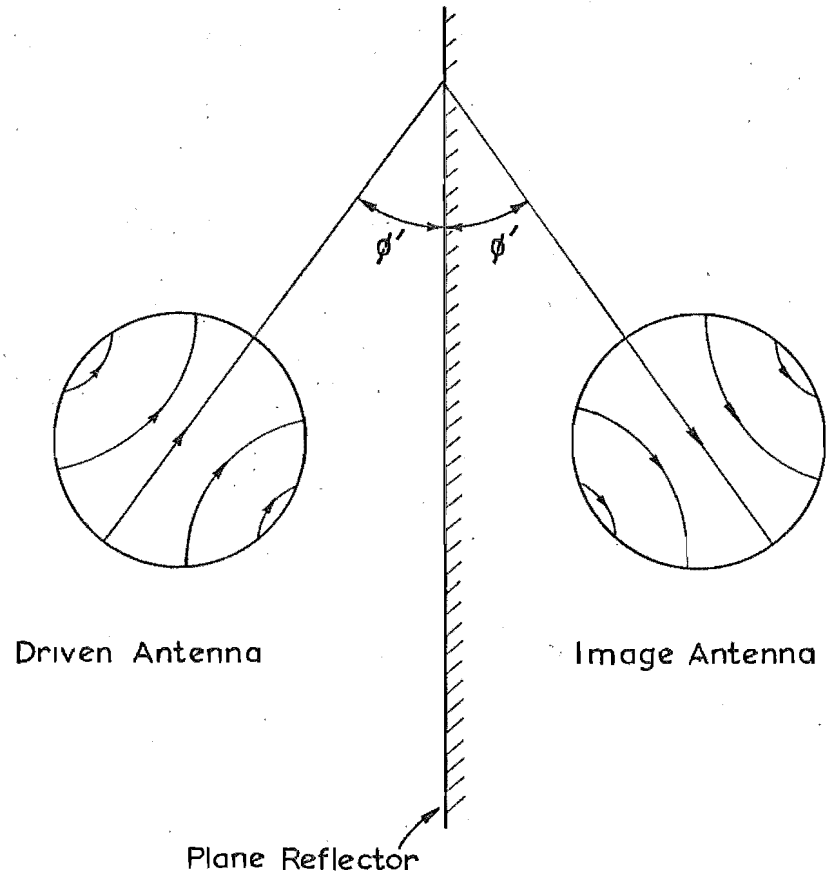

FIGURE 4-3 ANTENNA IMAGE PAIR

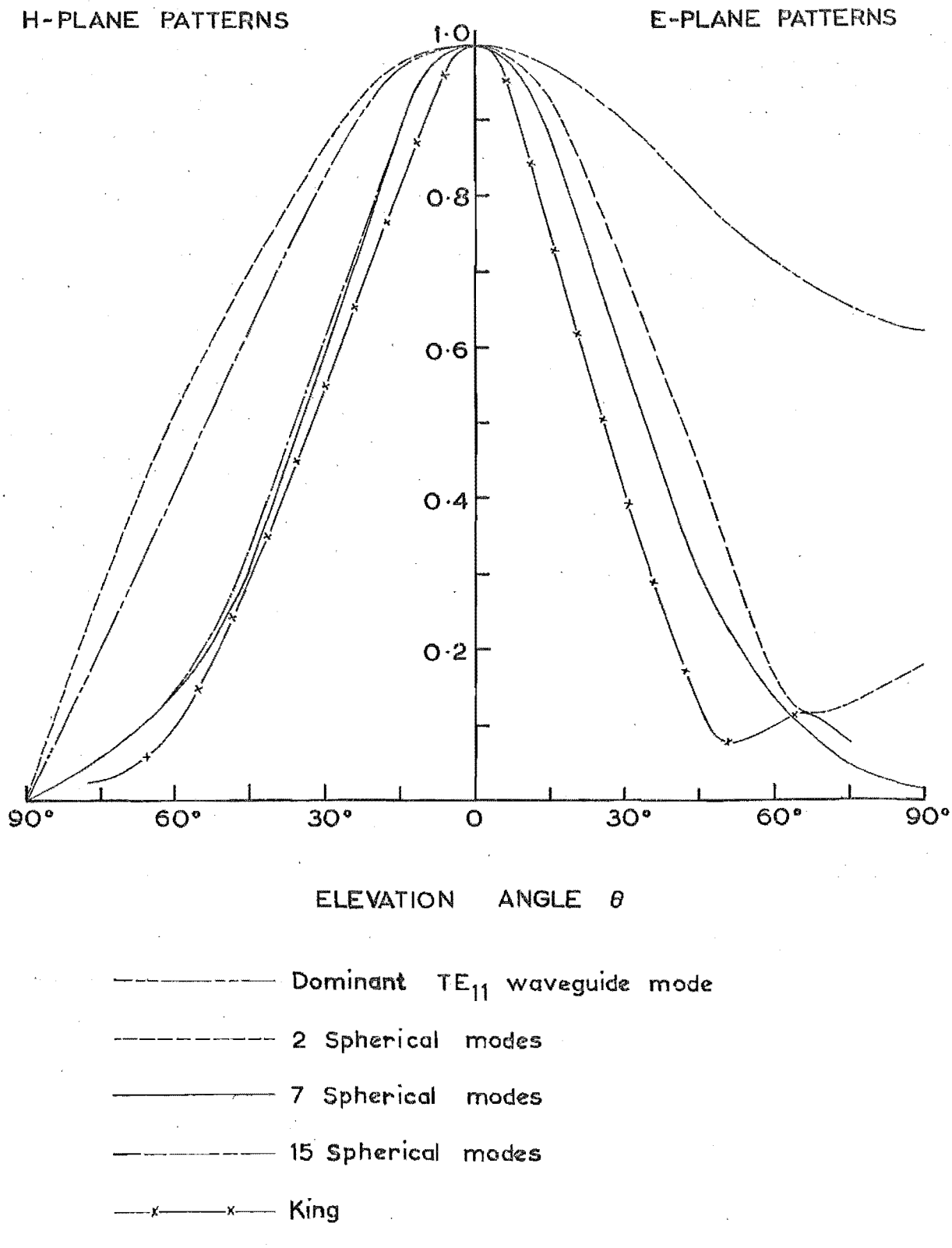

Figure 4·4 Far-field radiation patterns

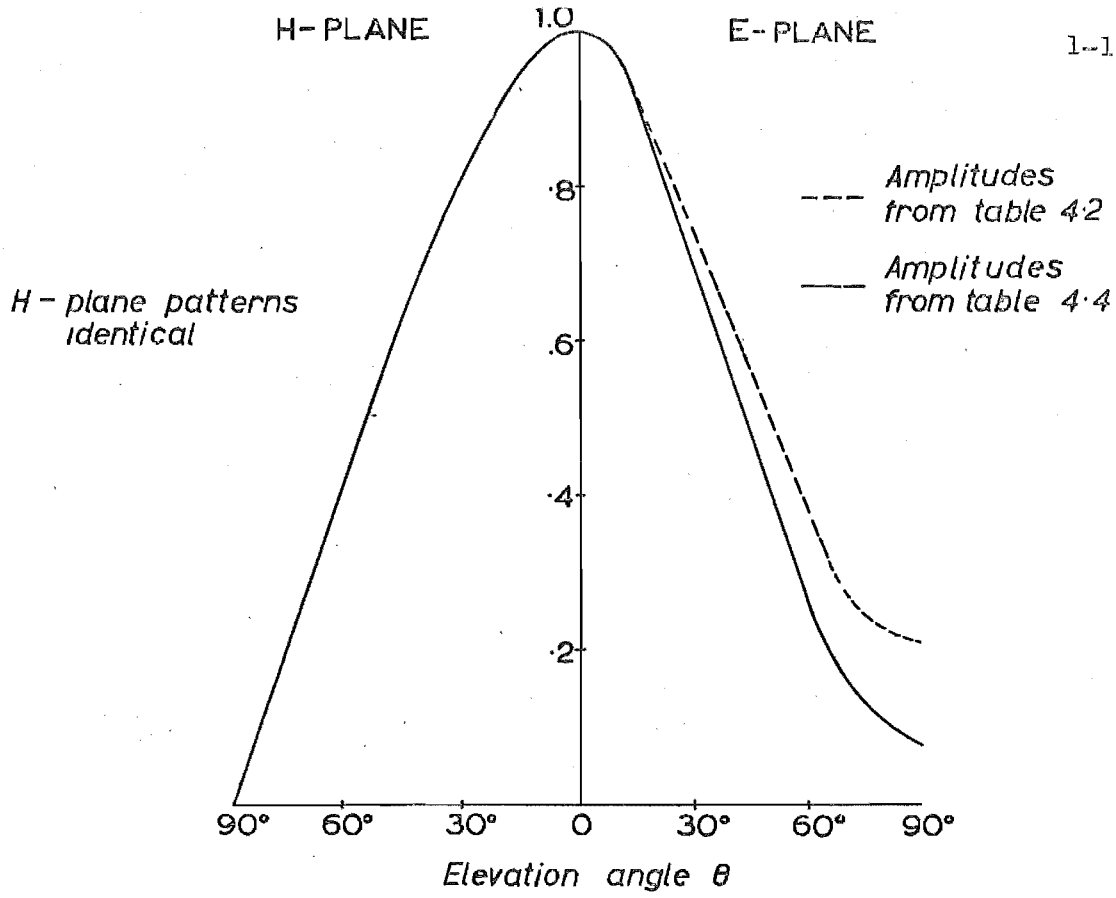

FIGURE 4·5 : FIELD PATTERNS FROM WAVEGUIDE MODES

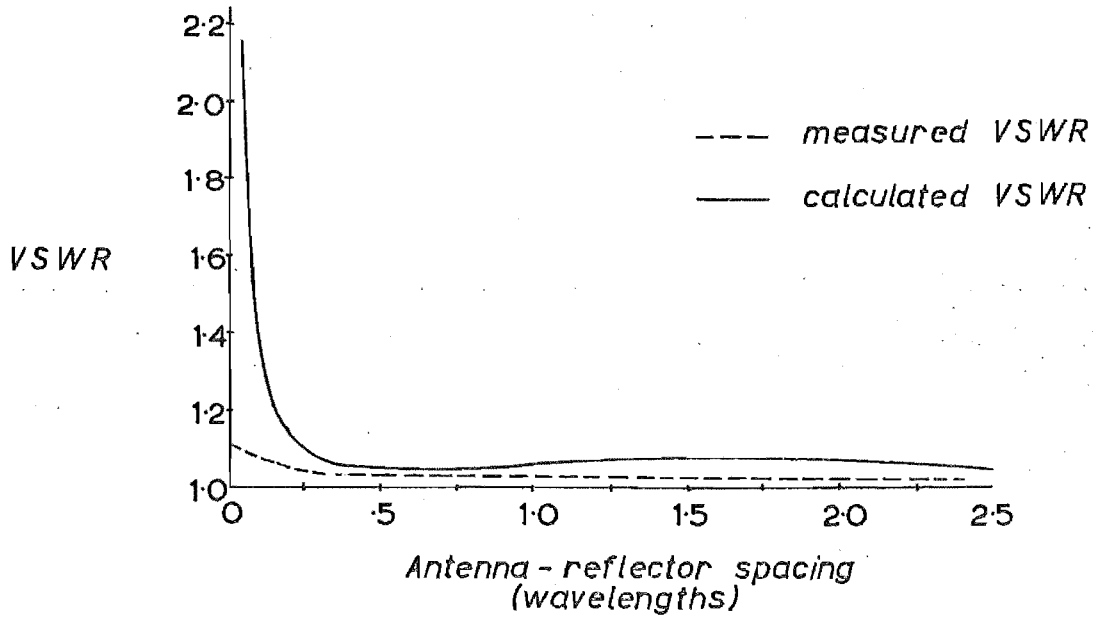

FIGURE 4·6 : ANTENNA MATCH $\phi' = 0°$

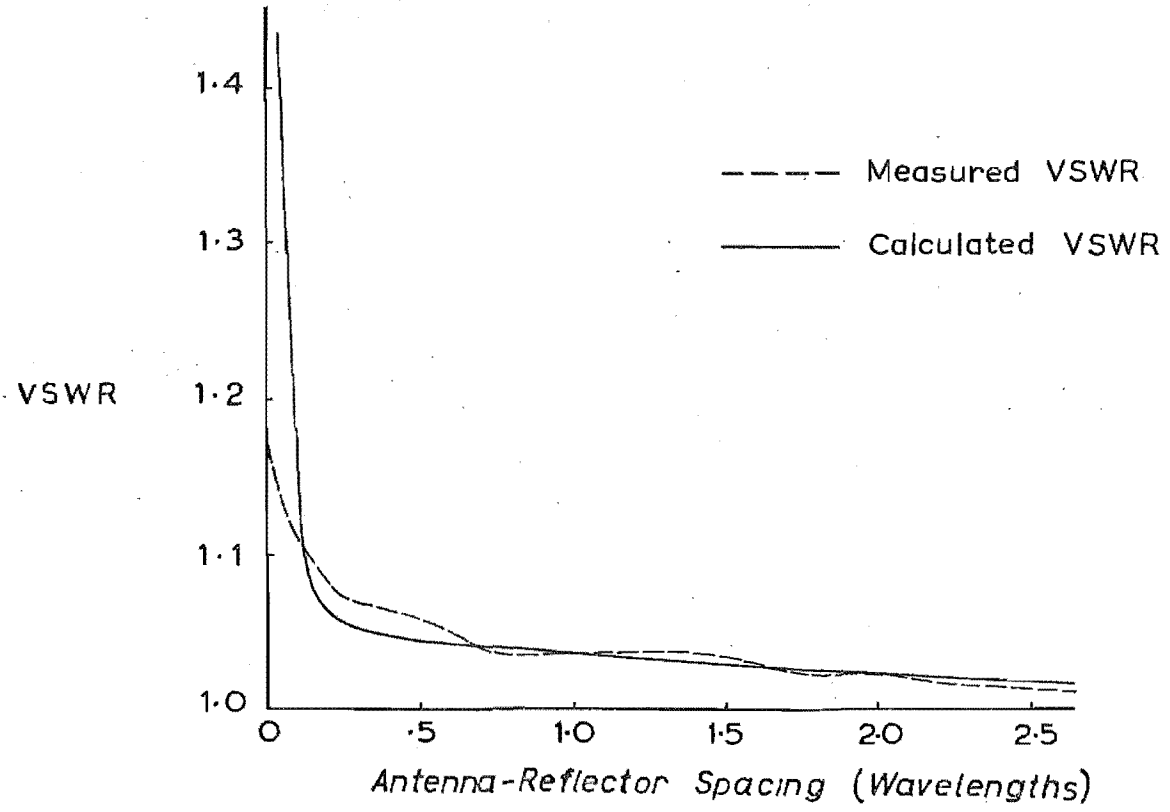

FIGURE 4·7 ANTENNA MATCH $\phi' = 90°$

P A R T 2

THE COAXIAL ANTENNA

CHAPTER 5.

The Coaxial Antenna.

5.1 Introduction.

In recent years many surveillance radar and communication systems employing large planar array-type antennas have been developed. The volumetric scan determined by the maximum and minimum detection ranges and the elevation and azimuth angular scans, is a basic design consideration in such systems. For applications where complete hemispherical coverage is required, the array system must be capable of scanning in all spatial directions, and furthermore, must be polarization insensitive to the extent that arbitrarily polarized signals can be transmitted and received. The latter is necessary, since, in general, the received signal will be of different polarization from the transmitted signal because of magneto-ionic effects[101] and the polarization characteristics of radar targets. To satisfy these conditions, the individual array radiators must act as isotropic point sources, radiating equally well in all directions and polarizations. No single radiator fulfils such a performance specification[102], and hence, combinations of simple, wide beam radiators are necessary to achieve the desired array scan and polarization capabilities.

The polarization state of any plane, electromagnetic wave can be specified completely as the sum of two orthogonal linear

polarizations perpendicular to the direction of propagation of the wave. The relative magnitudes and phases of the component linear polarizations are determined by the polarization state of the wave, whether linear, circular, or elliptical, of either left or right handed sense. To transmit or receive arbitrarily polarized signals, therefore, an antenna must be capable of radiating, with complete control of the relative magnitudes and phases, two orthogonal linear polarizations perpendicular to each direction of propagation. Consequently, an array consisting of such antennas, is polarization insensitive and can scan the complete hemispherical volume within the bounds of the detection ranges.

The simplest radiating element configurations consistent with the radiation and polarization requirements of the array are those composed of elemental crossed dipoles or their aperture duals, mounted on or above ground planes. The choice between the two approaches is dependent upon the particular system specifications, but in most electronically scanned array applications the aperture-type radiator is preferable. With no structural projections above the ground plane, the aperture radiator has greater mechanical rigidity and simplicity, allowing for increased array ruggedness or hardness, as compared with an array of dipoles. In addition, if the aperture holes are small compared with the array inter-element spacing, there is less tendency for the physical structure of the aperture array to support a leaky wave giving rise

to the surface resonance phenomenon[103]. However, when the aperture dimensions and the inter-element spacing are of the same order, the aperture array is as susceptible to this phenomenon as is the dipole array.

In order to develop a systematic basis for design, it is convenient to delineate the design specification of a radiating element suitable for inclusion in an electronically scanned array. The array is characterised as being polarization insensitive, to the extent that arbitrarily polarized signals can be transmitted and received, mechanically hard, and capable of scanning in all directions. The specification is in two parts. Firstly, the element design which gives the constraints on the radiating element parameters both electrical and mechanical, and secondly, the system design which specifies the design radiation and input characteristics of the element, and the conditions subsequently imposed upon the associated control circuitry. Although expressed from the point of view of a transmitter, by reciprocity the specifications are equally applicable to a receiver, and may be summarized as:

(A) Element design constraints.

(i) Compatibility with the array environment requires that whenever possible, the individual radiator should be designed to minimize the detrimental effects on the array performance caused by mutual coupling between elements, and the surface resonance

phenomenon. The radiator dimensions must be chosen in conjunction with the array spacing to inhibit the incidence of grating lobes.

(ii) The element should be capable of radiating the required polarizations over the scan volume specified for the array, since the ability of the array to scan in any particular direction and polarization is limited by the radiation properties of the individual radiator elements.

(iii) The hardness specification for the array must be reflected in the mechanical robustness of the element.

(iv) The element should be capable of efficient operation over as wide a frequency bandwidth as possible. For an antenna the bandwidth can be defined variously with respect to radiation, polarization, or impedance characteristics[104], but for the purposes of the present design the impedance definition will be applied.

(v) To reduce the cost per element and hence the total array cost, the radiator should be of simple construction in accordance with (iii), and to minimize the circuitry requirements, should use the simplest possible feed and excitation configurations.

(B) System design constraints.

(vi) Further to (v), compatibility of the radiator with a large array system requires simplicity of circuitry and a minimum of circuit elements consistent with the attainment of the specified array performance.

(vii) Under the various modes of operation of the radiator corresponding to particular radiated polarizations, constant power must be absorbed from the generator. Expressed in terms of the array performance, this condition is equivalent to stating that the input power to each radiator is independent of the scan angle and the radiated polarization. Furthermore, it is desirable from an efficiency viewpoint, that this power be the maximum possible which the generator can deliver.

(viii) Provision for high power handling capability when transmitting and for low losses when receiving are also desirable in the system and element designs.

From this specification an optimum design for an antenna suitable for inclusion in a large array will be developed.

The polarization condition and the hardness specification govern the choice of the basic antenna element. Thus, a triple-polarized radiator, which can radiate three orthogonal linear polarizations (for example, three mutually perpendicular dipoles), satisfies the polarization condition (ii). This follows as the three radiated polarizations can always be resolved into two resultant linear polarizations transverse to each particular scan direction. Then given complete control of the magnitude and phases of the signals corresponding to any two such transverse linear polarizations, any arbitrarily polarized wave can be transmitted or received[105]. The hardness specification (iii) is satisfied by an aperture radiator. If this is flush mounted in a ground plane the mechanical ruggedness of the element will be even further improved. Consequently, a triple-polarized, flush mounted, aperture radiator is the most suitable element for the array application.

The simplest antenna element commensurate with this description is a coaxial waveguide aperture radiator utilizing three orthogonal waveguide modes of propagation, the transverse electromagnetic TEM mode, and two space orthogonal transverse electric TE_{11} modes. The TEM mode aperture field radiates in a manner similar to a vertical monopole, while the radiation field of the TE_{11} mode is similar to that of a horizontal dipole mounted over a ground plane. It will be shown that the coaxial antenna produces the necessary

polarizations, and that proper control of the relative strengths of the modes radiating these polarizations, ensures that any arbitrary polarized signals can be transmitted or received.

A review of literature relevant to the coaxial antenna will be given, covering both theoretical studies and application notes. The derivation of the field expressions for the coaxial waveguide modes of propagation will be presented in a summarized form, and finally, a comparison between the coaxial antenna and the equivalent multiple dipole antenna will be given.

5.2. Literature review for the coaxial antenna.

Almost all existing studies of coaxial antennas have been concerned with determining the antenna's input and radiation characteristics from a knowledge of the aperture field distribution, which has frequently been assumed to be the field of the dominant mode alone. Schelkunoff[106] applied the equivalence principle to calculate the radiation from an open-ended coaxial waveguide supporting the TEM mode. This method relied on representing the far-field form of the Green's function by only the first two terms in its power series expansion, which is valid provided that the waveguide radius is small compared with the wavelength. Hence, higher order modes present in the aperture were strongly evanescent, and only the TEM mode contributed

significantly to the far-field. Applying the variational technique of Levine and Schwinger[89], Levine and Papas[107] and Marcuvitz[108] formulated the aperture admittance of the semi-infinite, TEM mode coaxial waveguide, flush mounted in an infinite perfectly conducting ground plane. Numerical results for various aperture dimensions were obtained by this method, assuming the TEM mode to represent the aperture field. As the ratio of the radii of the outer and inner conductors increases for fixed outer conductor radius, the higher order modes in the aperture become progressively more strongly evanescent. Consequently the accuracy of the tabulated results improves, as the assumption that the TEM mode field represents the actual aperture field becomes more accurate.

The narrow gap coaxial antenna, or annular slot antenna, has many vehicular and aircraft applications[109], and was dealt with by Pistolkors[110] who assumed the slot field to have the same distribution as the TEM mode field in coaxial waveguide. For very small slots, the radiation field was shown to approach a sinusoidal variation with elevation angle. Following Pistolkors' method, Rhodes[111] designed an annular slot antenna fed in the TEM mode for a VHF mobile application. This demonstrated the similarity in performance between the annular slot antenna and the more commonly used vertical monopole antenna. Cumming and Cormier[112] tabulated design data

relating the slot and input admittances of small, cavity backed, annular slot antennas to the aperture and cavity dimensions. These calculations were based upon the dominant mode fields. The radiation conductance of a hemispherical cavity backed annular slot antenna was calculated by Wait[113], but the analysis, which allowed for the finite conductivity of the cavity walls, was restricted to narrow slot antennas. The effects of cylindrical and coaxial back-up cavities were incorporated by Galejs and Thompson[114] into the variational formulation for the slot admittance of annular slot antennas. However, as with previous studies, only contributions from the dominant mode field were considered.

Cohn and Flesher[115] developed an iterative method for evaluating the integral equation formulation of the radiation and aperture characteristics of a flush mounted coaxial antenna supporting the TEM mode. Expressions for the aperture admittance and radiation field, based upon the dominant mode approximation, were given. These were shown to be most accurate for the case when the waveguide radii are small compared with the wavelength, which is equivalent to considering all modes of higher order than the TEM mode as being strongly evanescent. The dependence of the approximated radiation pattern on the ratio of the radii also was demonstrated. A similar iterative method and a variational

technique were used by Samaddar[116] to calculate the aperture admittance of a TEM mode, coaxial antenna, flush mounted in an infinite ground plane covered by a plasma or dielectric layer. The results of the two approaches were shown to be the same for any particular order of accuracy; that is, for any particular modal representation of the aperture field distribution. Samaddar's work, to a degree, paralleled that of Yeh and Wait[117] who studied the radiation from a dielectric coated, flanged (ground plane mounted), coaxial antenna in a warm plasma, and formulated a variational expression for the aperture admittance following the method of Levine and Papas. This analysis was primarily concerned with the radiation and admittance effects in the plasma region. However, as with the results obtained by Samaddar, admittance expressions for the limiting case, when the antenna radiates directly into free space, are implicit in the general expressions.

Ling et. al.[118] developed a general method for calculating the far-field radiation patterns of arbitrary, scalar, aperture field distributions for various shaped aperture antennas, including coaxial. The net radiation pattern of the aperture antenna was found by representing the aperture field distribution as a set of characteristic solutions to the scalar Helmholtz equation, and applying the well known bidimensional Fourier transform relating the aperture and far-field distributions[47]. Since the method depends upon a

complete knowledge of the aperture field representation, which can be derived only from a known aperture illumination function, the method is better suited to the antenna synthesis problem than the analysis problem. The TE_{11} and TE_{12} modal radiation patterns for an unflanged coaxial antenna were calculated by Scheffer[119], using the aperture field method of Silver[93]. For a moderately large sized aperture (two-and-a-half wavelengths diameter), the agreement obtained between the calculated and measured field patterns of these two modes was good in directions close to the main beam axis but deteriorated for directions off-axis, as a result of the errors inherent in the aperture field method[120].

Recent applications of coaxial antennas include that of Jamieson and Bates[121], who designed a coaxial antenna capable of transmitting and receiving arbitrarily polarized signals. A feature of this design, which was based upon an experimental study at L-band, was the use of both TEM and TE_{11} modal fields to achieve the desired polarization diversification. Koch and Scheffer[122] adapted a four ring coaxial antenna as a feed radiator for parabolic reflector antennas. Each coaxial region between pairs of conductors was excited in the TE_{11} mode and the phases of each region adjusted so that the total aperture distribution generated the optimum spherical sector shaped radiation pattern. Experimental results on the matching of electric field excitation probes for a coaxial cavity radiator illuminating a parabolic antenna have been

presented by Malowicki[123]. For this application, the high power handling requirements of the radiator restricted the shapes of the probes. The input VSWR and bandwidth behaviour were shown to be strongly dependent upon the probe shape.

To summarize, theoretical studies of coaxial antennas usually have dealt with simple structures supporting a single propagating mode, whereas practical antennas, and in particular the triple-polarized coaxial antenna, may involve electrically short, multi-mode structures. Therefore, the techniques reviewed above will be useful only as a basis for the design of a practical antenna. The optimum antenna design, defined with respect to the fulfillment of the design specification, has in general to be derived experimentally.

5.3 Coaxial waveguide modes of propagation.

The solution to the homogeneous boundary-value problem of determining the field configurations characteristic of a coaxial waveguide, is found by solving Maxwell's equations subject to the appropriate boundary conditions existing at the waveguide walls. Assuming that the guide walls are perfect conductors, and that the dielectric within the guide is homogeneous, isotropic, and source-free, of permeability μ, and dielectric constant ε, then the differential form of Maxwell's equations in a source free region are

$$\begin{aligned} \underline{\nabla} \times \underline{H} &= j\omega\varepsilon\underline{E}, \\ \underline{\nabla} \times \underline{E} &= -j\omega\mu\underline{H}, \\ \underline{\nabla} \cdot \underline{E} &= \underline{\nabla} \cdot \underline{H} = 0, \end{aligned} \qquad (5.1)$$

where time variations of the form $e^{j\omega t}$ are understood. Introduce a cylindrical polar coordinate system (r,γ,z) such that the axis of the guide is parallel to the z-axis as shown in Figure 5.1. Since the guide is homogeneous in the z-direction, the z-dependence of all field components is of the form $e^{\mp\gamma z}$, where the upper sign corresponds to propagation in the positive z-direction, and the lower sign corresponds to propagation in the negative z-direction, and γ is the propagation constant. From the cylindrical components of (5.1), the transverse field components E_r, E_ψ, H_r, and H_ψ can be expressed solely in terms of the two longitudinal field components E_z and H_z[124]. Further substitution in (5.1) yields the scalar wave equation in cylindrical coordinates,

$$\frac{\partial^2 U}{\partial r^2} + \frac{\partial^2 U}{r^2 \partial \psi^2} + \frac{\partial^2 U}{\partial z^2} + \frac{\partial U}{r \partial r} + k^2 U = 0, \qquad (5.2)$$

where U is either E_z or H_z. Since the transverse components are entirely derivable from E_z and H_z, two sets of independent solutions of (5.1) are possible: transverse electric (TE) modes derived from H_z with E_z zero, and transverse magnetic (TM) modes derived from E_z with H_z zero. In addition, there is a solution corresponding to the case when both E_z and H_z are zero. This is the transverse electromagnetic (TEM) mode. Hence, a wave representing the general solution of Maxwell's equations in a coaxial guide, is a linear combination of all three fundamental mode categories.

5.31 TEM mode

The TEM mode which is the principal or lowest order mode in coaxial waveguide, has both electric and magnetic fields entirely transverse to the direction of propagation, and is analogous to a plane wave in the unbounded medium. It can be shown[125], that the non-zero field components E_r and H_ψ are axially symmetric and are given by,

$$H_\psi = \sqrt{\frac{\varepsilon}{\mu}}\, E_r = \sqrt{\frac{\varepsilon}{\mu}}\, \frac{\kappa}{r}\, e^{-\gamma z}, \qquad (5.3)$$

where κ is a constant for a particular waveguide. The TEM mode propagates without attenuation for all frequencies (dielectric assumed perfect and lossless), with a propagation constant equal to the wave number in the unbounded medium. Unlike all other waveguide modes, therefore, the TEM mode does not have a cutoff frequency.

5.32 TE and TM modes.

The field vectors for all the higher order modes are found by imposing the boundary conditions appropriate for the TE or TM set of modes, to the characteristic solutions of (5.2). By the method of separation of variables, these solutions are found to be of the general form

$$U(r,\psi) = [A\, J_m(hr) + B\, Y_m(hr)]\, \cos m\psi, \qquad (5.4)$$

where $J_m(hr)$ and $Y_m(hr)$ are the m^{th} order Bessel and Neumann functions, respectively, A and B are model coefficients, and h is defined by

$$\gamma^2 = h^2 + \omega^2\mu\epsilon = h^2 + k^2, \tag{5.5}$$

where k is the wave number in the unbounded medium.

The boundary conditions require tangential electric field components to be zero on the guide walls. For the TE modes, this condition is equivalent to the transcendental equation

$$-\frac{B}{A} = \frac{J'_m(h'_n a)}{Y'_m(h'_n a)} = \frac{J'_m(h'_n b)}{Y'_m(h'_n b)}, \tag{5.6}$$

where the prime on the functions denotes differentiation with respect to the argument, h'_n corresponds to the n^{th} root of the equation, and a and b are defined in Figure 5.1. Similarly, for TM modes the boundary conditions reduce to

$$-\frac{B}{A} = \frac{J_m(h_n a)}{Y_m(h_n a)} = \frac{J_m(h_n b)}{Y_m(h_n b)}. \tag{5.7}$$

The denumerably infinite sets of values of h'_n and h_n satisfying (5.6) and (5.7), respectively, correspond to the denumerably infinite sets of TE and TM modes, and furthermore, it can be shown[124] that the field components of the general modes, denoted by TE_{mn} and TM_{mn}, which are members of these sets, can be derived from

$$H_z = \frac{h'^2_n}{j\omega\mu} e^{-\gamma_{mn} z} [A J_m(h'_n r) + B Y_m(h'_n r)] \cos m\psi \tag{5.8}$$

for TE_{mn} modes, and from

$$E_z = \frac{h_n^2}{j\omega\varepsilon} e^{-\gamma_{mn} z} \left[A J_m(h_n r) + B Y_m(h_n r) \right] \cos m\psi \qquad (5.9)$$

for TM_{mn} modes. The modal propagation constant γ_{mn} is defined by (5.5), and the cutoff wavelength is $\lambda_{mn}^c = 2\pi/h$, with h given by the roots of (5.6) or (5.7).

5.4 Coaxial antenna - three dipole comparison.

An array element consisting of three coincident mutually perpendicular dipoles mounted above a ground plane is electrically similar to the three mode coaxial antenna. Both radiators are capable of radiating in all spatial directions, and, being triple-polarized, also satisfy the polarization requirements of the array. However the dipole radiator has particular inherent disadvantages when compared to the coaxial antenna, quite apart from its obvious lack of mechanical ruggedness.

In the ideal radiator, the three dipoles which are orthogonal in space have coincident feed points, and because of the symmetry of this configuration no mutual coupling occurs between the three elements[126]. However, in practice, the structure supporting the radiator above the ground plane, and the transmission lines connecting each dipole to the transmitter/receiver, introduce asymmetries into the radiator geometry. The fields radiated by the dipoles induce currents in these structures which in turn radiate, couple with the dipoles, and consequently modify the radiation pattern and

impedance match of the radiator. This coupling is dependent upon the mode of operation of the radiator, determined by the relative strengths of the signals fed to the three dipoles. Furthermore, if the ground plane is not flat, for example when the radiator is mounted on a vehicle or aircraft, then the mutual coupling between the dipoles is likely to be increased, because of multiple scattering effects. With the coaxial antenna, on the other hand, orthogonality conditions for the waveguide modes[127] ensure that mutual coupling between the three modes in the antenna is very low. Also, coupling effects due to the interaction of the physical structure of the feed circuitry with the radiation field are eliminated in the coaxial antenna, since the circuitry and all connections to the antenna are shielded from the field by the ground plane.

The effect of the ground plane upon the performance of the dipole radiator can be evaluated by replacing the ground plane with the image of the radiator. Because of mutual coupling effects between the radiator-image pair, the driving point impedance of the radiator differs from the expected free space value of the self impedance of the radiator. These mutual coupling effects, which are in addition to the coupling effects discussed above, are functions of the radiator-image spacing. Hence, the driving point impedance, which is the combination of the self impedance and the mutual impedance between the radiator and its image, varies with the mounting height[128]. Simple array theory predicts that the net radiation

pattern and gain functions of the radiator-image pair are dependent upon the mounting height, but for mounting heights less than or equal to a quarter of the operating wavelength, these properties remain substantially constant[129]. Furthermore, in the array application, mutual coupling effects between the radiators cause the array driving impedance to vary with scan angle, and it has been shown[129] for dipole arrays, that for each value of array spacing, there is a corresponding optimum mounting height at which the maximum impedance mismatch incurred during scanning is minimal. The optimum radiator mounting height for a given application is determined from the impedance and radiation characteristics of the radiator when isolated and when incorporated in the array environment.

In comparison, there are no similar ground-plane-induced mutual coupling effects to be considered in the operation of the flush mounted coaxial antenna. When this antenna is in an array configuration, it will nevertheless exhibit impedance variations with scan angle, because of the mutual coupling between the individual elements in the array.

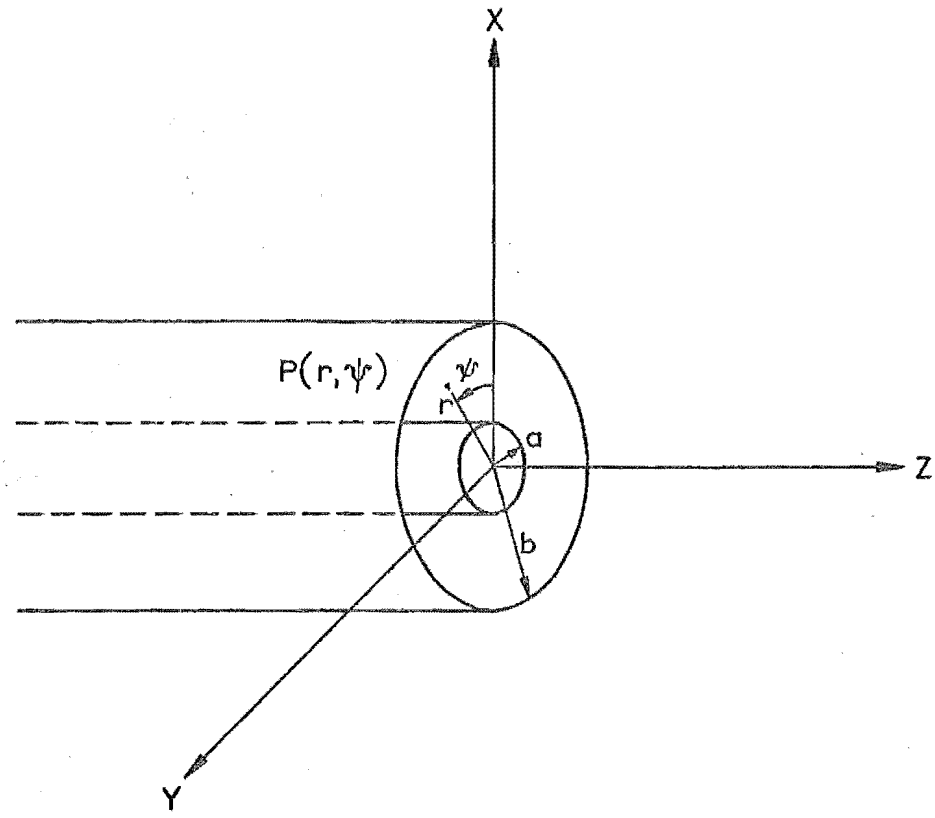

FIGURE 5·1 : COORDINATE SYSTEM FOR THE COAXIAL ANTENNA

CHAPTER 6.

Antenna Field Patterns.

6.1 Introduction.

The radiation pattern of a coaxial waveguide antenna supporting the TEM mode alone, can be calculated approximately by applying the equivalence principle method of Schelkunoff[106]. This method relies upon the assumption that the far-field form of the Green's function can be represented by only the first two terms in its power series expansion, which is valid either for propagation directions close to the axis of the guide, or if the guide radius is small compared with the wavelength. Furthermore, the radiation patterns of coaxial antennas supporting higher order modes can not be calculated by this technique. A more accurate estimation of the TEM modal radiation field was shown to be possible by using the electric and magnetic vector potentials method[115]. The field pattern calculated for the TEM mode is valid for all propagation directions and is not restricted to any particular range of guide dimensions. Higher order modal radiation patterns can also be calculated by this method, which is rigorous provided the antenna is flush mounted in an infinite, perfectly conducting, ground plane. The approximate solution for the radiation from an isolated coaxial antenna without a ground plane can be found[119] by applying Silver's aperture field method[93].

The approximation results from the assumption that all tangential components of the electric and magnetic fields in the aperture plane are zero outside the aperture itself. Consequently, the calculated solution is most accurate when the radiation is concentrated close to the direction of the guide axis, a characteristic of an antenna with a large aperture. The aperture field method solution is not rigorous, and may be considered as a compromise between the solutions obtained when the antenna is flush mounted in a perfect electric ground plane (tangential electric field components zero), and when flush mounted in a perfect magnetic ground plane (tangential magnetic field components zero)[120].

The radiation patterns for each mode of the coaxial antenna can be calculated exactly by applying the far-field form of the vector potential method discussed in Section 2.2. To recapitulate, the equivalence principle and the boundary conditions existing over the aperture plane, show that the total field from the antenna may be specified completely by an electric vector potential expressed in terms of the tangential electric field in the aperture. By substituting for each modal aperture field and applying the usual far-field approximations, the far-field form of the electric vector potential and hence the electric and magnetic fields can be determined. In essence, the method extends Schelkunoff's technique to all flush mounted aperture

antennas, equalling the rigour and range of validity of the previously outlined electric and magnetic vector potentials method. A significant advantage over the latter method is that instead of potentials of both types, only a single vector potential is required to determine the fields uniquely.

The radiation patterns corresponding to the dominant modes in the coaxial antenna will be calculated from a single electric vector potential. It will be shown that these modal patterns represent the radiation patterns of the antenna to a first approximation only. The complete radiation patterns can be determined by applying the N.F.T. introduced in Chapter 2, and the formulation of this technique for the coaxial antenna will be presented. Modifications to the radiation patterns caused by altering the antenna mounting will also be described.

6.2 Far-field modal radiation patterns.

6.21 Far-field vector potential radiation formula.

Following the notation of Chapter 2 an electric vector potential $\underline{F}$ is introduced with rectangular components F_x and F_y satisfying the scalar Helmholtz equation. From Appendix II F_x and F_y are defined for the coaxial antenna as

$$F_x = -\frac{1}{2\pi}\int_0^{2\pi}\int_b^a E_y(r,\psi,0)\,\frac{e^{-jkR}}{R}\,r\,dr\,d\psi, \qquad (6.1)$$

and

$$F_y = -\frac{1}{2\pi}\int_0^{2\pi}\int_b^a E_x(r,\psi,0)\,\frac{e^{-jkR}}{R}\,r\,dr\,d\psi, \qquad (6.2)$$

where the source and observational coordinates are defined in Figure 5.1. $E_x(r,\psi,0)$ and $E_y(r,\psi,0)$, respectively, are the $\hat{x}$ and $\hat{y}$ direction components of the aperture fields corresponding to the modes in the antenna.

In the far-field the Green's function assumes the limiting form

$$\lim_{R\to\infty} \frac{e^{-jkR}}{R} = \frac{e^{-jk(\rho-r\cos\gamma)}}{\rho}, \qquad (6.3)$$

where

$$\cos\gamma = \sin\theta\cos(\phi-\psi), \qquad (6.4)$$

as in Figure 5.1. By substituting (6.3) into (6.1) and (6.2), transforming the rectangular components of $\underline{F}$ into spherical components and applying the vector relation[130]

$$\underline{E} = \nabla \times \underline{F}, \qquad (6.5)$$

the far-field spherical components of the electric field for each modal aperture field are determined. Only terms that vary as ρ^{-1} need to be considered in (6.5), and hence,

$$E_\theta = \frac{jke}{2\pi\rho}^{-jk\rho} \int_0^{2\pi} \int_b^a [E_y(r,\psi,0)\sin\phi$$

$$+ E_x(r,\psi,0)\cos\phi]e^{jkr\sin\theta\cos(\phi-\psi)}\, r dr d\psi, \qquad (6.6)$$

and

$$E_\phi = -\frac{jk\cos\theta e}{2\pi\rho}^{-jk\rho} \int_0^{2\pi} \int_b^a [-E_y(r,\psi,0)\cos\phi$$

$$+ E_x(r,\psi,0)\sin\phi]e^{jkr\sin\theta\cos(\phi-\psi)}\, r dr d\psi. \qquad (6.7)$$

The magnetic field components can be found in a similar manner.

6.22 Modal radiation patterns.

(a) TEM mode.

From section 5.3 the sole tangential component of the aperture electric field for the TEM mode is

$$\underline{E}(r,\psi,0) = \hat{\underline{r}}\,\frac{\kappa}{r}. \qquad (6.8)$$

Substituting rectangular components of (6.8) and (6.7), using the expansion[131]

$$e^{jkr\sin\theta\cos(\phi-\psi)} = \sum_{m=0}^{\infty} \varepsilon_m\, jm\, J_m(kr\sin\theta)\cos m(\phi-\psi), \qquad (6.9)$$

where ε_m is the Neumann factor, and the integration formula

$$\int_b^a J_1(hx)\,dx = \frac{1}{h}[J_o(hb) - J_o(ha)], \qquad (6.10)$$

the far-field electric components are found to be

$$E_\theta = \frac{e^{-jk\rho}}{\rho \sin\theta} [J_o(ka\sin\theta) - J_o(kb\sin\theta)], \qquad (6.11)$$

and

$$E_\phi = 0. \qquad (6.12)$$

Due to the symmetry of the TEM mode aperture field no radiation can occur in the direction $\theta = 0$. Since for small values of θ the ascending series form of the Bessel functions[132] shows that

$$J_o(ka\sin\theta) - J_o(kb\sin\theta) = k^2 \frac{(b^2 - a^2)}{4} \sin^2\theta, \qquad (6.13)$$

the limiting value of (6.11) as $\theta \to 0$ is zero. Hence, to a first approximation, the TEM modal radiation pattern varies as $\sin\theta$ and is analogous to the radiation pattern of a vertical monopole. The pattern given by (6.11) is normalized and plotted in Figure 6.1.

(b) TE_{11} mode

Consider the TE_{11} mode to be excited such that its aperture field is polarized predominantly in the $\hat{y}$ direction. From Section 5.3 the tangential components of the aperture electric field of this mode are

$$\underline{E}(r,\psi,0) = -\hat{r}\,\frac{\sin\psi}{r}\,[AJ_1(h_1' r) + BY_1(h_1' r)] + \hat{\psi}\, h_1' \cos\psi [AJ_1'(h_1' r) + BY_1'(h_1' r)]. \qquad (6.14)$$

As above, substituting the rectangular components of (6.14) into (6.6) and (6.7), using (6.9) and the Lommel integration formulae[133], the far-field electric field components are found to be

$$E_\theta = \frac{je^{-jk\rho}\sin\phi}{\rho\sin\theta}\left[J_1(ka\sin\theta)C_1(h_1'a) - J_1(kb\sin\theta)C_1(h_1'b)\right], \quad (6.15)$$

and

$$E_\phi = \frac{je^{-jk\rho}\, h_1'^2 a\cos\phi\cos\theta}{\rho(h_1'^2 - k^2\sin^2\theta)}\left[J_1'(ka\sin\theta)C_1(h_1'a) - J_1'(kb\sin\theta)C_1(h_1'b)\right], \quad (6.16)$$

where

$$C_1(h_1'x) = AJ_1(h_1'x) + BY_1(h_1'x). \quad (6.17)$$

The aperture electric field of the TE_{11} mode is symmetrical about the plane defined by $\phi = \pi/2$, which is therefore designated as the E-plane for this mode. Similarly, the $\phi = 0$ plane is the H-plane. Upon substituting these values of ϕ into the above expressions, it follows that (6.15) and (6.16) are, respectively, the E-plane and H-plane TE_{11} modal radiation patterns. The TE_{11} mode radiates in a similar manner to a horizontal dipole oriented in the same direction and mounted above a perfect ground plane. Normalized field patterns corresponding to (6.15) and (6.16) are plotted in Figure 6.1.

The modal radiation pattern for the TE_{11} mode oriented in the $\hat{x}$ direction is the same as that for the $\hat{y}$ direction oriented mode, except that the E-plane is the $\phi = 0$ plane, and the H-plane is the $\phi = \pi/2$ plane.

6.3 Coaxial antenna radiation patterns.

The modal radiation patterns discussed above represent the complete radiation patterns of the coaxial antenna to a first approximation only. As discussed in Chapter 4, the edge conditions at the aperture rim require a denumerable infinity of higher order modes to be present at the discontinuity, in addition to the dominant modes. Consequently, the aperture fields of the dominant modes alone are insufficient to represent accurately the actual aperture field of the coaxial antenna.

6.31 Aperture higher order modes.

The necessary infinite set of higher order modes must include, in general, all TE_{mn} and TM_{mn} modes. But in the coaxial antenna, because of the symmetry of the aperture, the excited higher order modes will have the same azimuthal orientation and dependence as the dominant modes. The circularly symmetric TEM mode excites only those modes that are fully symmetrical and independent of azimuthal variations. From Section 5.3 the only modes fitting such a description are the TM_{0n} modes. The TE_{11} mode oriented in the $\hat{y}$ direction excites higher order modes of the form TE_{1n} and TM_{1n} oriented in the $\hat{y}$ direction. Similarly, the $\hat{x}$ direction oriented TE_{11} mode excites TE_{1n} and TM_{1n} modes oriented in the $\hat{x}$ direction.

The complete aperture field of the coaxial antenna can be represented, therefore, as the fields of the dominant TEM and TE_{11} modes plus the fields of the denumerably infinite set of TM_{0n}, TM_{1n}, and TE_{1n} modes. All modes are both reflected back into the antenna and transmitted across the aperture plane into space, so that the radiation pattern of the antenna and its aperture admittance differ from the values calculated on the assumption that the coaxial waveguide supports only the dominant modes.

6.32 Estimation of total radiation pattern.

Since an accurate analytic solution for a practical coaxial aperture antenna design is impractical, as discussed in Chapter 5, the aperture field distribution, as represented by the set of waveguide modal functions, can not be determined analytically unless *a priori* knowledge of the radiation field exists, such as in the antenna synthesis problem. A complete description of the radiation from the coaxial antenna requires either far-field measurement of the radiation pattern or the inferring of this pattern from measurements performed at or near to the antenna. Far-field pattern measurements and direct sampling of the aperture field are difficult to achieve accurately for such a wide beam antenna, due to the reasons stated in Chapters 2 and 4. But by representing the fields as a set of spherical vector modes, performing limited field measurements in the near field of the coaxial antenna, and applying the N.F.T.

in Chapter 2, the complete radiation pattern can be determined.

From the vector potential expressions for the electric field components of the modal radiation patterns and the dependence of the azimuthal variations of the higher order modes in the aperture upon the forms of the dominant modes, the electric field radiated can be considered in two parts. The first varies as $\sin\phi$ or $\cos\phi$, and the second is constant with the azimuthal coordinate. Thus, the E_θ and E_ρ field components each have terms proportional to $\sin\phi$ and further terms independent of ϕ, whereas the E_ϕ field component has terms proportional to $\cos\phi$ in addition to the terms independent of ϕ. A similar set of conditions applies for the magnetic field components, where H_θ and H_ρ have the same azimuthal dependence as E_ϕ, and H_ϕ has the same azimuthal dependence as E_θ and E_ρ. Together with the forms of the vector modes and the application of the appropriate boundary conditions existing on the ground plane, these azimuthal variations of the field components show that the fields radiated by the coaxial antenna can be represented fully by

$$\underline{E}(\rho,\theta,\phi) = \sum_{n=1}^{\infty} [a_{2n}\underline{^{m}e}_{\rho,0,2n}(\rho,\theta,\phi) + a_{2n-1}\underline{^{m}e}_{\rho,1,2n-1}(\rho,\theta,\phi)$$

$$+ b_{2n-1}\underline{^{n}e}_{\rho,0,2n-1}(\rho,\theta,\phi) + b_{2n}\underline{^{n}o}_{\rho,1,2n}(\rho,\theta,\phi)], \qquad (6.18)$$

and $\underline{H}(\rho,\theta,\phi) = \frac{jk}{\omega\mu}\sum_{n=1}^{\infty}[a_{2n}\underline{n}_{e,0,2n}(\rho,\theta,\phi) + a_{2n-1}\underline{n}_{e,1,2n-1}(\rho,\theta,\phi)$

$+ b_{2n-1}\underline{m}_{e,0,2n-1}(\rho,\theta,\phi) + b_{2n}\underline{m}_{o,1,2n}(\rho,\theta,\phi)]$, (6.19)

where the form of the vector modes are given in Appendix I, and the subscripts o and e denote odd or even functions of ϕ, respectively. From (6.18) and (6.19) the non-vanishing field components on the ground plane in the near field are

$$E_\theta = \sum_{n=1}^{\infty}\Big[\sin\phi\{-a_{2n-1}P^1_{2n-1}(0)h^{(2)}_{2n-1}(k\rho)$$

$$+ \frac{b_{2n}}{2(4n+1)}[2n(2n+1)P_{2n}(0)-P^{(2)}_{2n}(0)][(2n+1)h^{(2)}_{2n-1}(k\rho)-2nh^{(2)}_{2n+1}(k\rho)]\}$$

$$+ b_{2n-1}\frac{2(n+1)}{4n-1}P_{2n}(0)\,[(2n-2)h^{(2)}_{2n-2}(k\rho)-(2n-1)h^{(2)}_{2n}(k\rho)]\Big], \quad (6.20)$$

$$H_\phi = \frac{jk}{\omega\mu}\sum_{n=1}^{\infty}\Big[\sin\phi\{-\frac{a_{2n-1}}{4n-1}P^1_{2n-1}(0)[2nh^{(2)}_{2n-2}(k\rho)-(2n-1)h^{(2)}_{2n}(k\rho)]$$

$$-\frac{b_{2n}}{2}[2n(2n+1)P_{2n}(0)-P^2_{2n}(0)]h^{(2)}_{2n}(k\rho)\} - b_{2n-1}2nP_{2n}(0)h^{(2)}_{2n-1}(k\rho)\Big], \quad (6.21)$$

and

$$H_\rho = \frac{jk}{\omega\mu}\sum_{n=1}^{\infty}[a_{2n-1}\cos\phi\,2n(2n+1)P^1_{2n-1}(0)\,\frac{h^{(2)}_{2n-1}(k\rho)}{k\rho}$$

$$+ a_{2n}\,2n(2n+1)P_{2n}(0)\,\frac{h^{(2)}_{2n}(k\rho)}{k\rho}]. \quad (6.22)$$

Following the N.F.T. procedure the modal amplitudes and hence the complete radiation pattern can be determined from measurements performed on the tangential magnetic field components on the ground plane.

An inspection of (6.21) and (6.22) shows that the two azimuthal modes included in the field representation (m=0 and 1) are associated with different orthogonal radial modes. Hence, it is not necessary to separate the azimuthal modes by performing measurements of each component in both the $\phi = 0$ and $\pi/2$ directions. The a_{2n-1} and a_{2n} can be deduced with respect to a_1 from H_ρ component field measurements in the $\phi = 0$ direction, and the b_{2n-1} and b_{2n} can be deduced with respect to a_1 from H_ϕ component field measurements in the $\phi = \pi/2$ direction. Further from (6.21) and (6.22), in the directions $\phi = \pi/2$ for H_ϕ component and $\phi = 0$ for H_ρ component all the radial modes are included in the field representations, whereas in the directions $\phi = 0$ for H_ϕ component, and $\phi = \pi/2$ for H_ρ component, only even index radial modes are included. An application of the recurrence relations for the radial modes[134] to the elements of the matrices formed from the field representations (as occurs in the NFT), shows that when all radial modes are included, matrix elements in adjacent columns only differ by a factor $1/k\rho$, where ρ is the radius to the field point corresponding to the row of the matrix. When only the even index modes are present, adjacent elements differ by a factor $1/(k\rho)^2$. Thus, the latter matrix will be

better conditioned numerically than the former for the same matrix order.

The sets of a_{2n} and b_{2n-1} modal amplitudes can be determined with the maximum numerical accuracy from H_ρ measurements in the $\phi = \pi/2$ direction and H_ϕ measurements in the $\phi = 0$ direction, respectively. But since the NFT relies on relative field measurements, the two sets of magnetic field measurements must be normalized with respect to the same reference measurement for the b_{2n-1} to be determined in proper relation to the a_{2n}. The remaining sets of a_{2n-1} and b_{2n} modal amplitudes are found subsequently from H_ρ component measurements in the $\phi = 0$ direction and H_ρ component measurements in the $\phi = \pi/2$ direction, respectively. By separating the terms corresponding to the known modal amplitudes from those of the unknown modal amplitudes, the matrices to be inverted numerically in the solution for the a_{2n-1} and b_{2n} consist of the odd index radial modes only. Consequently, these matrices will be as well conditioned numerically as the even mode matrices discussed above.

To summarize, the determination of N complex modal amplitudes in the vector mode field representations (6.18) and (6.19) requires N total field measurements of the magnitude and phase of the H_ϕ and H_ρ field components on the ground plane. Performing measurements of H_ϕ in the $\phi = \pi/2$ direction and H_ρ in the $\phi = 0$ direction enables all N modal amplitudes to be determined from the numerical solution of two

matrix equations of order N/2. The numerical accuracy of this solution can be improved by measuring both field components in both ϕ directions, a technique which requires the numerical solution of four matrix equations of order N/4. This method also reduces the total computational time and effort, as the number of numerical operations involved in the inversion of a matrix of order m is proportional to m^3. Moreover, since each field point is used twice, once for each field component, only half the number of actual field points required in the first method are necessary to determine the same number of modal amplitudes.

6.33 Effects of aperture higher order modes.

By choosing the coaxial antenna waveguide dimensions so that only the dominant TEM and TE_{11} modes propagate freely and without attenuation, all the higher order modes excited in the aperture are evanescent. Apart from the dominant modes the lowest order modes present in the aperture are the TM_{01}, TM_{11}, and TE_{12} modes. Comparing the cutoff wavelengths of these modes with that of the TE_{11} mode shows that even these three modes are well into the cutoff region. Hence, all the excited higher order modes are strongly evanescent. The modes contribute, in particular, to the reactive field surrounding the aperture of the antenna, so that their effects on the radiation pattern are limited. Because of the similarity between the modal radiation patterns of the TE_{11} mode in the coaxial antenna and the TE_{11} mode

in the cylindrical waveguide, aperture antenna (see Chapter 4), an indication of the actual performance of the former can be gained from a comparsion with the radiation pattern of the latter, as derived by applying the N.F.T. It is apparent, therefore, that of all the higher order modes excited by the TE_{11} mode, the TE_{12} and TM_{11} modes alone will account for almost all of the differences between the actual radiation pattern of the coaxial antenna fed in the TE_{11} mode, and the TE_{11} modal radiation pattern plotted in Figure 6.1. Similarly, the differences between the actual radiation pattern of the coaxial antenna fed in the TEM mode, and the TEM modal radiation pattern plotted in Figure 6.1, will be caused almost entirely by the TM_{01} mode. By virtue of this similarity, it is anticipated that the radiation patterns of a practical coaxial antenna of comparable performance to the circular antenna discussed in Chapter 4, are likely to be of the forms shown in Figure 6.2.

Inside the waveguide section of the antenna, the excited higher order modes are confined to the immediate vicinity of the aperture. The modes, being strongly evanescent, have large attenuation constants so that penetration of reflected modes back into the waveguide region is limited. Hence, the most significant effect of the higher order aperture modes is on the aperture admittance of the antenna. The extent of this effect is difficult to estimate theoretically, because there is no definite knowledge of the true aperture

field distribution, and furthermore, the geometry of the practical coaxial antenna precludes an accurate theoretical analysis. In practice, aperture admittance effects must be accounted for experimentally.

6.4 Ground plane effects.

The radiation patterns of the flush mounted coaxial antenna on the ground plane provide only a single electric field component E_θ, due to the TEM mode. In most applications, this single field polarization will be sufficient, since for propagation directions close to the ground plane, only vertical polarized fields can propagate. However, in certain circumstances, notably when the antenna is elevated above the ground plane, or when the ground plane is imperfect permitting tangential electric field components to exist across its surface, horizontally polarized signals may be present for these propagation directions. To transmit or receive such signals, the coaxial antenna must be modified. By mounting the antenna above the ground plane, as shown in Figure 6.3, radiation will continue into the shadow regions below the aperture plane in the same manner as for dipole antennas mounted above a ground plane[135,136]. Raising the antenna also alters its impedance, and the optimum height must be found experimentally.

The modal radiation patterns calculated for the flush mounted antenna are not valid representations for the radiation from the raised antenna. The vector potential method used

in these calculations was based upon the boundary condition that tangential electric field components in the aperture plane were zero outside the aperture of the antenna. This condition does not apply to the raised antenna. It has been shown that the radiation patterns of aperture antennas not mounted in ground planes, and whose aperture dimensions are greater than a wavelength, can be predicted with reasonable accuracy by the approximate method of Silver, even for the shadow regions beyond the aperture plane[94,119]. Although this method is inconsistent, in that the far-field expressions when evaluated in the aperture plane do not reduce to the initially assumed boundary conditions (that is, all tangential field components are zero in the aperture plane outside the aperture itself), it gives a more accurate estimation of the modal radiation patterns for the raised antenna than does the vector potential method. However, full scale pattern measurements are necessary to specify the complete radiation patterns of the raised antenna.

6.5 Conclusion.

The usefulness of the coaxial antenna depends upon its ability to radiate at least two independent linear polarizations transverse to each direction of propagation. From the modal radiation patterns of the TEM and TE_{11} modes, it is apparent that by utilizing these modes the coaxial antenna fulfils the polarization requirement, with the proviso

noted in Section 6.4. The aperture higher order modes modify the shape of each modal radiation pattern but do not introduce any cross-polarization terms into the radiated field, since they have the same azimuthal dependence as the corresponding dominant mode. Hence, the control of the far-field polarization states of the actual antenna can be described in terms of the control exercised over the three dominant modes.

Although the radiation from the coaxial antenna can be specified completely by applying the N.F.T. discussed in Chapter 2, it is possible to estimate the radiation pattern by comparing this antenna with the cylindrical waveguide, aperture antenna. Extending the results of Chapter 4, the higher order modes present in the coaxial aperture having the most significant effect upon the antenna radiation patterns are the TM_{01} mode for the TEM modal pattern and the TE_{12} and TM_{11} modes for the TE_{11} modal pattern. Since the TM_{01} and TEM modal radiation patterns are similar, the pattern of the coaxial antenna supporting the TEM mode remains of the same form, whereas the pattern when the antenna supports the TE_{11} mode is similar to that given in Chapter 4. This first approximation to the aperture field can also be used in a variation formulation to estimate the antenna's aperture admittance. In practice, such a calculation is of limited value, since an actual antenna is likely to be of complicated geometry and design details must be acquired experimentally.

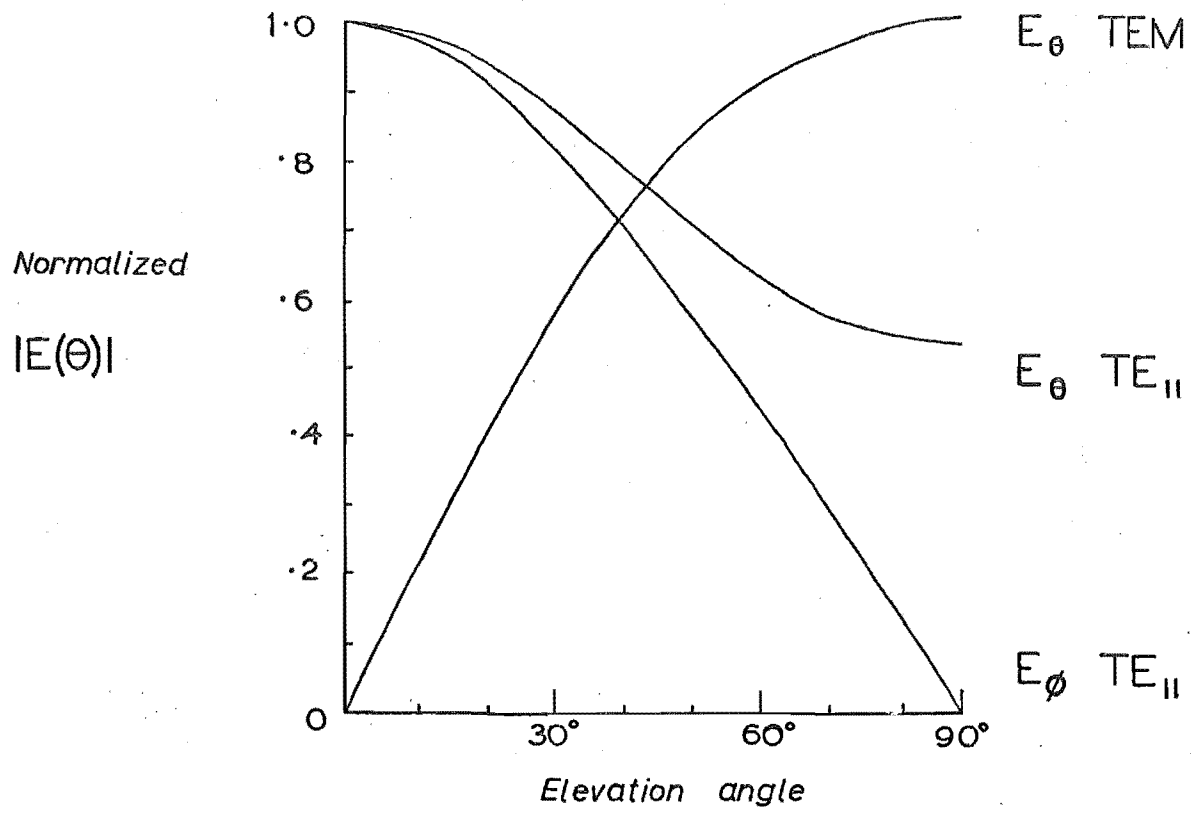

FIGURE 6·1 : MODAL RADIATION PATTERNS

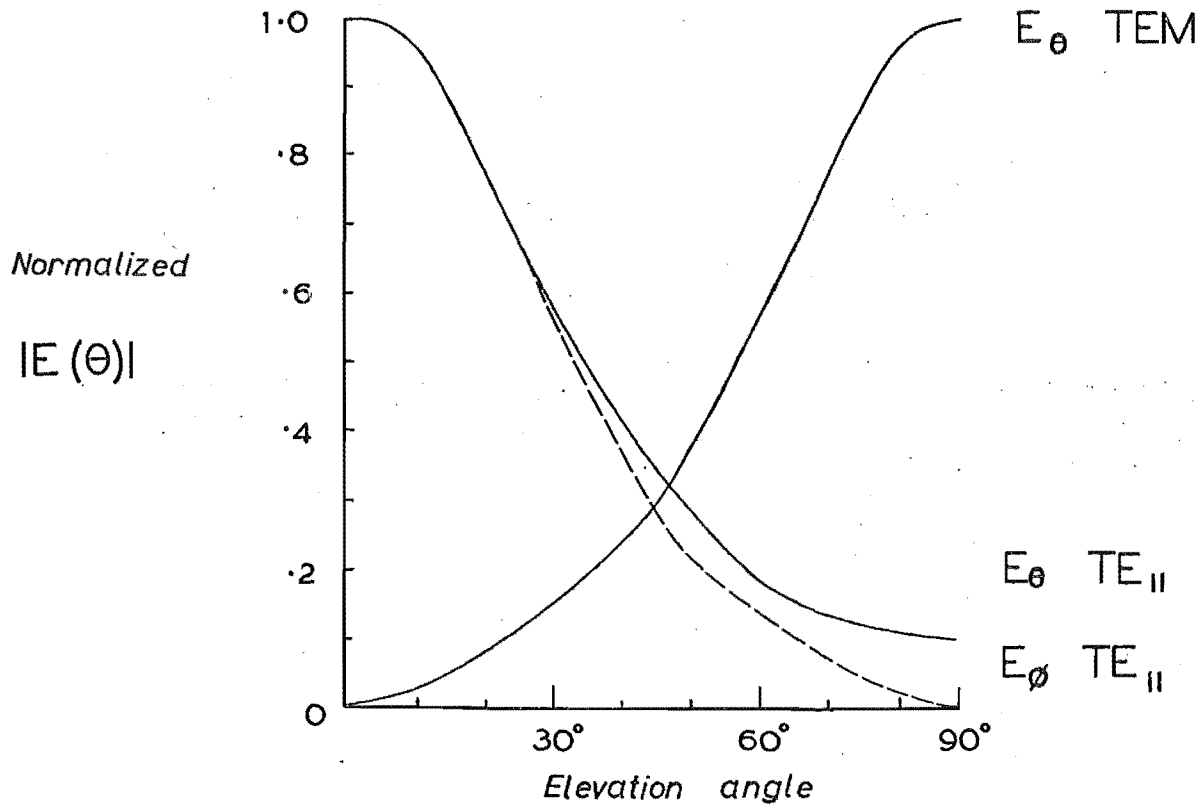

FIGURE 6·2 : ESTIMATED RADIATION PATTERNS

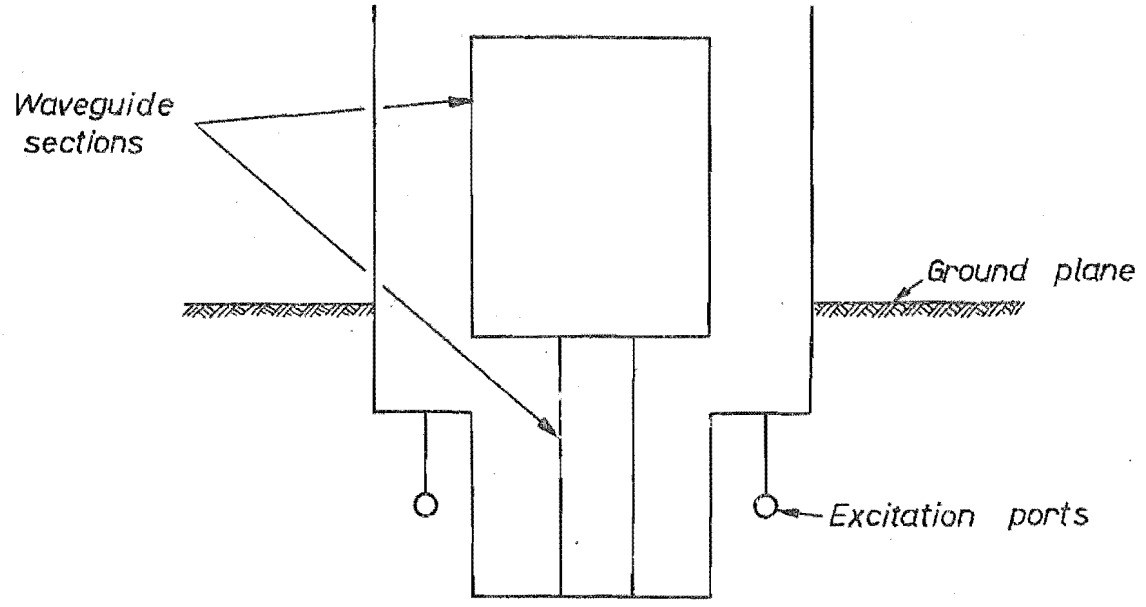

FIGURE 6·3 : RAISED COAXIAL ANTENNA

CHAPTER 7

System Design.

7.1 Introduction.

The system design was defined in Chapter 5 as that part of the total antenna design specifying the radiation and input characteristics of the antenna element together with the conditions subsequently imposed upon the associated control circuitry. The system consists of the generator or receiver, the antenna, and the inter-connecting feed circuitry which provides the means of control over the antenna's mode of operation. For convenience it is assumed that the antenna is matched to the feed circuitry, and consequently any matching networks required, will be regarded as part of the element design. This particular division is justified since the antenna input impedance is a function of the antenna design rather than of the circuitry design. Hence, the system design falls into two sections, the far-field radiation of the antenna, and the design of the feed circuitry extending from the transmitter or receiver to the input or excitation ports of the antenna. The design will be described from the perspective of a transmitting system, but by reciprocity it applies equally to a receiving system.

If the coaxial antenna is to be suitable for inclusion in a planar array, the optimally designed system must satisfy the design constraints outlined in Chapter 5. To comply with the maximum power condition, the total input power

to the system must be independent of the mode of operation of the antenna. This is equivalent to requiring the sum of the individual powers associated with each mode in the antenna to be constant and at the same time independent of which particular modes are excited at any given instant. Thus, provided the input power is independent of the feed circuitry parameters, the power condition will be satisfied. In an array application, the cost per element is largely determined by the complexity of the feed circuitry. If the array contains many elements, it is essential that the feed circuitry be as simple as the desired array performance will permit. The simplicity of the antenna excitation affects the circuitry design as well as the element design, and once again it is important, from a cost point of view, to operate with the simplest possible excitation configuration. Finally, the polarization diversity condition, defined as the capability of radiating at least two orthogonal linear polarizations transverse to any direction of propagation, should be satisfied. This is not as general a capability as being able to radiate any polarization state in any direction, but it is as useful in practice. Given signals in any two orthogonal polarizations, it is always possible to compute the signals which would have been transmitted in any other polarization state[105].

The polarization structure of the coaxial antenna will be discussed in relation to the fields of the dominant modes. It will be shown that in the design of the system circuitry to control these modes, the circuitry simplicity and the polarization diversity design constraints can not be satisfied simultaneously. Two compromise system designs will be presented. In the first system, the emphasis is placed on satisfying the former constraint, while the second system is designed in accordance with the latter constraint. The performance of these systems will be evaluated with special regard to the control exercised over the polarization states radiated by the antenna.

7.2 Polarization structure.

7.21 Polarization vectors.

The transformation of a set of right-handed, cartesian coordinate axes through the Euler angles[137] can be divided into three sub-transformations corresponding to the rotation about each individual axis. Each rotation is described by a matrix of the form

$$\begin{bmatrix} \cos\alpha & \sin\alpha \\ -\sin\alpha & \cos\alpha \end{bmatrix}, \tag{7.1}$$

where α is the angle of rotation. Combining matrices of this form, the complete transformation of the set of rectangular coordinate unit vectors $(\hat{\underline{x}},\hat{\underline{y}},\hat{\underline{z}})$ through the Euler angles (ϕ,θ,ψ) to give the set of unit vectors $(\hat{\underline{\xi}},\hat{\underline{n}},\hat{\underline{\zeta}})$, is described

by the matrix equation

$$\begin{bmatrix} \hat{\xi} \\ \hat{\eta} \\ \hat{\zeta} \end{bmatrix} = \begin{bmatrix} \cos\psi\cos\theta\cos\phi-\sin\psi\sin\phi & \cos\psi\cos\theta\sin\phi+\sin\psi\cos\phi & -\cos\psi\sin\theta \\ -\sin\psi\cos\theta\cos\phi-\cos\psi\sin\phi & -\sin\psi\cos\theta\sin\phi+\cos\psi\cos\phi & \sin\psi\sin\theta \\ \sin\theta\cos\phi & \sin\theta\sin\phi & \cos\theta \end{bmatrix} \begin{bmatrix} \hat{x} \\ \hat{y} \\ \hat{z} \end{bmatrix} \tag{7.2}$$

where the first rotation is through ϕ about the z axis, the second is through θ about the y axis, and the third is through ψ also about the z axis, and the positive direction of rotation is defined as in the sense of rotation of a right-handed screw. When compared with the spherical coordinate system, it is apparent that the Euler angles ϕ and θ are equivalent to the spherical azimuth and elevation angular coordinates, respectively. From (7.2) with ψ assumed zero, in a spherical coordinate system (ρ,θ,ϕ), $\hat{\xi}$ is the θ direction unit vector, $\hat{\eta}$ is the ϕ direction unit vector, and $\hat{\zeta}$ is the ρ direction unit vector.

Consider an arbitrary antenna radiating into space and located at the origin, 0. Then, in Figure 7.1, $\hat{\zeta}$ corresponds to a particular direction of propagation, and the vectors $\hat{\eta}$ and $\hat{\xi}$ correspond to the directions of two orthogonal, linear polarizations transverse to the direction of propagation and which describe the polarization state of a wave propagating in the $\hat{\zeta}$ direction. If the antenna is to be capable of transmitting or receiving any polarization state in any direction, then it must be capable of radiating two linear polarizations corresponding to the directions of $\hat{\xi}$ and $\hat{\eta}$ for all propagation

directions. From (7.2) it can be shown that for these polarization vectors to exist for all scan angles (that is all values of ϕ and θ), the antenna must radiate three independent polarizations parallel to $\hat{x}$, $\hat{y}$, and $\hat{z}$. For example, the fields radiated by three coincident and mutually perpendicular dipoles oriented in the $\hat{x}$, $\hat{y}$, and $\hat{z}$ directions, can be resolved into two linear polarizations transverse to any propagation direction.

The radiation patterns of the triple polarized coaxial antenna analysed in Chapter 6 show that this antenna is also capable of radiating the three required component polarization vectors. Each dominant mode excites higher order modes in the aperture. However, since these modes do not introduce cross-polarization terms into the radiation fields associated with this or any other dominant mode, the far-field polarization vectors are completely determined by the input signals to each dominant mode at the excitation ports of the antenna. Proper control of the relative strengths of the three dominant modes ensures that any arbitrarily polarized signal can be transmitted or received.

7.22 Polarization group structure.

To establish the existence of a group, certain conditions must be satisfied[138]. Rotational transformations about coordinate axes, as represented by (7.1) and (7.2), fulfil these conditions and form a rotation group, with respect to multiplication, for all values of the Euler angles,

modulo 2π. The angles ϕ and θ specify a particular propagation direction $\hat{\xi}$ of the field radiated by the antenna, and from the group structure of (7.2) with ψ assumed zero, there are two and only two transverse, linear polarization vectors associated with each $\hat{\zeta}$ direction. This is because with $\psi = 0$, each value of ϕ and θ in (7.2) uniquely determines the $\hat{\xi}$ and $\hat{n}$ directions as well as the $\hat{\zeta}$ direction.

The polarization state of the total aperture field determines the polarization state of the radiated field. Consider propagation in the $\hat{z}$ direction, and represent the directions of the polarization vectors corresponding to the aperture fields of the two TE_{11} modes by $\hat{x}$ and $\hat{y}$. With a general phase shift α between these vectors, the transverse polarization vectors in the far-field, $\hat{\xi}$ and $\hat{n}$, are as shown in Figure 7.2, where χ in general is a function of the Euler angles ϕ and ψ. The resultant electric field in the far-field is

$$\underline{E} = \hat{\xi}(ae^{j\alpha}\cos\chi + b\sin\chi) + \hat{n}(-ae^{j\alpha}\sin\chi + b\cos\chi) \quad (7.3)$$

and the general locus of (7.3) on any plane transverse to the propagation direction, is an ellipse of ellipticity dependent upon the ratio a:b. The orientation of the major axis with respect to the $\hat{\xi}$ direction is a function of α. For a=b, the limiting polarization states of (7.3) in the far-field is summarized in Table 7.1.

α	Polarization state
$-\pi$	linear
$-\pi/2$	left-handed circular
0	linear
$\pi/2$	right-handed circular
π	linear

Table 7.1: Polarization states for $\theta = 0$.

An elliptical polarization state results for all intermediate α values and also when the two component linear polarizations are not equal in magnitude. The polarizations corresponding to $-\pi < \alpha < 0$ form the left-handed polarization state subgroup, while those corresponding to $0 < \alpha < \pi$ form the right-handed polarization state subgroup. These subgroups are orthogonal, since a member of one is orthogonal with the equivalent member of the other sub-group. For example, if the two $TE_{1,1}$ modes are excited so that the antenna radiates a left-handed, circularly polarized wave in the $\underline{\hat{z}}$ direction, then a right-handed, circularly polarized wave incident upon the antenna from the $\underline{\hat{z}}$ direction will not be accepted.

The polarization state locii for all scan angles can be developed in a similar manner. In general, for each direction of propagation $\underline{\hat{\zeta}}$, the linear polarizations

radiated by the antenna in the $\hat{x}$, $\hat{y}$, and $\hat{z}$ directions will be resolved into two equivalent linear polarization components that are transverse to $\hat{\zeta}$. The relative strengths of these two components will then define the polarization locus corresponding to the particular direction of propagation.

7.3 System circuitry design.

The polarization versatility condition and the control circuitry complexity specification (see Section 5.1) are two of the more restrictive design constraints to be considered in the system design. It will be shown that, in fact, these are mutually opposing, so that a compromise design will be necessary. Two designs will be developed. In the first, the satisfaction of the circuitry specification will be emphasised, and in the second the compromise will favour the design of a system capable of complete polarization state control.

7.31 Simple four-port system.

Waveguide modes of propagation can be excited conveniently by either electric probes mounted parallel to the electric field of the mode, or magnetic probes whose loops are oriented in planes normal to the magnetic field of the mode[139]. The three dominant modes in the coaxial antenna are excited and detected by four such probes, equally spaced around the circumference of a cross-sectional plane of the antenna. The electric probes and the planes

of the magnetic loops are oriented radially. A complete discussion of the particular probe design will be delayed until Chapter 8, and for the present, it will suffice to regard the input terminals of the four probes as the input or excitation ports of the antenna.

If two signals of equal magnitude arriving at diametrically opposed probes from a common feed point, are in phase with each other, then the TEM mode is excited, and conversely if the signals are exactly out of phase, the TE_{11} mode is excited. For the reciprocal condition of reception, only those signals at the probes which are in phase will be passed onto the receiver by the probes phased for TEM mode excitation. Similarly, only out of phase signals will be detected by the receiver coupled to the probes phased for TE_{11} mode excitation. To excite the third mode, a variable phase shifter is placed in the feed line connected to the input port of one of the two probes exciting the TEM mode. Varying the phase shift continuously between zero and π radians controls the relative magnitudes of the modes excited by this set of probes from solely TEM mode corresponding to zero phase difference, to TE_{11} mode corresponding to π radians phase difference.

To achieve as simply as possible complete independent control of the relative strengths of the signals fed to the input ports, the two sets of probes are connected to the sum and difference output arms of a ring hybrid[140],

as shown in Figure 7.3. The generator signal is divided equally between the two channels of equal electrical length which feed the input ports of the hybrid. One channel contains a variable phase shift α. When $\alpha = 0$ the two equal input signals add in the sum output port and exactly cancel in the difference output port, since the electrical path lengths from each input port to the sum port are equal, and, to the difference port, are different by a half a wavelength. When $\alpha = \pi$ the signals cancel in the sum port and add in the difference port. Intermediate values of α divide the input signals proportionately between the two output ports, and hence between the two sets of probes.

With reference to Figure 7.3, probes 1 and 3 excite the TE_{11} mode oriented in the $\hat{x}$ direction while probes 2 and 4 excite the TE_{11} mode oriented in the $\hat{y}$ direction. The phase shifters γ and δ placed in the feed lines to the input ports of probes 1 and 4, are adjusted so that either probes 1 and 3 or probes 2 and 4 excite the TEM mode. At any given instant the TEM mode is excited by only one set of probes. Thus, γ and δ are restricted to the ranges,

$$\begin{aligned} &\text{(i)} \quad \delta = \pi \quad , \quad \text{for } 0 \leq \gamma < \pi \\ &\text{(ii)} \quad 0 \leq \delta \leq \pi, \quad \text{for } \gamma = \pi \end{aligned} \qquad (7.4)$$

The relative magnitudes of all three modes are controlled by the α, γ, and δ phase shifters, and the relative phase of the signals fed to each set of probes is controlled by the

β phase shifter. However, when probes 1 and 3 excite both the TEM and TE_{11} modes, the value of γ determines the phase as well as the magnitude of the TEM mode with respect to the $\hat{x}$ direction oriented TE_{11} mode. Similarly, when probes 2 and 4 excite both TEM and TE_{11} modes, δ determines both the magnitude and phase of the TEM mode with respect to the $\hat{y}$ direction oriented TE_{11} mode. The phases of the modes excited by the same probes, therefore can not be specified independently of their relative magnitudes. The modes excited by one set of probes can be fully controlled with respect to the mode excited by the other probes, since the signals fed to each set of probes are fully controlled in both magnitude and phase. Because there is only limited provision for independent phase and magnitude control between the three modes, the relative strengths of the far-field polarization vectors associated with these modes are correspondingly interdependent, and the polarization states for each scan angle can not be chosen arbitrarily.

The principal feature of the system circuitry shown in Figure 7.3 is that it is the simplest possible design consistent with independent control of the signals fed to the input ports of the probes. But because of the inherent limited control of the relative modal strengths, the polarization versatility of the system is restricted.

7.32 Modified system.

Complete satisfaction of the polarization requirement discussed in Section 5.1 can be obtained for the coaxial antenna at the cost of increased complexity of the feed circuitry. Thus, the sum output port of the ring hybrid in the simple four-port system is connected to the set of probes exciting the $\hat{x}$ direction oriented TE_{11} mode, and the difference output port is connected to a feed line, which in turn feeds an additional ring hybrid. The difference port signal from the first hybrid then divides equally between the two input channels of the second hybrid, and a variable phase shifter γ, in one channel, controls the relative output signals in the sum and difference ports of this hybrid. The sum port is connected to a set of probes exciting the $\hat{y}$ direction oriented TE_{11} mode, and the difference port is connected to a set of probes exciting the TEM mode. Each mode, therefore, is excited by a separate set of probes.

The two phase shifters β and δ are placed in the respective sum output lines of each hybrid, as shown in Figure 7.4, to control independently the relative phases of the signals exciting the three modes. The two phase shifters α and γ then completely control the relative magnitudes of the three signals, so that the relative strengths of the three modes in the antenna can be varied continuously over all values. Hence, these four phase shifters, fully control

the relative strengths of the far-field polarization vectors, permitting the coaxial antenna to transmit or receive arbitrarily polarized signals for all scan angles, within the bounds imposed by the radiation patterns discussed in Chapter 6.

Although the complexity of the feed circuitry has been increased in this system, the simplicity of the four probe excitation of the antenna can be maintained by utilizing the same probes for the excitation of both the TEM mode and the $\hat{y}$ direction oriented TE_{11} mode. Introducing a further ring hybrid and feeding the TE_{11} mode signal into the difference port and the TEM mode signal into the sum port, gives complete isolation between the two input channels. The TE_{11} mode signals divides equally in magnitude between the two remaining ports but with the signal appearing at one port lagging the signal at the other port by π radians. Similarly, the TEM mode signal divides equally, providing output signals of equal magnitude and in phase with each other. The two output ports are connected to the two probe ports.

To recapitulate, the modified system enables the coaxial antenna to satisfy the full polarization versatility design specification by increasing the complexity of the system circuitry. Moreover, the simple four probe excitation of the antenna can be maintained at the cost of additional circuit elements. The alternative method of excitation requires six probes, that is, a set of two probes per mode, which significantly increases the complexity of the antenna element design

problem.

7.4 System performance.

7.41 Maximum power condition.

The power absorbed from the generator is the sum of the powers associated with each mode in the antenna. Each modal power is a function of the values of the phase shifters controlling the modal magnitudes. In the simple system, the α phase shifter determines the power of the signals fed to each set of probes, and the γ and δ phase shifters determine the respective modal powers. The α and γ phase shifters in the modified system completely specify the modal powers, such that when $\alpha = 0$ all the generator power is absorbed in the TE_{11} mode oriented in the $\hat{x}$ direction, while for $\alpha = \pi$ the power is divided between the TEM mode and the $\hat{y}$ direction oriented TE_{11} mode, depending upon the particular value of γ.

By allowing for the phase shifts in the input signals fed into a ring hybrid due to the different electrical path lengths around the device, it can be shown that the magnitudes of the two output port signals are proportional to,

$$\text{(i)} \quad \sin\frac{\nu}{2} \quad \text{- for the sum port} \qquad (7.5)$$

$$\text{(ii)} \quad \cos\frac{\nu}{2} \quad \text{- for the difference port}$$

where ν is the variable phase shift in one input channel. The power associated with each output signal is proportional

to $\sin^2(\nu/2)$ and $\cos^2(\nu/2)$, respectively, so that the total output power from the hybrid is a constant independent of ν. In the simple system, since the input power to the set of probes exciting both the TEM mode and one of the TE_{11} modes is not dependent upon the settings of the γ or δ phase shifters, the total input power to the system is constant for all phase shifter settings. Similarly, the power absorbed from the generator by the modified system is independent of the three particular modal powers. The constant power absorbed by each system will be the maximum power deliverable by the generator, provided that the system circuitry is matched to the generator impedance.

The maximum power condition of the system design specification is satisfied completely by each of the feed circuitry systems described above. Also the refinement to the modified system, permitting the retention of the four probe excitation of the antenna, by introducing a zero or π radian phase shift only, does not affect the power absorbed by the system.

7.42 Polarization state control.

Control of the far-field polarization state is achieved by the individual control of the component, linear, polarization vectors. The relative strengths of these two component vectors are directly related to the strengths of the three dominant modes in the antenna, which in turn are determined by the system circuitry. With all three modes excited,

the general electric field components at a point in the far-field are as shown in Figure 7.5. The field component parallel to the $\hat{p}_x$ direction is the radiation field due to the $\hat{x}$ direction oriented TE_{11} mode. As shown in Chapter 6, this field has in-phase components in the $\hat{\theta}$ and $\hat{\phi}$ directions which combine to give a single linear polarization vector in the $\hat{p}_x$ direction determined by the relative magnitudes of the two components. Since these magnitudes are different functions of azimuth angle ϕ, the direction of $\hat{p}_x$ also varies with ϕ. For $\phi = 0$ $\hat{p}_x$ is parallel to the $\hat{\theta}$ direction, whereas when $\phi = \pi/2$, $\hat{p}_x$ is parallel to $\hat{\phi}$. The phase shifter settings of the system circuitry determine the magnitude a and the phase factor $\exp(j\alpha')$. Similarly, the field component parallel to $\hat{p}_y$ is the radiation field due to the $\hat{y}$ direction oriented TE_{11} mode. As before, c and γ' are set by the system circuitry. The field component parallel to the $\hat{\theta}$ direction is the radiation field due to the TEM mode. This component is always parallel to $\hat{\theta}$, since the TEM mode radiation field has only a single E_θ component which is independent of azimuthal angle. Once again, the magnitude and phase of this field component are functions of the mode radiation pattern and the system circuitry settings. Hence, the resultant electric field at a point in the far-field is

$$E = \hat{\theta}(ae^{j\alpha'}\cos\nu + be^{j\beta''} + ce^{j\gamma''}\cos\chi) + \hat{\phi}(-ae^{j\alpha''}\sin\nu + ce^{j\gamma''}\sin\chi) \tag{7.6}$$

where ν and χ specify the directions of $\hat{p}_x$ and $\hat{p}_y$, respectively, with respect to $\hat{\theta}$. This expression is of the same

form as (7.3), and for $\theta = 0$, (7.6) in fact reduces to (7.3). The locus of (7.6) on any plane transverse to the direction of propagation is an ellipse dependent upon the relative strengths of the three component fields.

It has been shown that the polarization capability of the simple four-port system is limited. When both TE_{11} modes are excited, since each mode is fed from a different set of probes, the magnitude and phase of each mode are controlled independently, and in the far-field all polarization states are available. However, because the radiation field due to the TE_{11} mode tends to zero for both field components as $\theta \to \pi/2$, the magnitude of the resultant far-field polarization approaches zero for directions close to the ground plane. When all modes are excited, for these directions the far-field polarization state approaches vertical linear, which is the component due to the TEM mode. In the remaining directions for which all modes contribute, only particular elliptical states are available. The system circuitry provides full control of the relative magnitudes of the three component linear polarizations, but the phases are partially dependent upon the magnitudes, as discussed in Section 7.3. From the circuitry of this system, for each value of b in (7.6) there corresponds a particular value for each of c, β', and γ', when probes 2 and 4 excite the TEM and TE_{11} modes simultaneously. Similarly, when both modes are excited by probes 1 and 3, each value of b determines the values of a, α', and β'. For each value of the relative

magnitudes, therefore, the only independent phase variations are those due to α' in the former and γ' in the latter. Inspection of (7.6) shows that these are insufficient to provide complete phase variations of the far-field polarization vectors. This means that, corresponding to each magnitude ratio, only a limited range of polarization states is possible with this system.

The far-field polarization state performance of the simple four-port system is summarized in Table 7.2. The modal fields are the dominant modes excited in the antenna and the subscripts x and y denote the orientation of the TE_{11} mode, whether parallel to the $\hat{x}$ or $\hat{y}$ directions, respectively.

Elevation angle	Azimuth angle	Modal fields	Polarization states
$\theta=0$	-	$(TE_{11})_x$ & $(TE_{11})_y$	All states
$0 < \theta < \pi/2$	$0 \leq \phi \leq 2\pi$	$(TE_{11})_x$ & $(TE_{11})_y$	All states but decreasing magnitude
$0 < \theta < \pi/2$	$0 \leq \phi \leq 2\pi$	All modes	Restricted elliptical states
$\theta = \pi/2$	$0 \leq \phi \leq 2\pi$	TEM	Vertical linear.

Table 7.2: Polarization state control of the simple four-port system.

The polarization state capability of an antenna in particular directions of propagation can be recorded conveniently by mapping the surface of the polarization sphere[141] onto its upper and lower equatorial planes. The upper plane corresponds to the left-handed polarization group whilst the lower plane corresponds to the right-handed polarization group. As an example, the polarization states associated with the radiation from the TEM and $\hat{y}$ direction oriented TE_{11} modal fields in the $\phi = 0$ plane are plotted in Figure 7.6. In plotting these as functions of the elevation angle, it is assumed that the individual component magnitudes are given by the modal radiation patterns discussed in Chapter 6. This requires the system circuitry settings to be such that equal signal strengths are radiated by both modes in their respective directions of maximum radiation. Continuous variation of the circuitry elements controlling the phase of each component polarization ensures that all polarization states corresponding to each magnitude ratio are available. By varying the magnitude as well as the phase of these signals, all polarization states are available for all elevation scan angles, with the exception that the limiting values of $\theta = \pi/2$ and $\theta = 0$ permit only vertical and horizontal linear polarization states, respectively. Also for scan angles close to these directions, the sensitivity of the polarization state control is correspondingly limited.

The polarization state diversity of the modified system is complete, since the input signals associated with each far-field component polarization are fully controllable in both magnitude and phase. Not only are these signals de-coupled from each other, but also the magnitude and phase of each signal are unrelated. The far-field polarization state performance of the modified system is summarized in Table 7.3.

Elevation angle	Azimuth angle	Modal fields	Polarization states
$\theta = 0$	-	$(TE_{11})_x$ & $(TE_{11})_y$	All states
$0 < \theta < \pi/2$	$0 \leq \phi < 2\pi$	All modes	All states
$\theta = \pi/2$	$0 \leq \phi \leq 2\pi$	TEM	Vertical linear

Table 7.3: Polarization state control of the modified system.

As for the simple system, in the propagation directions close to the ground plane, the polarization states approach vertical linear as the horizontal components progressively approach zero. Furthermore, if only one TE_{11} mode is excited together with the TEM mode, the limiting polarization state in the $\theta = 0$ direction is horizontal.

7.5 Discussion.

The most important system design constraints were deemed to be the maximum power condition, the minimum circuit complexity condition, and the requirement for full

polarization state versatility. Both the systems considered satisfy the first constraint entirely, but it has been demonstrated that the second and third constraints are mutually exclusive to the extent that they can not be fulfilled simultaneously. Each system is a compromise solution to the design problem, with the simple four-port system meeting the requirements of the first and second constraints, whereas the modified system satisfies the first and third constraints at the cost of the second.

The circuitry shown in Figure 7.3 is the simplest system permitting independent control of the signals fed to each set of probes. Although the relative strengths of the modes excited by the same probes are not independent, the degree of control over the resultant far-field polarization states that is obtained for the whole system is adequate for many array applications. Frequently, the actual polarization state of a signal need not be known, as it is sufficient to adjust the system parameters to maximise the strength of the signal. In such instances the simple system would be preferred, especially if the antenna is in an array involving a large number of elements.

Complete polarization versatility demands an increase in the complexity of the system circuitry, and the simplest circuitry consistent with this requirement is the modified system shown in Figure 7.4. As a direct consequence of the need to isolate each input signal, the three modes are excited by three separate pairs of probes. Further extension of the circuitry permits the four probe excitation of the antenna to be retained, while preserving the independence of the control over the three input signals. But because of the significantly greater cost per element when compared with the simple system, the modified system in either the six or four probe configuration, would not be considered for use in a large array application. The system is useful, however, when the antenna is required to radiate a specified polarization or detect the particular polarization of an incoming signal. Examples of such applications include polarization sensitive radar scattering measurements[142], and radar measurements of propagation path magneto-ionic effects[143].

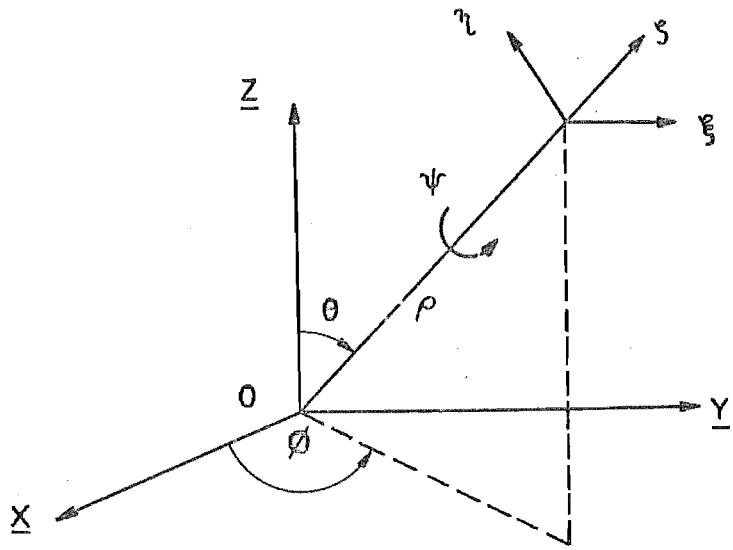

FIGURE 7·1 : COORDINATE TRANSFORMATION

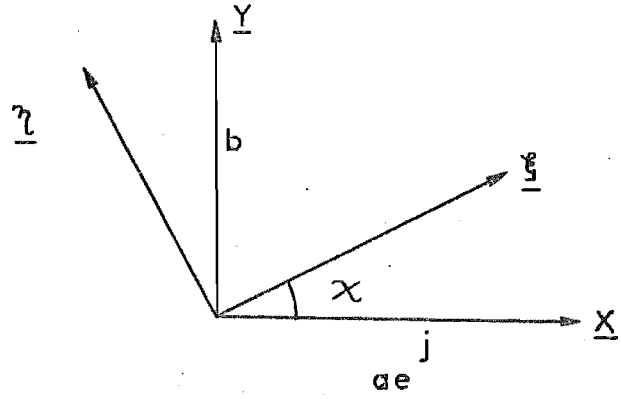

FIGURE 7·2 : POLARIZATION STATE REPRESENTATION

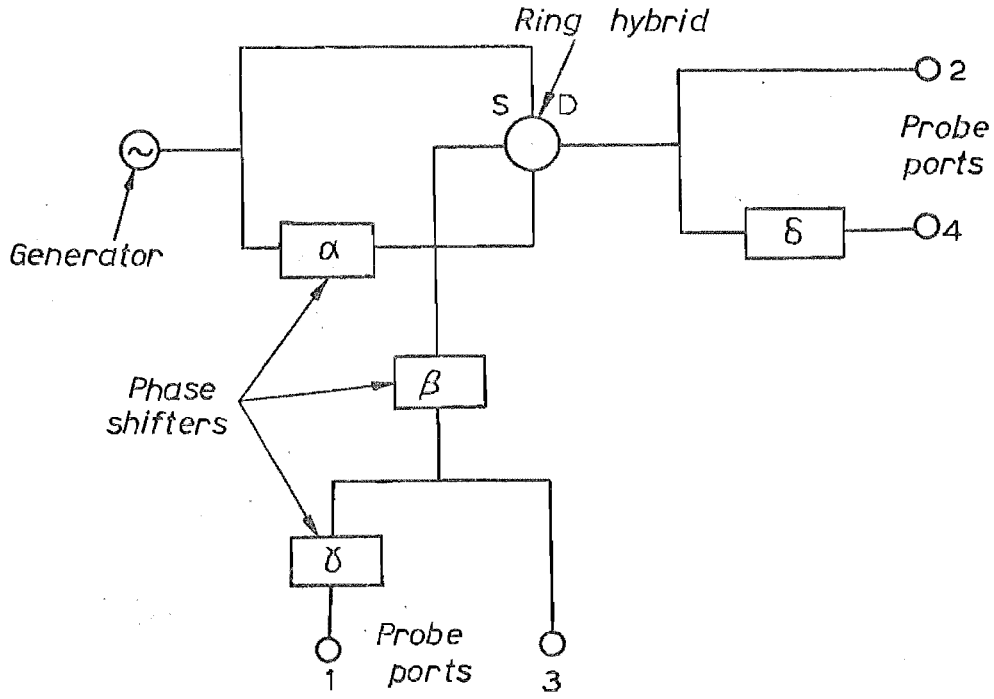

FIGURE 7·3 : SIMPLE FOUR PORT SYSTEM CIRCUITRY

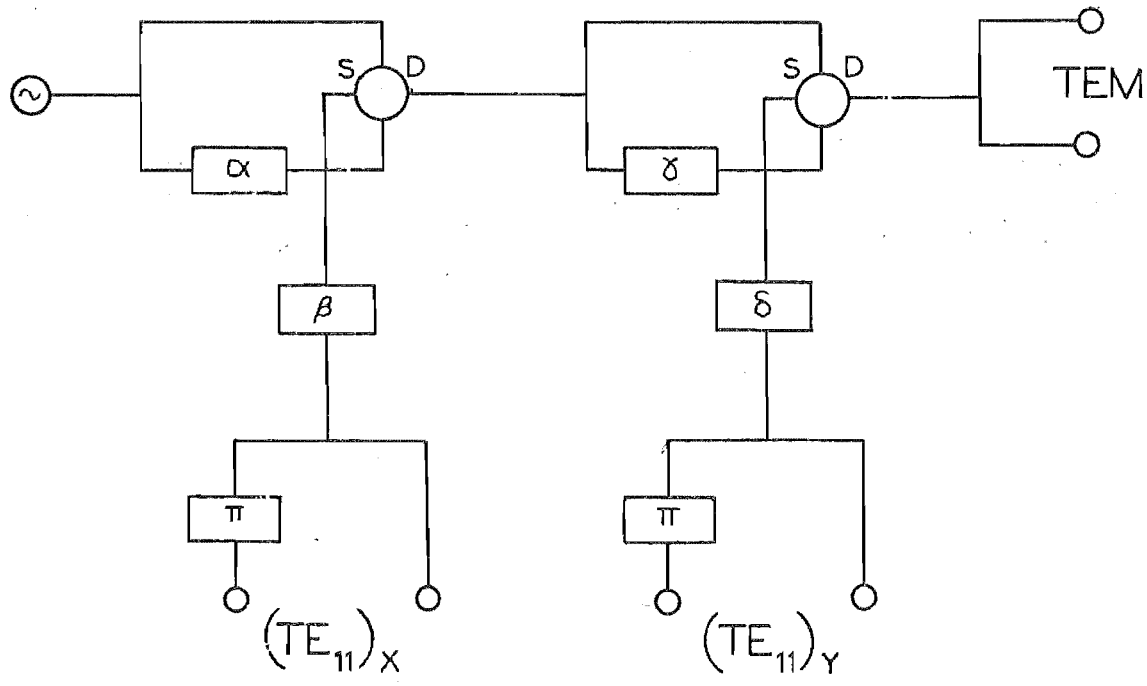

FIGURE 7·4 : MODIFIED SYSTEM CIRCUITRY

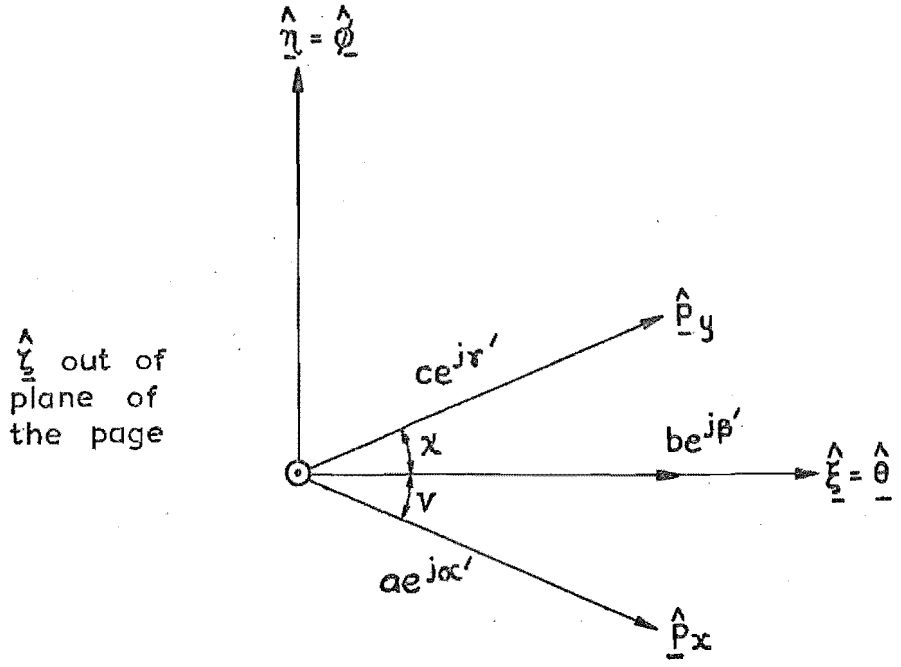

FIGURE 7·5 : POLARIZATION STATE CONTROL

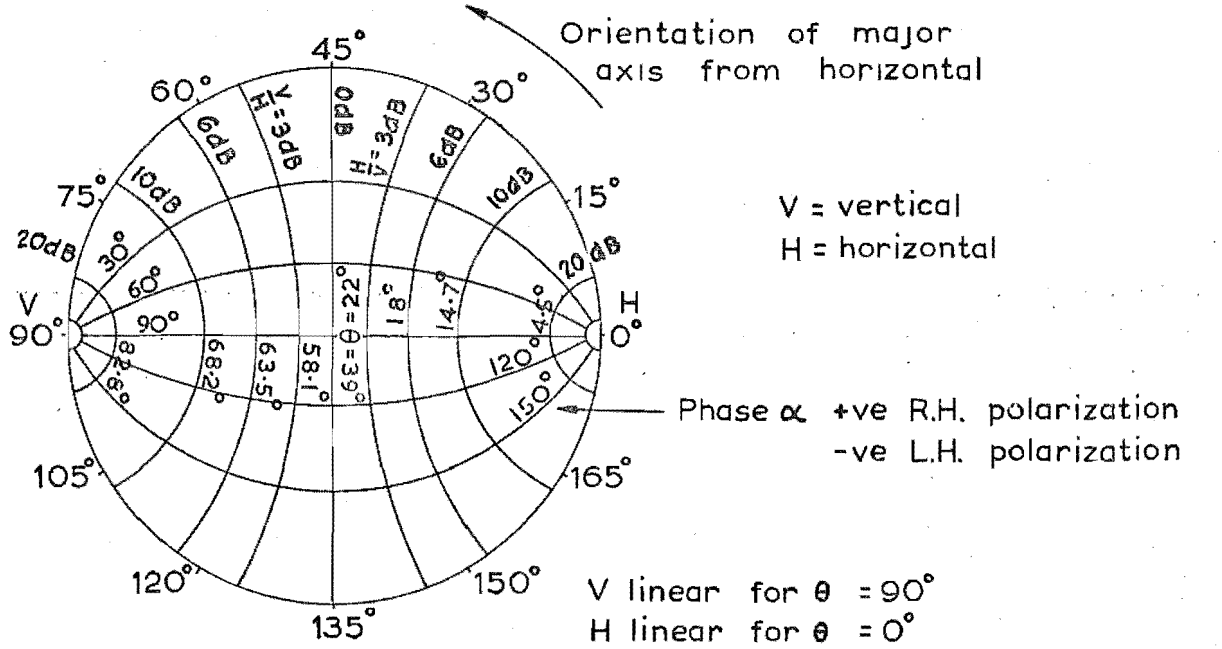

FIGURE 7·6 : POLARIZATION CHART

CHAPTER 8

Element Design.

8.1 Introduction.

In Chapter 5, the element design was defined as that part of the total antenna design specifying the electrical and mechanical parameters of the element. For the coaxial antenna this includes the design of the waveguide sections supporting the necessary TEM and TE_{11} modes, the choice and design of the excitation method for these modes, and the design of any required matching networks. The coaxial antenna can be considered as having input ports corresponding to the signals fed to each dominant mode, and output ports corresponding to the radiation fields associated with each mode. In general, mutual coupling will occur between these various ports. The element design must therefore attempt to eliminate, or at least compensate for, their effects. Hence, the element design falls into three distinct sections, the waveguide design, the method of excitation and probe design, and finally, the design of the compensation networks. Once again, the design will be described in terms of a transmitting antenna, but it applies equally to a receiving antenna.

The complexity of the coaxial antenna design limits the application of analytical techniques, and it is more convenient to derive the optimum design experimentally.

This design is based upon measurements performed on a prototype L-band coaxial antenna, flush mounted in a nine wavelengths square ground plane.

The design constraints outlined in Section 5.1 will be applied to the design of the coaxial antenna. In particular, the requirement for compatibility with an array environment and a predetermined array performance, will be shown to constrain the waveguide design by imposing maximum and minimum restrictions on the antenna aperture dimensions. The design specification for the probes derives almost entirely from the bandwidth condition requiring efficient operation over the frequency band considered. By specifying the input match, this condition also defines the required performance of the compensation networks. Because of the constraint restricting the complexity of the antenna excitation method, the optimum element design will be developed principally for the four probe system considered in Chapter 7. However, a qualitative description of the design for the alternative six probe system will be presented. Considerable attention will also be focussed on the effects of cross-coupling between the antenna input ports. The detrimental effects on the antenna performance will be discussed, and the design of compenation networks will be given. Finally, the overall performance of the coaxial antenna will be evaluated specifically with relation to the bandwidth condition.

8.2 The waveguide design.

In the coaxial antenna two types of mode propagate, the TEM mode and the two space orthogonal TE_{11} modes. To provide an independent tuning facility for the TEM mode, the antenna has been designed in two principal sections linked by a short transitional section of waveguide, as shown in Figure 8.1. In the main section both types of mode propagate freely, but in the tuning section only the TEM mode can propagate. By varying the length of the tuning section, extra tuning of the TEM mode can be achieved independently of the other two dominant modes.

Analytical techniques have been developed to evaluate the admittances of step discontinuities in coaxial waveguide[144-146], but have dealt with structures supporting the TEM mode as the sole dominant wave. The coaxial antenna, however, is multimodal with three dominant modes. To accurately estimate the effects of waveguide steps that are electrically close to each other, requires that there be negligible coupling between the discontinuities. In the coaxial antenna, the transition section not only contains two closely spaced steps which excite, at least in part, the same higher order modes, but is also further complicated by the presence of the excitation probes. Hence, the optimum dimensions of each waveguide section can be derived most conveniently by experimentation.

8.21 The main section.

Apart from the need to discriminate against the undesirable higher order modes, the most important feature of the main section design is the choice of the aperture dimensions. If the TEM and TE_{11} modal aperture fields are to radiate efficiently, then the aperture diameter cannot be very much less than a wavelength[106]. Conversely, in order to inhibit the incidence of grating lobes when the antenna is included in an array the maximum aperture dimension should not exceed half a wavelength. The most reasonable design compromise is to choose the diameter to be half a wavelength. This permits the respective radiation efficiences to remain substantially unaltered, as is apparent from the radiation expressions developed in Chapter 6. Furthermore, the radiation patterns corresponding to each mode are significantly broader for the half wavelength diameter aperture than for a full wavelength diameter aperture, thus giving a more complete coverage of the radiated half space.

After considering the cutoff wavelengths for the various modes, the diameter of the inner conductor was chosen as a quarter of a wavelength. With an outer conductor diameter of half a wavelength, all modes except the TEM and TE_{11} modes are strongly evanescent in this region. The higher order modes in this section are generated by the discontinuities at the aperture and at the waveguide step junction to the tuning section. In Chapter 6 it was shown

that, because of the aperture symmetry, the aperture higher order modes have the same field symmetries as the dominant modes exciting them. Hence, the excited modes are the TM_{0n}, TM_{1n} and TE_{1n} modes. Invoking the same symmetry argument, the modes excited at the circularly symmetric step junction will also be the TM_{0n}, TM_{1n} and TE_{1n} modes. The characteristics of the dominant modes and the lowest order evanescent modes of each type, present in the main section are summarized in Table 8.1.

Dominant mode	Phase constant	Guide wave-length	Evanescent mode	Attenuation constant	Cutoff wave-length
TEM	0.314 rad/cm	20cm	TM_{01}	10.5 dB/cm	5.03cm
TE_{11}	0.159 rad/cm	39.45cm	TM_{11}	10.55 dB/cm	4.91cm
			TE_{12}	11.07 dB/cm	4.79cm

Table 8.1: Mode characteristics in main waveguide section (frequency of operation = 1.5 GH_z).

In most applications, for reasons of economy and convenience, it will be desirable to keep the coaxial antenna as physically small as possible. While this limits the overall length of each waveguide section, the main section must still be of sufficient length to prevent the higher order modes excited at one discontinuity, from coupling with similar modes excited at the other discontinuity. If the section

is too short, the strengths of the evanescent modes increase with respect to the strengths of the dominant modes. Since more of the incident energy is then coupled to the reactive fields in the antenna, the input impedance match is degraded, and since the aperture field distribution is also altered, the radiation pattern of the antenna is modified.

By choosing the length of the main section to be half a wavelength, virtually complete isolation is obtained for even the lowest order evanescent mode. However, to allow for the mounting of the probes and the transition to the tuning section, the outer conductor extended further than the inner conductor. The optimum overall length of this section, which was chosen in conjunction with the probe design, was derived experimentally. A discussion of the basis of this experiment will be delayed until Section 8.3.

8.22 The tuning section.

To minimize the effects of the step junction discontinuities, the characteristic impedances of the two waveguide sections should be identical. However, the main section is multimodal, and, rather than having a single characteristic impedance, it has a wave impedance associated with each dominant mode. The tuning section supports the dominant TEM mode only, so that its characteristic impedance is the wave impedance of the TEM mode. This will be matched to the wave impedance of the TEM mode in the main section, provided the conductor radii ratios are the same for both sections.

With the 2:1 radii ratio in mind, an examination of the cutoff wavelengths of the modes led to the outer conductor diameter being chosen as a quarter of a wavelength. The lowest order evanescent modes present in this section are then the TE_{11} and TM_{01} modes whose salient characteristics are summarized in Table 8.2.

Evanescent mode	Attenuation constant	Cutoff wavelength
TE_{11}	3.83 dB/cm	11.6 cm
TM_{01}	21.53 dB/cm	2.51 cm

Table 8.2: Mode characteristics in tuning section.

As with the main section, the overall length of the tuning section was optimized experimentally. The dependence of the input impedance of the excitation probes upon the length parameters of both sections will be discussed in Section 8.3.

8.23 The transition section.

For this section the outer conductor diameter was half a wavelength and the inner conductor diameter was an eighth of a wavelength. In a coaxial waveguide of these dimensions only the TEM mode can propagate freely. The symmetry of the region ensures that in addition to the TEM mode the higher order TM_{0n}, TM_{1n} and TE_{1n} modes are present. The TE_{11} mode is the lowest order evanescent mode, and with a small

attenuation constant is just beyond cutoff. Hence, more power must be supplied to the TE_{11} mode at excitation than to the TEM mode if these two modes are to radiate equal power. To prevent excessive loss of the energy associated with the TE_{11} mode, it is essential that the transition section be kept as short as possible. As mentioned previously, this length was determined by experiment. The characteristics of the lowest order evanescent modes are summarized in Table 8.3. It is apparent that apart from the TE_{11} mode, all higher order modes are strongly evanescent within this region.

Evanescent mode	Attenuation constant	Cutoff wavelength
TE_{11}	0.84 dB/cm	19.11 cm
TM_{01}	6.57 dB/cm	7.67 cm
TM_{11}	7.23 dB/cm	7.06 cm
TE_{12}	8.25 dB/cm	6.28 cm

Table 8.3: Mode characteristics in transition section.

The complete waveguide design for the coaxial antenna operating at a frequency of 1.5 GHz is given in Figure 8.1.

8.3 Probe design.

8.31 Method of mode excitation.

In Chapter 7 it was shown that the three dominant modes in the coaxial antenna can be excited equally well by four electric or magnetic probes. To excite the modes the electric probes are aligned in the direction of the predominant electric field polarization of each particular mode. For the TEM and TE_{11} modes, therefore, the probes are oriented in the radial direction, with the probe port mounted on the outer conductor of the main waveguide section. Conversely, the magnetic loop probes are oriented so that the plane of the loop is transverse to the direction of the magnetic field of each mode. For the TEM and TE_{11} modes the plane of the loops is radially directed with the probe ports mounted on either the main section outer conductor or the rear wall of the main section. The latter mounting, in conjunction with the use of a non-contacting short circuit plunger[147] as the rear wall, permitted the length of the main section to be varied in a simple and continuous manner. Furthermore, if the probes are mounted on the outer conductor side walls, it is necessary to optimize both the length of the main section, and also the spacing of the probes in front of the rear wall[37] Since continuous variation of this spacing is not possible without major modifications to the antenna, the rear wall mounted magnetic loop probes were chosen as the method of mode excitation.

8.32 Magnetic loop probe impedance.

The optimum probe design was derived experimentally in conjunction with the optimum waveguide design, upon the basis of the input impedance match of an individual probe with all remaining probes correctly terminated. The resistive component of the input impedance represents the power radiated into the antenna and propagating away from the probe in the dominant modes, whereas the reactive component represents the time average reactive energy stored in the antenna. Reactive energy is associated with the standing wave patterns of the dominant modes in the waveguide sections, so that the dominant modes as well as the evanescent modes contribute to the reactive component. By tuning the lengths of each waveguide section (facilitated by incorporating non-contacting short circuit plungers in the original design), the standing wave patterns are adjusted, until the reactive energy associated with the dominant modes cancels, at least in part, with the reactive energy of the evanescent modes.

For an electrically small probe with diameter less than a quarter of a wavelength, the self-inductance of the probe, due to the flux linkage resulting from the magnetic field excited by the probe current itself, predominates over the inductive effect of the evanescent modes[148]. Varying the length of the tuning section affects the TEM mode only, since the evanescent modes decay to negligible values at the short circuit position, while varying the

length of the main section effects principally the TEM and TE_{11} modes. Thus, the section lengths are tuned until the reactive energy of the dominant modes becomes capacitive and cancels with the inductive energy corresponding to the self-inductance of the probe, which, to a first order, remains independent of the lengths of the waveguide sections.

8.33 Grounded and capacitive loaded loop probes.

Two types of loop probes were investigated for the coaxial antenna. These were the grounded loop and the capacitive loaded loop as shown in Figure 8.2. In the former, the loop is fed from standard 50 ohm coaxial line and terminated on the waveguide wall. Provided the loop is small the current distribution around the loop can be assumed to uniform. For the latter loop, however, the free end is not terminated, forcing the current to be zero at this point and the current distribution around the loop to be non-uniform, similar to the current standing wave on an electric probe[148]. Since the self-flux linkage due to this current will be less than that linking with the equivalent grounded loop, the loaded loop will have the smaller self-inductance. Furthermore, the loop termination also determines the resistive component of the loop impedance, since this component is dependent upon the current standing wave which is directly related to the loop termination.

8.34 Experimental evaluation of loop probes.

As discussed previously the optimum probe design was derived experimentally upon the basis of the probe input impedance match with respect to the generator impedance of 50 ohms. In this section the results obtained from this experiment performed at 1.5 GHz will be presented for several loop probes. In particular, the impedance characteristics of grounded and loaded loops will be compared, and the effects of the probe and waveguide geometries on the probe impedance will be discussed. Finally, the impedance variation as a function of frequency will be given for selected probes.

(a) Effect of loop termination.

It has been shown that the self-inductance of small loop probes is dependent upon the loop termination. Table 8.4 gives a comparison between the measured input impedances of grounded and capacitive loaded loop probes of the same basic geometry, as depicted in Figure 8.3.

Probe Design (See Fig 8.3)	Loop termination	Probe parameters						Probe impedance ohms
		d	D	h	x	g	ℓ	
(a)	Grounded	2mm	8mm	1.7cm	1.0cm	0	3.7cm	52.5 + j 155
	Loaded					.2mm		13.5 - j 32.5
	Loaded					.1mm		12.5 - j 24.5
(a)	Grounded	2mm	8mm	2.7cm	2.0cm	0	5.7cm	200 + j 170
	Loaded					.5mm		24 + j 44
	Loaded					1.5mm		25.5 + j 30
(b)	Grounded	2mm	14mm	2.5cm	1.0cm	0	5.8cm	227.5 + j 120
	Loaded					1mm		27.5 + j 45.5
	Loaded					2mm		36 + j 32.5

Table 8.4: Probe impedance of grounded and loaded loops.

It is evident that the introduction of capacitive loop loading, by altering the probe current distribution, greatly reduces both components of the probe impedance. Consequently, the loaded loops are better suited to achieving the match impedance of 50 ohms than are the grounded loops.

(b) Impedance dependence of probe geometry.

By comparing the impedances of similar geometry probes in Table 8.4, it is apparent that the probe impedance, and

especially the resistance component, is a function of the probe perimeter. This is analogous to the radiation resistance characteristics of isolated loops in free space[149]. The probe impedance is dependent upon the current distribution on the loop, which for both grounded and loaded loops of type (a) and (b) is a standing wave. For a grounded loop, the current standing wave approaches the small loop approximation of uniform current distribution, as the loop becomes more uniform in shape and as its diameter decreases. Hence, as the perimeter of either type of probe varies, the current standing wave pattern varies, causing rapid changes of the probe impedance.

The measured impedances of three capacitive loaded loops of different thicknesses are plotted in Figure 8.4 as functions of probe perimeter. All impedance values were measured under conditions of optimum tuning of the main and tuning waveguide sections. These conditions were determined experimentally by varying the tuning length of each section until the best possible probe match was achieved. Furthermore, the coaxial feed line to the probe being measured was adjusted to be an integer multiple of half a wavelength, so that the impedance measured at the feed line terminal was the impedance of the probe. The probe impedance is shown to depend strongly upon the probe perimeter for all three probes, with a resonance condition occurring for a particular perimeter value close to a quarter of a wavelength. The effect of

increasing the probe thickness can be gauged by comparing the impedances of the two type (a) probes in this figure. Thus, for all values of probe perimeter considered, the probe with a section diameter d = 3.2mm has a lower reactance and a higher resistance than the corresponding 2mm section diameter probe. In general, as the thickness of the probe increases, the rate of change of probe impedance with change in probe perimeter, decreases. The probe thickness also determines the impedance at resonance. From the magnitude of this effect, it is reasonable to assume that the differences between the impedances of the 4mm section diameter probe, and the 3.2mm section diameter probe, are primarily due to the increase in probe thickness rather than the slight difference of shape. The effect of probe shape on the impedance function will be dealt with later, in greater detail, in relation to the frequency characteristics of the probes.

To summarize, loaded loop probes, when mounted in the coaxial antenna, are resonant for probe perimeters of approximately a quarter of a wavelength. The actual resonant probe perimeter is a function of the probe thickness, which also determines the probe impedance at resonance. This result for the coaxial antenna probes, complements the quarter wavelength resonance condition previously reported for simple grounded loop probes mounted in rectangular waveguides[148]. The distinction between the two cases is that the resonance condition refers in the former instance

to capacitive loaded loop probes, while in the latter case to grounded loop probes. Hence, the resonance of loop probes is dependent upon the enclosing waveguide cavity.

(c) Effect of waveguide section lengths on probe impedance.

It has been shown that the tuning effects caused by varying the lengths of the waveguide sections result from changes to the standing wave patterns of the dominant modes. Since the energy associated with the dominant modes contributes to the radiated and reactive energies in the antenna, the tuning lengths of the waveguide sections affect both components of the probe impedance.

Figure 8.5 gives the measured impedance variation of a type (b) loaded loop probe as a function of the tuning section length L_t, for constant main section lengths L_m. The impedance functions are shown to be repetitive, with the resonance points, where the probe impedance approaches the 50 ohm match impedance, occurring at L_t values a half a wavelength apart. These correspond to the ranges $(2n-1)\lambda/4 \leq L_t < n\lambda/2$ (n an integer) for which the tuning reactance of this section is capacitive. This is frequency dependent, since it is proportional to $\tan(\beta L_t)$, where β is the TEM mode phase constant and is directly proportional to the frequency. From the Figure, the optimum tuning lengths required are close to the quarter wavelength limit where $\beta L_t = \pi/2$ radians. Given this, the probe impedance

will be strongly dependent upon the frequency, since $\tan(\beta L_t)$ varies most rapidly as βL_t approaches $\pi/2$ radians. In practice, the shortest resonant length, n=1, would be preferred as the operating length. This choice minimizes the sensitivity of the impedance to changes in the operating frequency, as well as reducing the overall physical length of the antenna, and any energy loss due to attenuation in the tuning section guide walls.

The measured impedance variations of three loaded loop probes of the same length are plotted against L_m, in Figure 8.6, with L_t adjusted for the best probe match in each case. As expected, the impedances of all three probes are markedly dependent upon L_m, yielding optimum values close to three quarters of a wavelength for this section length. The figure also demonstrates the effects of probe geometry. Comparing the respective impedance functions of the two type (c) probes, shows that the reactance, in particular, of the thicker d=4mm probe is considerably less sensitive to changes in the tuning length than is the d=2mm probe reactance. Hence, the effect of increasing the probe thickness on the impedance-tuning length relation is the same as for the impedance-probe perimeter relation mentioned earlier. Similarly, the effect of probe shape is shown by comparing the impedance function of the d=2mm type (c) probe with that of the same section diameter type (b) probe. Over the range of L_m values considered, the impedance

of the latter does not vary as rapidly as the impedance of the former, indicating that the probe impedance is determined by the probe shape as well as by its thickness. Because of the difficulties in separating the individual contributions to the probe impedance of each change to the probe geometry, this description of the effects of changes to the probe thickness and shape necessarily must remain qualitative in nature.

To summarize, varying the waveguide section lengths L_m and L_t tunes both components of the probe impedance, and for each particular loop probe there exists an optimum length for each section, where the probe most closely satisfies the match condition. The quality of match achieved is a function of the probe geometry. A design value of three quarters of a wavelength can be assumed for L_m, provided the probes to be used are of substantially the same shape as the probes considered above. Final tuning of the antenna in a given application would then be accomplished by adjustment of L_t.

(d) Frequency characteristics of optimum loop probes.

From the results discussed previously, a quarter of a wavelength is the optimum perimeter for loaded loop probes. The impedance of several probes of this length, and of section diameter d=2mm, were measured as a function of frequency about the operating frequency f_o = 1.5 GHz. The results of this experiment in which the waveguide section lengths

were optimized for each probe at f_o, are given in Figure 8.7 - 8.9.

In Figure 8.7 the strong frequency dependence of the impedance for a typical loop probe in the antenna is demonstrated. The tuning effects of the waveguide sections are apparent in the restricted region close to f_o, where the inductive probe reactance variations have been almost completely cancelled by the capacitive contributions from the tuning section. This highly resonant impedance characteristic, which is somewhat reminiscent of the electric dipole impedance characteristic[150], restricts the operation of the coaxial antenna to a narrow frequency band centred at f_o. Concentrating on the band from 1.4 GHz to 1.6 GHz, the resistance and reactance characteristics of several selected probes are plotted in Figures 8.8 and 8.9 respectively. These plots show that changes to the probe shape significantly modify the impedance characteristics and effective bandwidths of the probes, defined upon the basis of the maximum permissible VSWR incurred over the frequency band. As before, it is difficult to develop a complete, quantitative description of the effects of probe shape. However, from the results obtained it is possible to formulate an empirically based design indicating the optimum choice of probe shape from those shown in Figure 8.3. Incorporating the bandwidth criterion, the optimum probe is now defined as the probe most closely satisfying the match condition over the widest frequency band. From the figures, and assuming a permissible VSWR of 1.75:1,

the optimum probes tested were the type (b) and type (d), implying that a substantially symmetrical loop geometry is required. The relative bandwidths of the two type (d) probes show that, within the physical limits imposed by the waveguide walls, increasing the loop diameter D increases the effective bandwidth of the probe. This may be further increased by increasing the probe thickness, but from Figure 8.6, it can be seen that this will have the additional effect of degrading the probe match at f_o. By comparing the type (d) probe of D = 1.6cm with the type (b) probe, it is evident from the respective tuning section lengths required, that the former probe has the lower self-inductance. This follows from the variation of the tuning reactance with L_t, since the larger the value of L_t, within the ranges discussed previously, the smaller the capacitive tuning reactance, indicating a smaller value of inductance to be tuned. With all parameters apart from probe shape remaining constant, this implies a reduction in the probe self-inductance. Furthermore, the lower tuning reactance also signifies that this probe is less sensitive to frequency fluctuations than is the type (b) probe. The VSWR's incurred by these two probes over the frequency band of operation are plotted in Figure 8.10. The type (d) probe with D = 1.6cm is clearly the optimum choice for the coaxial antenna, since it has a wider 1.75:1 VSWR bandwidth, and also is better matched at f_o, than the type (b) probe.

(e) Summary of loop probe design.

The optimum probe design has been defined as the probe incurring the minimum VSWR with respect to a match impedance of 50 ohms, over the frequency band of operation. Capacitive loaded loop probes, because of their inherently lower input impedances, were found to be more suitable than grounded loop probes for satisfying this match condition. It has been established that the former probes are resonant for a mean probe perimeter of a quarter of a wavelength, with the probe resistance at resonance being a function of the probe geometry. This compares with a previously reported resonance condition for grounded loop probes. Furthermore, for each probe, there correspond optimum lengths for the main and tuning waveguide sections, so that the optimum probe design must be derived in conjunction with the optimum waveguide design.

The effects of probe shape and thickness on the probe impedance have been studied in relation to the optimum choice of waveguide section lengths and the frequency characteristics of the probes. For the probes investigated, a design length of three quarters of a wavelength has been shown to be optimum. Final tuning in any given application would be achieved by adjustment of the tuning section length. The highly resonant nature of the probe impedance - frequency characteristic restricts the operation of the coaxial antenna to a narrow frequency band centred on f_o = 1.5 GHz. However, it has been shown that the bandwidth of the optimum

loop probe, defined with respect to a permissible VSWR of 1.75:1, is 5%, which compares favourable with the bandwidth of the equivalent dipole antenna.

It has been shown that the experimentally derived optimum probe design for the coaxial antenna is a resonant capacitive loaded, loop probe with a quarter of a wavelength perimeter. The optimum probe shape, based upon the criteria of probe match and bandwidth, was found to be of type (d), the design details of which are given in Table 8.5, together with the associated optimum waveguide section lengths. The VSWR incurred by this probe, as a function of frequency, is plotted in Figure 8.10, and compared with the performance of a similar type (b) probe, whose design is also given in Table 8.5.

Probe Type	Probe parameters						Waveguide parameters		Impedance at f_o (ohms)	1.75:1 VSWR Bandwidth
	d	D	h	x	g	ℓ	L_m	L_t		
(d)	2mm	1.6cm	2.35cm	2mm	-	5cm	15cm	5.4cm	47.35+j 3.78	5.2%
(b)	2mm	1.3cm	2.5 cm	5mm	8mm	5cm	15cm	5.2cm	47.0 +j 9.9	5.0%

Table 8.5: Optimum probe design.

8.4 Coupling network.

8.41 Loop probe cross-coupling effects.

The orthogonality conditions for waveguide modes of propagation[127] ensure that ideally no cross-coupling can occur between the different modes in the coaxial antenna. In particular there will be no coupling between the two TE_{11} modes because of the orthogonality, across the antenna cross-section, of the trigonometrical functions describing the different orientations of these modes. However, energy conversion from one mode to another can occur if there are imperfections present in the waveguide geometry, conductivity, or method of excitation. For most practical waveguide antennas, such effects will be negligible provided care is taken in the antenna construction. In the coaxial antenna, it will be essential to maintain the precise location of the excitation probes to minimize any cross-coupling between the two TE_{11} modes, which is likely to be the principal coupling effect in the antenna. Any coupling between these modes and the TEM mode will be negligible, provided no asymmetrical discontinuities are present. Therefore, since the signals associated with each mode will be independent of the signals associated with the remaining modes, negligible coupling will occur between the input signals to each set of probes. This condition applies equally to both of the circuitry systems considered in Chapter 7, and is also independent of whether the four or six probe configuration is used.

Conversely, the symmetry of the two probes in each probe set results in a strong cross-coupling effect between diametrically opposite probes. This can be demonstrated by considering a set of probes exciting the TEM mode. Each probe, by itself, is capable of exciting the TEM mode. Hence, the mode can be excited by one probe and detected by the diametrically opposite probe, which indicates that when both probes are used to excite this mode, strong cross-coupling must occur between the two probes. At the input port to each probe, this coupling signal is manifested as a reflection from the antenna, degrading the impedance match.

8.42 Coupling elimination.

As previously suggested for array antennas[74 - 78] the cross-coupling signal between probes can be eliminated effectively by providing electrical coupling between the two input lines feeding each probe, as shown in Figure 8.11. A signal sampled from one feed line is adjusted in magnitude and phase in the coupling line to cancel the reflected signal in the other feed line. Because of the symmetrical nature of the cross-coupling effect, the coupling line must be reciprocal, modifying the magnitudes and phase of both the sampled signals identically. For each type of probe used in the antenna there will correspond optimum values of the coupling line magnitude and phase control parameters. The optimum condition is defined as the particular adjustment yielding, at each input port, the best impedance match with all remaining ports

correctly terminated, together with the minimum cross-coupling signal when the diametrically opposite probe is excited.

The optimum values of the coupling line parameters were derived experimentally using the line detailed in Figure 8.11. The variable penetration of the sampling probes into each respective feed line, provided control of the magnitudes of the sampled signals. A continuously variable, reciprocal phase shifter incorporated into the coupling line provided the necessary phase control.

The effects of the cross-coupling on the performance of the antenna can be taken into account by postulating an effective input impedance at each port, based upon the total reflected signal from the antenna. This signal will combine the reflection due to the probe mismatch, with the remainder of the cross-coupling signal, that may not be cancelled completely by the coupling line signal. Since the effect of the coupling line is phase dependent, and hence, frequency dependent, the degree of cancellation of the cross-coupling signal is also sensitive to changes in the frequency about f_o. Moreover, the impedance characteristic of the loop probe is also a function of the frequency, so that the effective input impedance at each port is strongly frequency dependent. The effective input impedance, and the impedance measured at a typical port with all remaining ports correctly terminated, are plotted as functions of

the operating frequency in Figure 8.12. The VSWR's corresponding to these plots are given in Figure 8.13 and are compared with the VSWR characteristic of the optimum loop probe discussed above. For these measurements the coupling line was adjusted to the optimum position, as previously defined, at the frequency f_o. Furthermore, the introduction of the coupling line led to the probe shape being modified to a type (c) probe with g = 8mm requiring a tuning section length L_t = 6.3 cm. All other probe parameters remained unchanged. This modification permitted an improvement in the match at f_o.

From the VSWR plots, it is evident that the effect of the cross-coupling signals is to reduce drastically the antenna bandwidth. Compared with the optimum probe 1.75:1 VSWR bandwidth of 5.2%, the bandwidth is more than halved to 2.3%, by accounting for the coupling signal. However, without the coupling signal (especially at frequencies close to f_o), cross-coupling signals appearing at the ports would almost render the antenna inoperable with an effective VSWR of 4.5:1 at f_o. The effect of the coupling on the antenna impedance is shown by comparing the frequency plots of the measured probe impedance and the effective input impedance. The former plot rotates clockwise around the Smith Chart with increasing frequency, which is characteristic of a passive impedance function of an antenna[151]. Conversely, because of the cross-coupling signals appearing as reflections

from the antenna, the latter plot rotates anticlockwise around the Smith Chart. Thus, the antenna acts as an active device in the sense that at each port the predominant reflected signal is not dependent upon the input signal to that particular port.

8.5 Matching network.

The antenna bandwidth can be increased by incorporating a suitably designed compensating network into the element design. However, the form of the effective input impedance variation over the frequency band of operation, precludes the broadband matching of the antenna by a single matching element. A primary matching device is required to transform this impedance function into a form from where a second device can improve the match over the frequency band.

The impedances corresponding to the frequencies furthest removed away from f_o in the band, must be increased to improve the match. This indicates that a parallel resonant stub will be required as the broadbanding device. A line transformer will then be required to transform the input impedance function into a form more convenient for the stub device.

8.51 The line transformer.

Although the effective input impedance values of the midband frequencies are already well matched, the impedance values at frequencies corresponding to the extremes of the

frequency band considered, are too low to be compensated for by the stub device alone. Therefore, the line transformer must increase these latter values without affecting the impedance values at midband. A line transformer an odd multiple of a half a wavelength long, provides the required impedance transformation. The effective length of the device is half a wavelength at f_o, so that the impedance values at midband are not affected by the transformer. At frequencies higher than f_o, the effective length is longer than a half a wavelength, and hence the associated impedance values are transformed in a clockwise sense around the Smith Chart, with respect to their original values, to increase in value. For frequencies lower than f_o, the effective length is shorter than a half a wavelength, so that the associated impedance values are transformed to higher values in the anticlockwise sense around the Smith Chart. The increase in the transformed values is a function of the overall physical length of the transformer, but it will be necessary usually to restrict the length of the line to a half a wavelength, in order to limit the extent of the standing wave existing between the antenna and the matching network. The transformed impedances are also dependent upon the characteristic impedance of the line transformer. Therefore, a particular value of the effective impedance is matched completely by choosing the appropriate length and characteristic impedance of the transformer. From the impedance plot given in Figure 8.12, a more advantageous approach is to design the transformer to match

an intermediate impedance value. Although no particular value of the impedance is compensated for completely, the overall bandwidth performance is improved.

To facilitate the determination of the optimum values of the line transformer parameters, a computer program was developed to evaluate the transformed impedance from the effective input impedance at the ports. These values were derived in conjunction with the design of the parallel stub device, and are summarized in Table 8.6. The transformed impedance is plotted against frequency in Figure 8.14.

8.52 The parallel stub matching network.

This device is required to compensate the impedance transformed by the line transformer over as wide a bandwidth as possible. As previously, the maximum compensation will be necessary at the frequencies corresponding to the extremes of the frequency band. A parallel resonant stub an odd multiple of a quarter of a wavelength long if short circuited, or an even multiple if open circuited, provides the necessary compensation. At f_o the stub appears as an open circuit, so that the midband impedance values are little affected. For frequencies higher than f_o, the stub provides a capacitive shunt reactance to cancel with the inductive input reactance. Conversely, for frequencies lower than f_o, the stub reactance appears inductive, and consequently, cancels with the capacitive input reactance.

The tuning reactance of the stub is determined by the length and characteristic impedance of the transmission line or waveguide forming the stub. For the present application, to provide the necessary reactance values over such a narrow frequency band, the characteristic impedance of the stub must be small. This introduces difficulties of construction and connection to the antenna feed lines. However, the characteristic impedance required increases as the length of the stub increases, since a longer stub is more frequency sensitive, causing the tuning reactance of the stub to change more rapidly over the band. The length restrictions on the stub are less stringent than on the line transformer, because the stub is a parallel element and only its effect at the connection to the feed line is important to the performance of the antenna. Consequently, the stub length may be increased in quarter or half wavelength steps until a more acceptable characteristic impedance value is obtained.

The stub for broadband matching of the coaxial antenna was designed by following the procedure of Nelson and Stavis[152]. A computer program was developed to evaluate and optimize the design in conjunction with the line transformer outlined above. The design parameters of the stub are given in Table 8.6, and the final transformed input impedance to the total matching network of stub and line transformer is plotted in Figure 8.14. The VSWR incurred

by the matched antenna over the frequency band is given in Figure 8.15, by whence it is apparent that the effect of the matching network is to more than double the 1.75:1 VSWR bandwidth to 5%.

Element	Characteristic impedance (ohms).	Electrical length
Line transformer	27.5	.4563λ
Parallel short-circuited stub.	8.75	1.2511λ

Table 8.6: Design of matching network.

8.53 Strip-line network.

The matching network has been described in terms of coaxial air-line devices, but the design parameters apply equally well to strip-line devices[153]. This latter method of construction is preferable in applications where the overall physical lengths of the line transformer and stub are restricted. By employing a concertina configuration for the centre conductor in the strip-line, the required electrical lengths of the devices can be concentrated into shorter physical lengths than are possible for the equivalent coaxial air-line devices. Moreover, this

technique also allows longer stub lengths of subsequently higher characteristic impedance to be used in the parallel stub element. For example, a strip-line stub of 2.252 wavelengths electrical length (at f_o) and of 15.75 ohms characteristic impedance, has the same performance as the stub detailed in Figure 8.14.

8.6 Discussion.

The element design of the coaxial antenna has been presented. The design parameters which were optimized experimentally at L-band, are summarized in Figure 8.1 and Table 8.7, and the antenna performance as a function of the operating frequency is shown in Figures 8.14 and 8.15.

In the design, major emphasis was placed upon satisfying the constraints resulting from the requirement for compatibility with an array environment, and the need for efficient performance over the band of operating frequencies. The former imposes stringent restrictions on the waveguide design, limiting the maximum overall dimensions, but also requiring substantial radiation from both the TEM and TE_{11} modes. Conversely, the latter constraint primarily affects the probe desing, and hence, due to the strong cross-coupling effect between diametrically opposite probes, the design of the coupling and matching networks.

Of the secondary constraints, most attention was given to providing a simple method of exciting the necessary modes in the antenna. Thus, the four probe configuration has been preferred.

Section	Description						
(a) Waveguide	Refer to Figure 8.1 $L_m = 0.75\lambda$ $L_t = 0.315\lambda$						
(b) Probes	Type (c) loaded loop probes:						
	Probe parameter	d	D	h	x	g	ℓ
	Electrical length (wavelengths)	.01	.08	.12	.01	.04	.25
(c) Compensation networks	Coupling network: 0.455λ electrical length (magnitude coupling to be adjusted). Matching network: Line transformer and parallel stub. (See Table 8.6).						

Table 8.7: Summary of optimum design parameters.

In the six probe excitation method, the additional set of either electric or magnetic probes exciting the TEM mode are located in the tuning section. The input impedance to each probe is then dependent upon not only the probe type and geometry, but also upon the tuning section geometry and the

position of the probe in the guide. Thus, the optimum probe design is determined most conveniently by experimentation. The remaining two probe sets exciting the TE_{11} modes, are designed and positioned exactly as in the four probe configuration. Because the introduction of the tuning section probes alters the tuning lengths of both the waveguide sections, and subsequently, the impedances of the TE_{11} probes, the design of all six probes and the two waveguide sections must be optimised experimentally, in conjunction with each other. In addition to the cross-coupling effects present in the four probe configuration, cross-coupling also occurs between the two TEM probes, requiring further compensation networks. Moreover, modifications to the four probe coupling and matching networks are also necessary, so that the six probe configuration greatly increases the complexity of the element design.

The power handling capacity of the coaxial antenna is limited principally by the loaded loop probes. At high power levels, breakdown may occur across the loop gap, because of the high electric field stresses generated by the abrupt discontinuity at the free end of the loop. This effect is minimised by increasing the probe thickness and chamfering the edges at the loop end. The effect on the probe impedance is small (as discussed in Section 8.3), but necessitates slight modifications to the tuning section length and the compensation networks. Similarly, the electric stresses on the waveguide step edges are also lessened by chamfering.

For most large array applications, however, although the array may be required to radiate very large amounts of power, the power handled per elemental radiator is likely to be quite small.

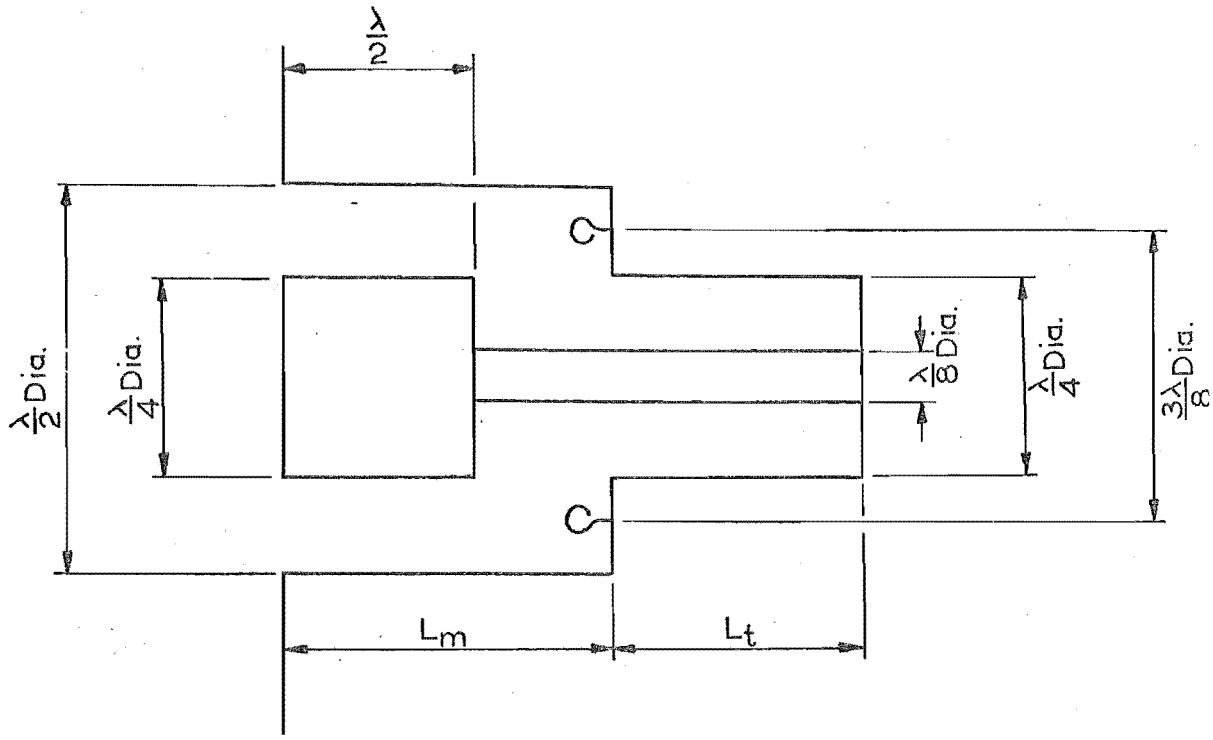

FIGURE 8·1 : WAVEGUIDE DESIGN

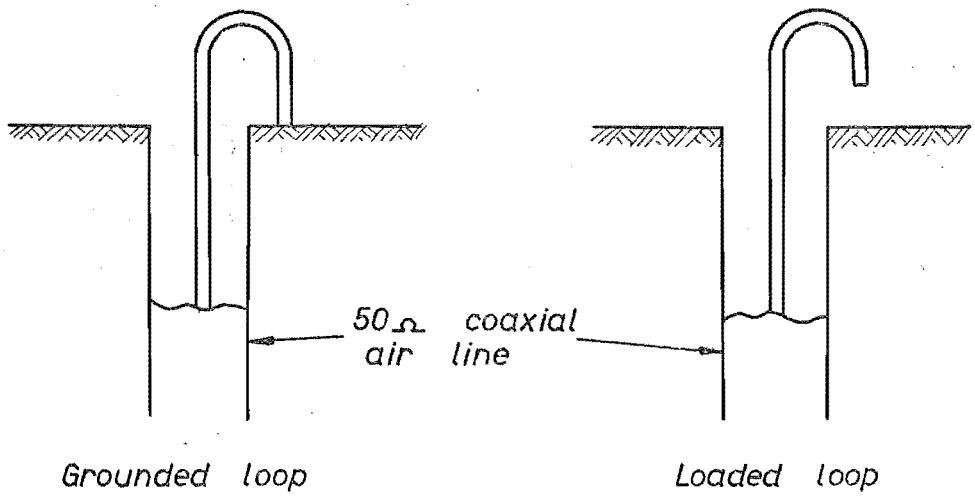

FIGURE 8·2 : MAGNETIC LOOP PROBES

l = mean probe perimeter
c = 1 cm. for probes (a) and (b)

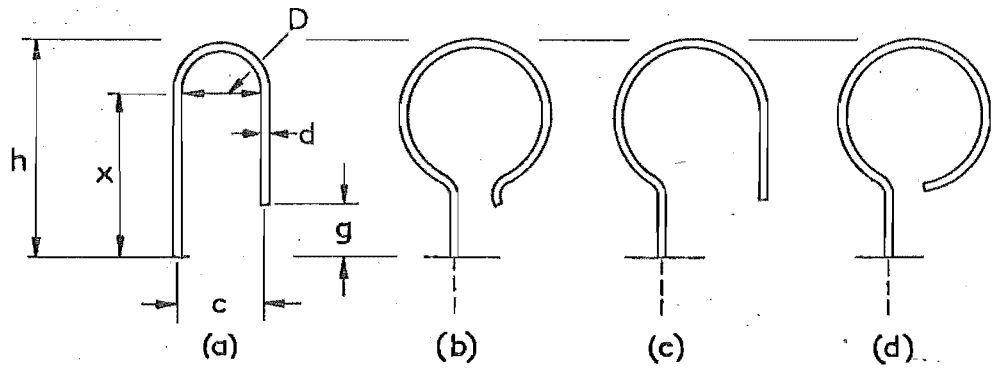

FIGURE 8·3 : LOOP PROBE DESIGN

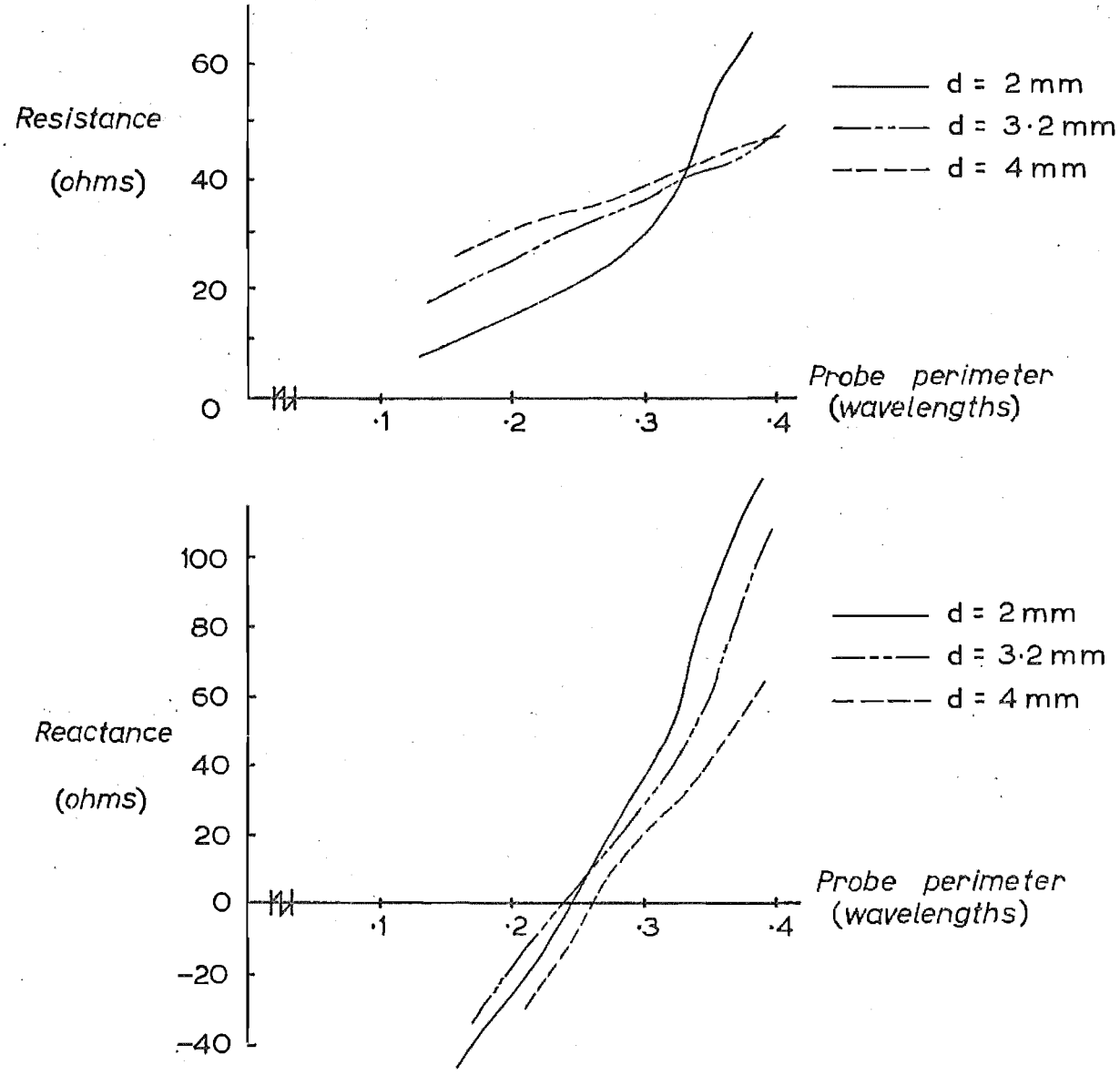

FIGURE 8·4 : EFFECT OF PROBE PERIMETER

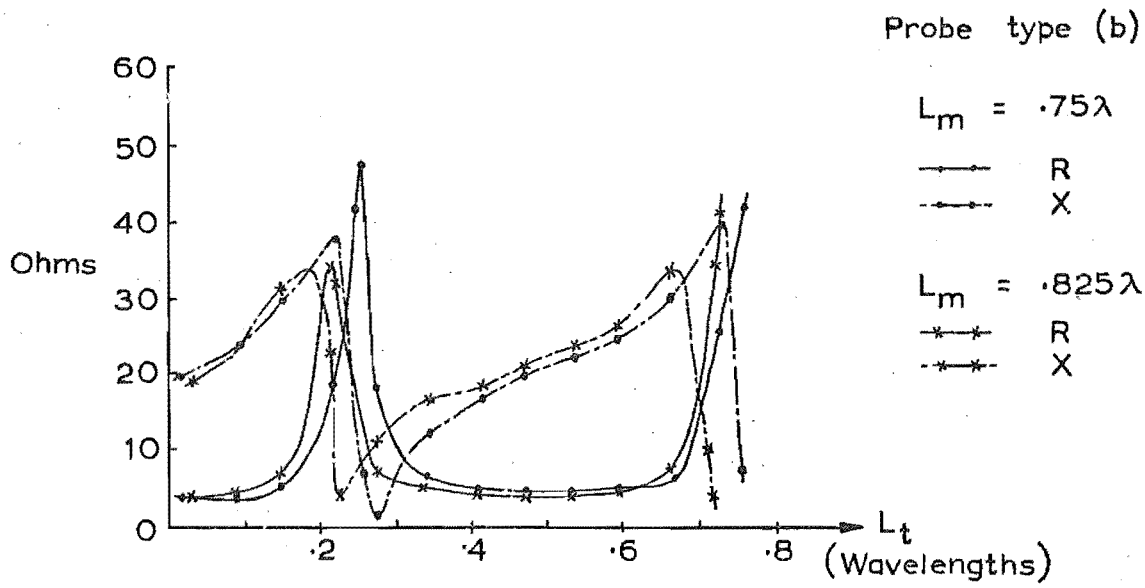

FIGURE 8·5 : EFFECT OF TUNING SECTION LENGTH

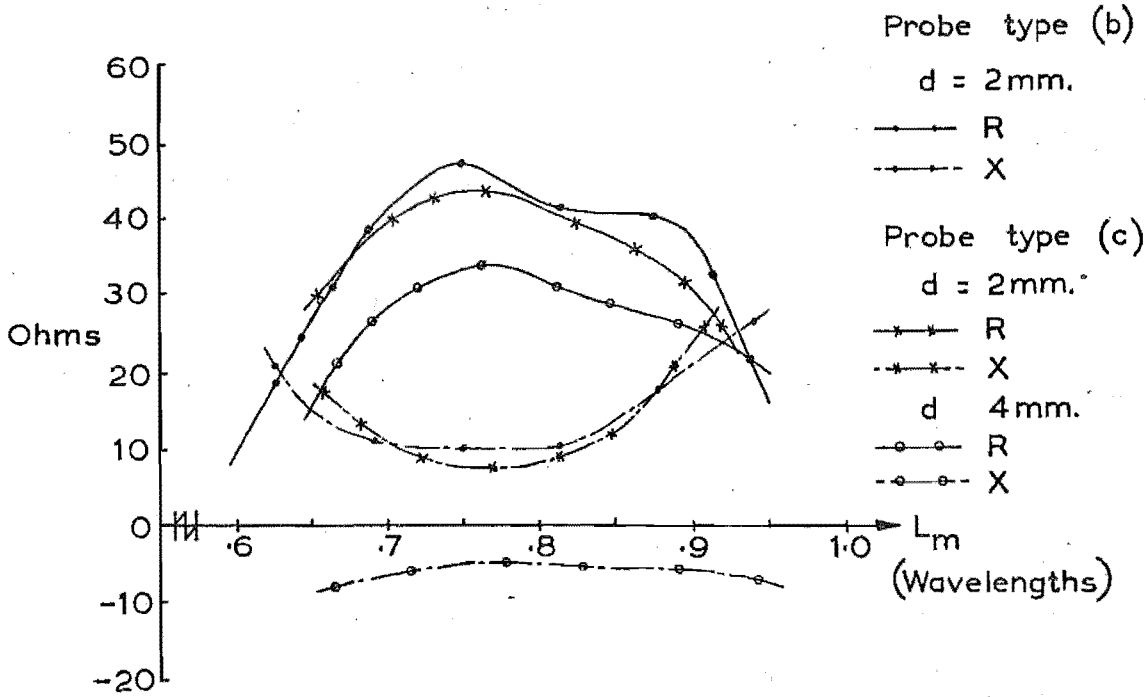

FIGURE 8·6 : VARIATION OF PROBE IMPEDANCE WITH MAIN SECTION LENGTH

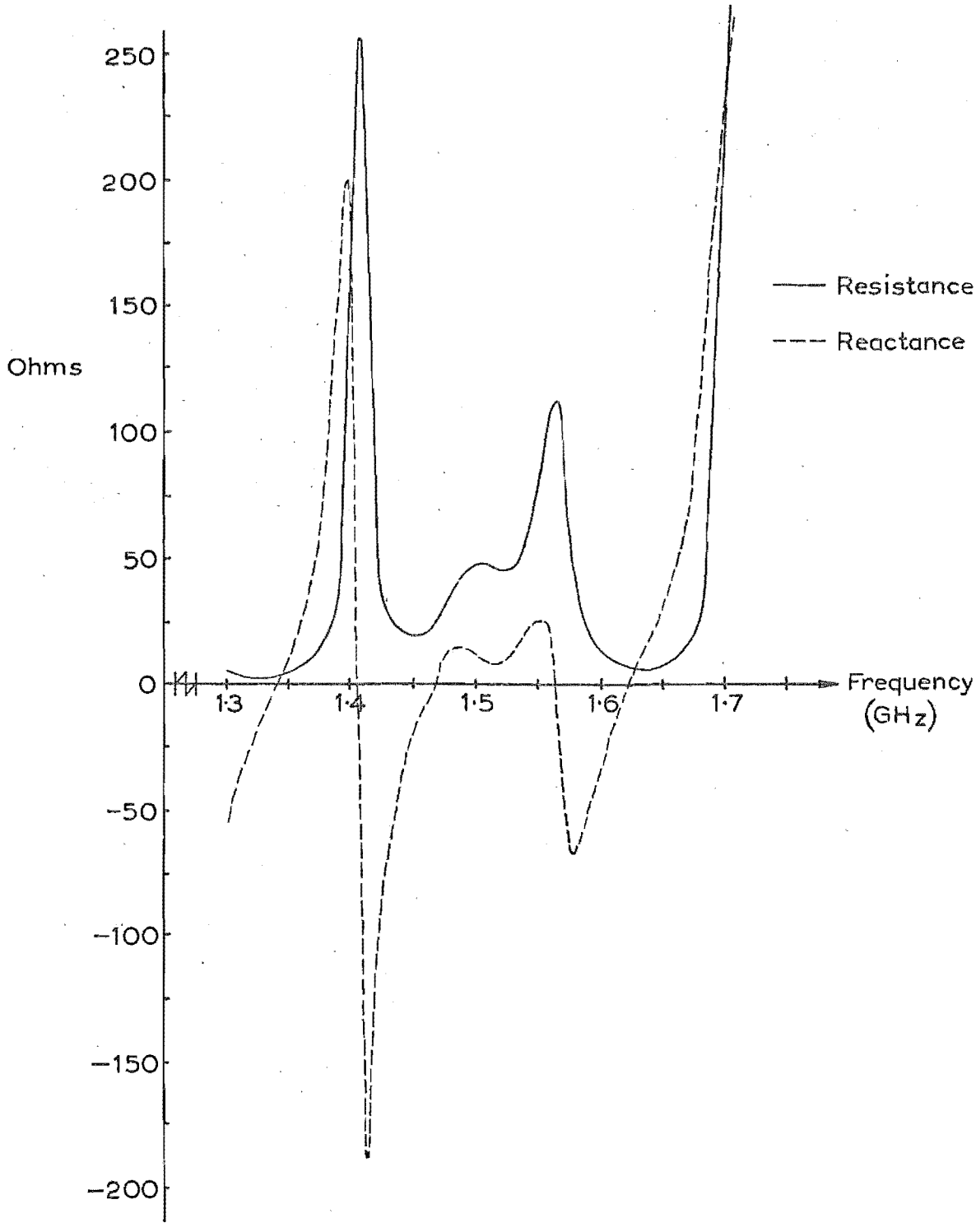

FIGURE 8·7 : FREQUENCY RESPONSE OF TYPICAL LOOP PROBE

KEY FOR FIGURES 8·8 AND 8·9

Figure	Curve	Probe	Probe dimensions (cms)				
			D	d	g	h	x
8·8 (a)	———	(a)	·8	·2	·5	2·65	2·0
and	—·—	(c)	1·6	·2	·45	2·35	·2
8·9 (a)	– – –	(c)	1·4	·2	·8	2·45	·7
8·8 (b)	———	(b)	1·3	·2	·7	2·5	·6
and	—·—	(d)	1·3	·2	–	2·45	·7
8·9 (b)	– – –	(d)	1·6	·2	–	2·35	·2

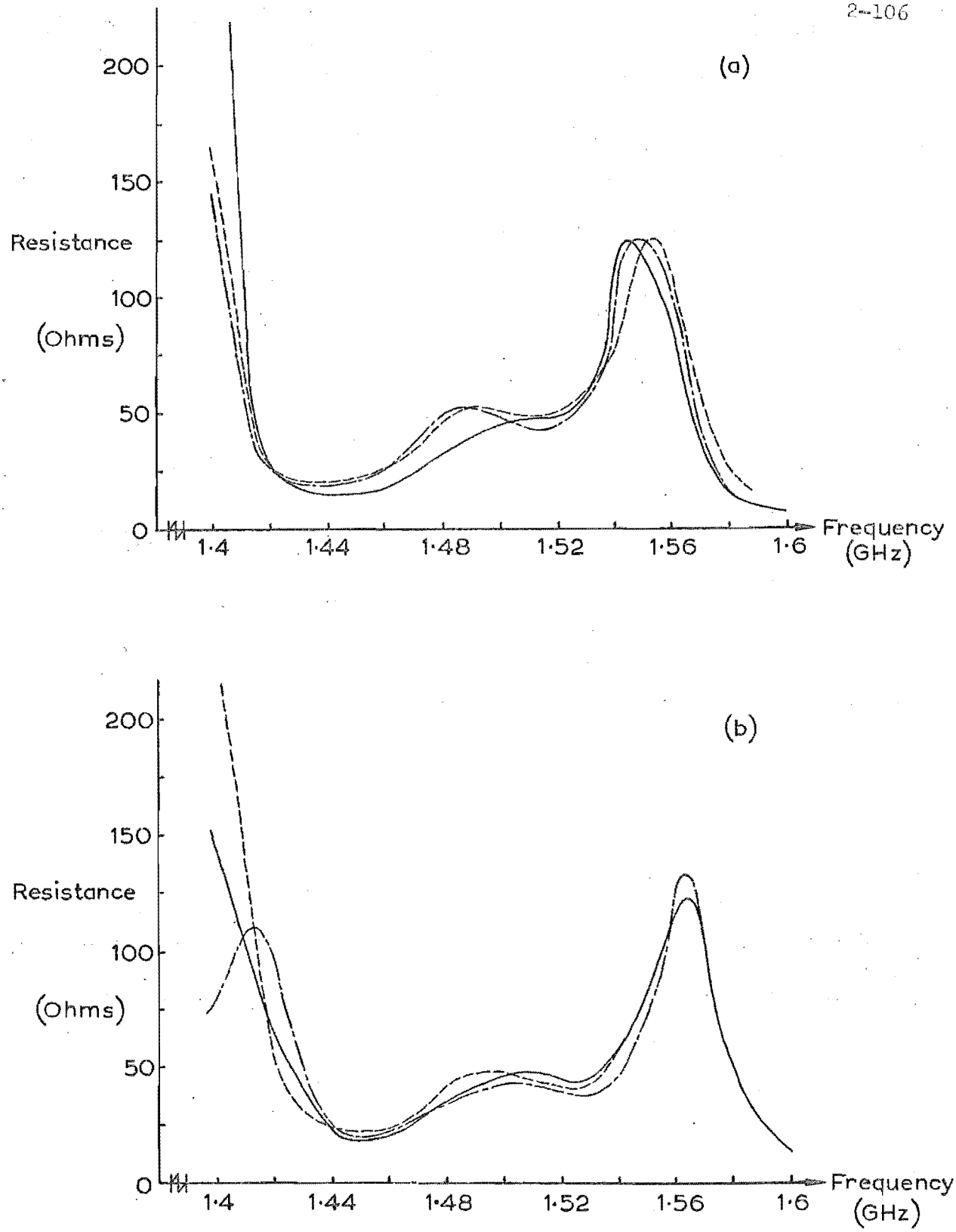

FIGURE 8·8 : PROBE RESISTANCE OVER FREQUENCY BAND OF OPERATION

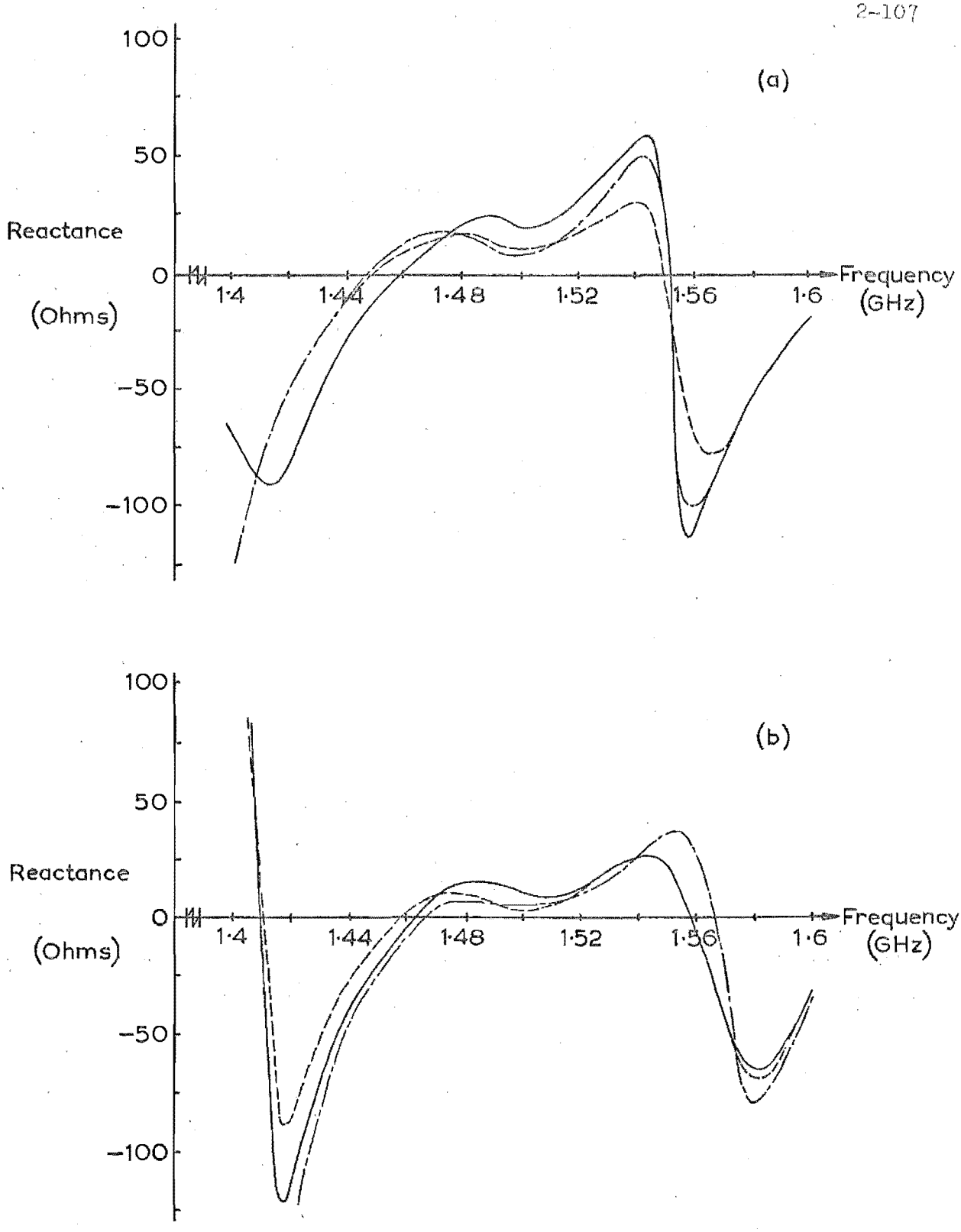

FIGURE 8·9 : PROBE REACTANCE OVER FREQUENCY BAND OF OPERATION

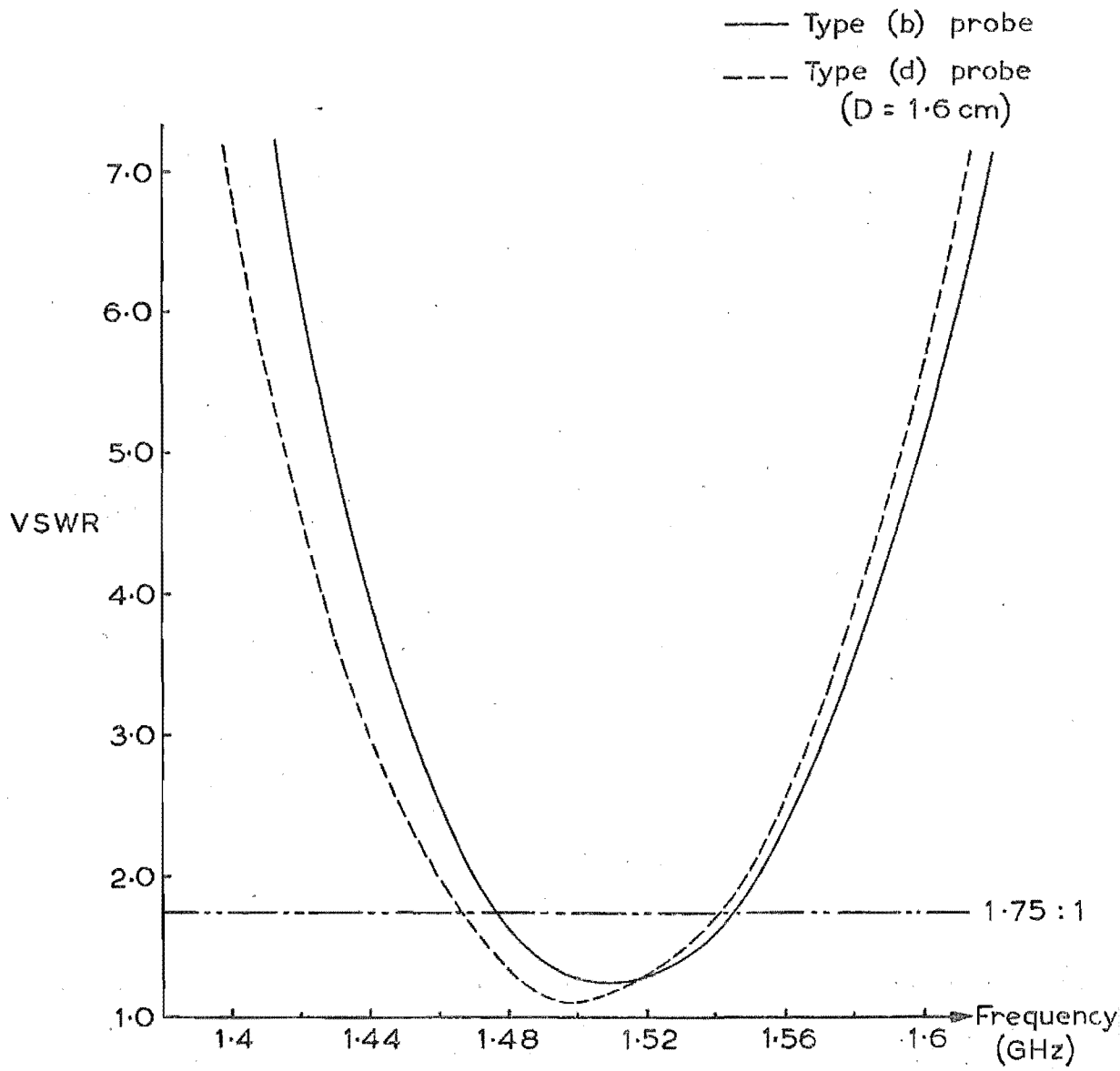

FIGURE 8·10 : VSWRs OF OPTIMUM PROBES

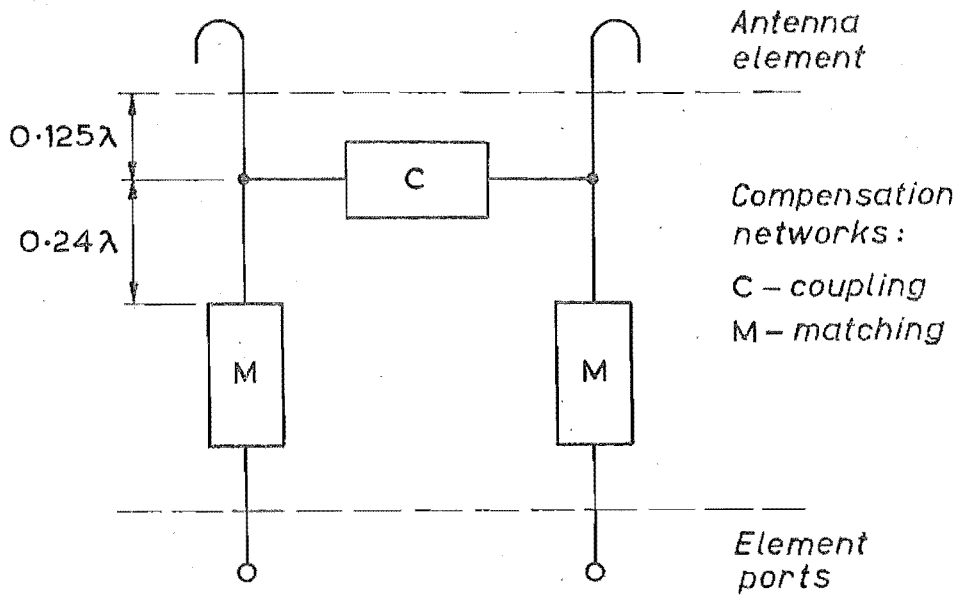

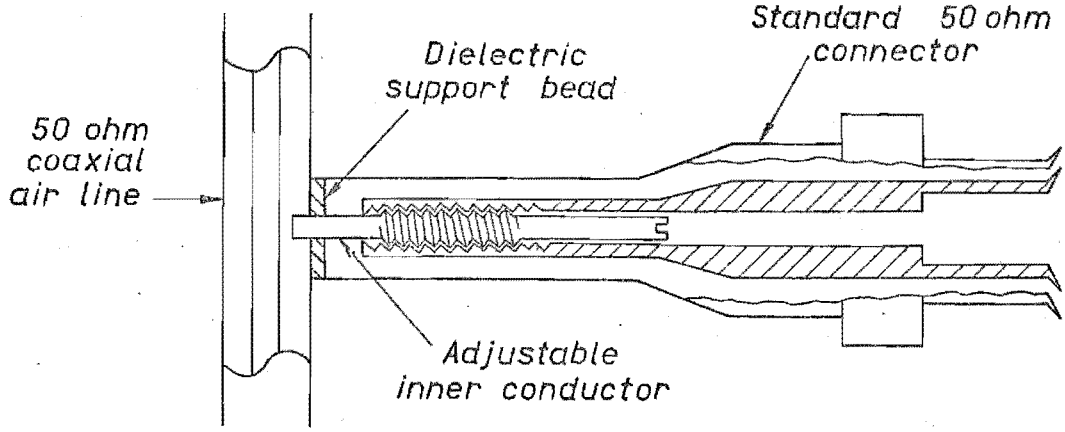

FIGURE 8·11 : COMPENSATION NETWORKS

$f_- = 1{\cdot}45$ GHz
$f_o = 1{\cdot}5$ GHz
$f_+ = 1{\cdot}55$ GHz

—— Effective input impedance

--- Port impedance with remaining ports terminated

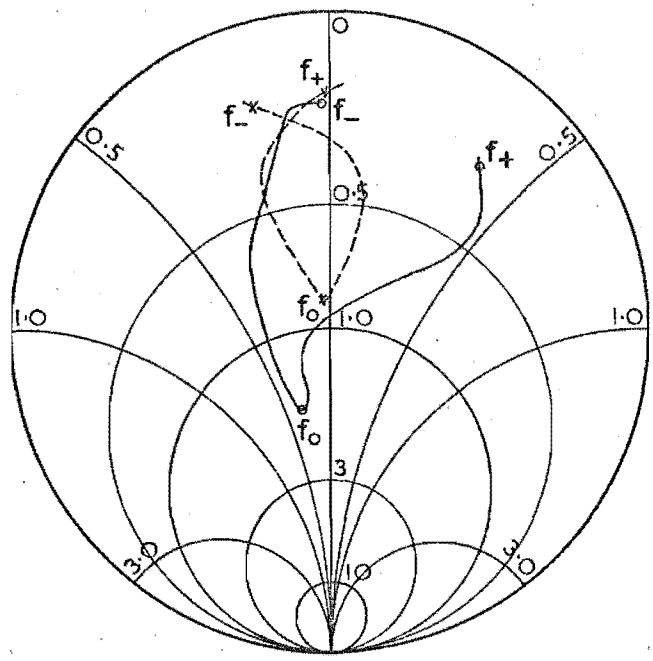

FIGURE 8·12 : EFFECTIVE INPUT IMPEDANCE AND PORT IMPEDANCE

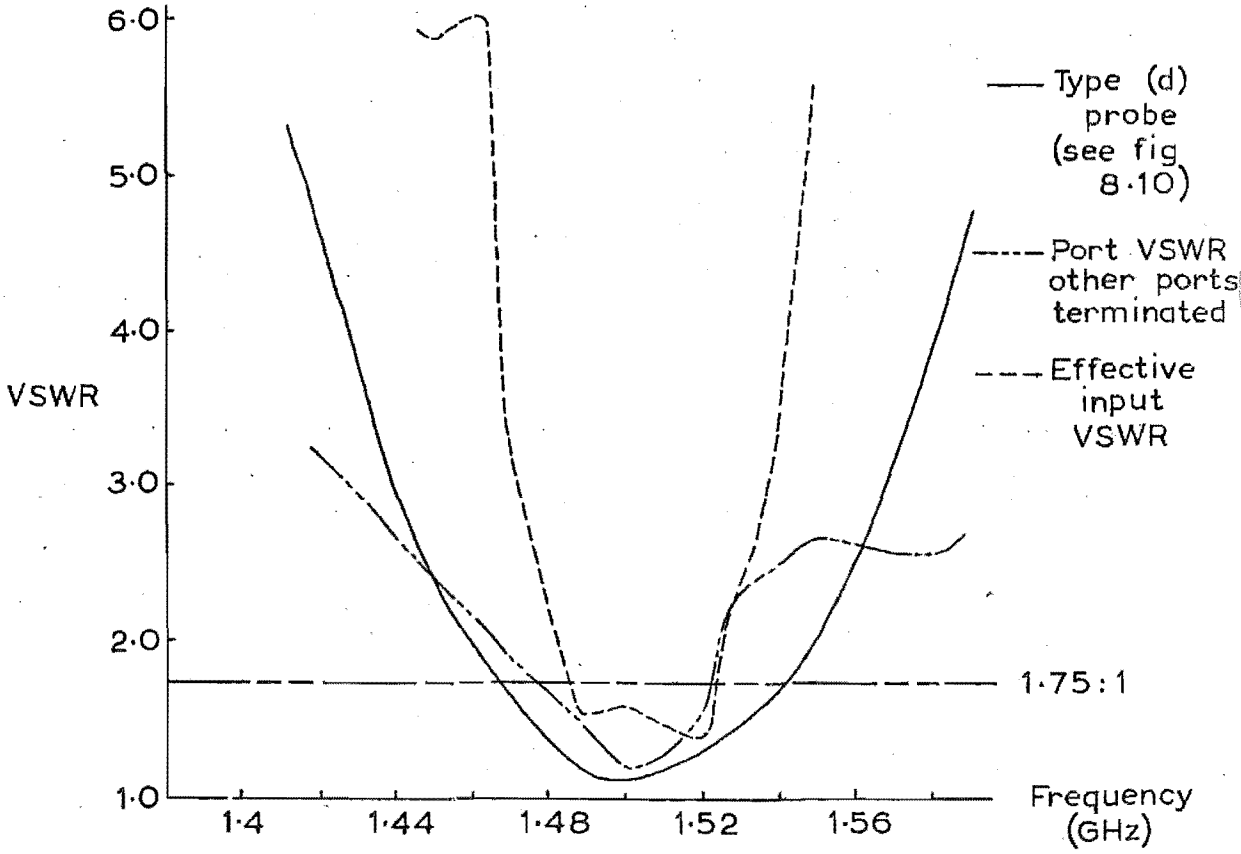

FIGURE 8·13 : EFFECT OF PROBE CROSS-COUPLING

$f_- = 1{\cdot}45$ GHz
$f_o = 1{\cdot}5$ GHz
$f_+ = 1{\cdot}55$ GHz

—— Impedance transformed by line transformer

--- Impedance transformed by matching stub

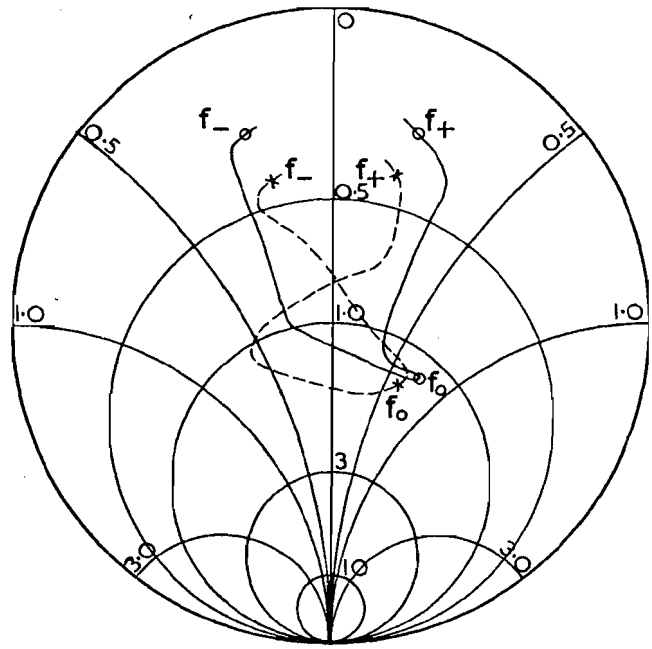

FIGURE 8·14 : ANTENNA IMPEDANCE

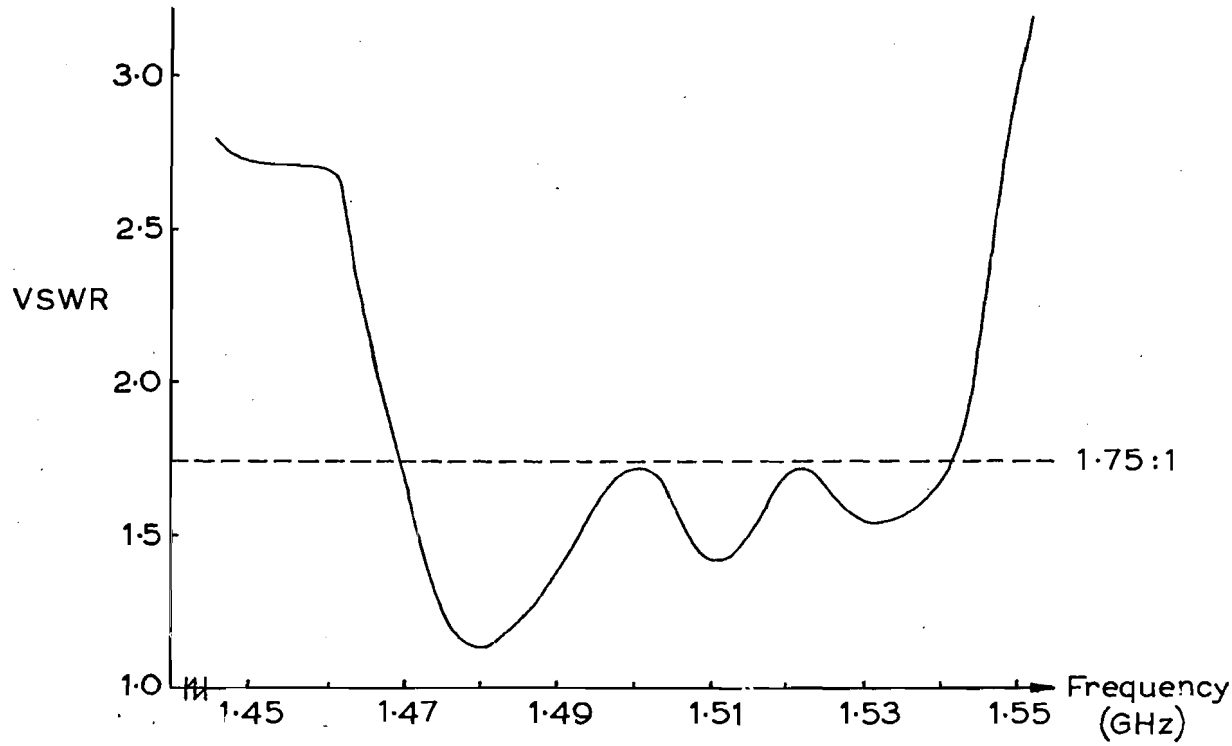

FIGURE 8·15 : MATCHED ANTENNA PERFORMANCE

CHAPTER 9

Discussion of the Coaxial Antenna.

9.1 Introduction.

The system and element designs of the coaxial antenna have been derived in accordance with a specific array application, and although this imposed certain constraints on the designs, the performance of the antenna is such that it will be useful in several other applications. For uses other than inclusion in arrays, the design constraints resulting from the need for compatibility with an array system can be relaxed. As an example, the aperture diameter of an isolated antenna can be appreciably greater than a half a wavelength. Increasing the aperture dimensions will tend to improve the radiation efficiency of the dominant modes in the aperture, but will also decrease the beamwidths of their radiation patterns. The optimum aperture diameter for an isolated antenna, therefore, will not be very much greater than a half a wavelength. Rather than introduce an entirely new element design for each individual application, it will be simpler to restrict the discussion to the original antenna designed for the array. The principles of antenna operation and control will be the same irrespective of the actual aperture dimensions, provided that these dimensions remain of the same order in all cases. The degree of control over the operation of the antenna will vary with the different performance requirements

of each application, so that the design of the control circuitry, unlike the design of the element, will be dependent upon the particular application. Two examples of the use of the coaxial antenna in systems other than large arrays will be discussed. A brief description of the necessary control circuitry for each application will also be included.

The design refinements which can be made in order to improve the performance of the antenna will be presented. Attention will be focussed on the design parameters of the waveguide sections, since, apart from the lengths of each section, the full optimisation of these parameters was not attempted in the experimental development of the optimum design of the antenna.

Although the optimum design has been derived, certain aspects of the operation of the antenna are not fully understood. An experimental study to complete this knowledge will be suggested. The estimation of mutual coupling effects between coaxial antennas in an array will be considered and two methods of analysis, an equivalent circuit and a scattering matrix approach, will be indicated. The latter method is an application of the technique formulated in Chapter 3. The suggested further study will also be extended to include an experimental verification of these methods.

9.2 Further applications of the coaxial antenna.

Although the coaxial antenna has been designed specifically for inclusion in a large surveillance radar or communication array system, its radiation characteristics make it useful as an isolated antenna. In particular, it is suitable for use in applications requiring an antenna with a wide beam radiation pattern that can be polarized arbitrarily. In most such instances, sufficient polarization diversity is achieved if the antenna radiates two independently controlled, orthogonal, linear polarizations transverse to each direction of propagation. This follows since the signals corresponding to these two component polarizations completely specify the polarization state of the wave that is transmitted or received by the antenna. Thus, complete control of the relative strengths of the signals controls all the possible polarization states of the wave.

9.21 V.H.F. mobile station antenna.

As an example of the application of an isolated coaxial antenna consider a V.H.F. 450 MHz. band mobile communications link. When operating over rough terrain, due to multiple scattering effects, both the angle of arrival and the polarization state of an incoming wave are uncertain. The angle of arrival is restricted mainly to those angles close to the horizontal plane, but, in general, the polarization is arbitrary. The transmission

and reception of such signals can be achieved readily by a coaxial antenna mounted vertically on a mobile vehicle. When compared with the equivalent dipole antenna, the coaxial antenna offers the advantages of flush mounting, mechanical rigidity, and simplicity of excitation.

The presence of the vehicle modifies the radiation patterns of the antenna, permitting substantial radiation of the far-field polarizations associated with the dominant modes, into the regions immediately above and below the aperture plane[121]. Thus, the coaxial antenna radiates the necessary component linear polarizations in the directions to which the waves are constrained. Complete polarization is not required, since satisfactory operation is obtained merely by tuning the transmitter/receiver to the predominant polarization. Because of the restricted propagation directions, therefore, adequate polarization diversity is achieved, at any given instant, by utilizing the fields of only two dominant modes, the TEM mode and one of the TE_{11} modes. For the directions of propagation considered, the TEM mode radiates a vertical linear polarization component, and the TE_{11} mode in its H-plane radiates a horizontal component. As the direction of propagation varies in azimuth, the excitation of the TE_{11} mode is switched from say the $\hat{x}$ direction oriented set of probes to the $\hat{y}$ direction probes, and simultaneously the excitation of the TEM mode is switched from the $\hat{y}$ direction to the $\hat{x}$ direction probes. The choice between the excitation of the TE_{11} modes is

determined by which of the two modal fields has the greater signal strength associated with its horizontal linear polarization for a particular direction of propagation. Since each set of probes excites only one dominant mode at a time, a simpler form of the four-port system discussed in Chapter 7 is used for the control circuitry. This system is shown in Figure 9.1. The α and β phase shifters control the relative magnitudes and phases of the two excited modes, respectively, and the two remaining phase shifters assume values of 0 or π radians depending on which mode each set of probes excites. Consequently, the coaxial antenna with this circuitry is capable of transmitting and receiving the arbitrarily polarized waves of a V.H.F. mobile section.

9.22 Polarization calibration antenna.

In the installation of a communications system, such as the V.H.F. mobile link in the previous example, it is often necessary to calibrate the radiation characteristics of the base station. A complete description maps the region served by the station in terms of the signal strength and the polarization state received at each point. To accomplish this calibration an antenna able to receive any arbitrarily polarized wave in any direction of propagation is required. From Chapter 7, the coaxial antenna controlled by the modified system circuitry, with the additional ring hybrid to retain the simple four probe excitation of the antenna, fits this description, since the circuitry completely and independently

controls the relative strengths of all the radiated component linear polarizations. Provided that the angle of arrival of the wave is known, and that the radiation patterns associated with the three dominant modes are known accurately, the polarization state of the received wave can be calculated from the settings of the phase shifters in the control circuitry. Since each relative setting of these phase shifters corresponds to a particular received polarization state for each direction of propagation, the phase shifters can be calibrated directly in terms of polarization states for each angle of arrival. Hence, the coaxial antenna can be used to perform definitive measurements of the polarization states radiated by an antenna.

9.3 Antenna design modifications.

The design of the coaxial antenna was optimised on the basis of the input port properties of the antenna, with the major emphases centred on the waveguide section lengths, and the probe design, since these were found to be the parameters most critically affecting the performance of the antenna. In this section modifications to the parameters of secondary design importance which will improve the performance of the antenna will be discussed.

The transition section of waveguide is the foremost feature of the antenna design that requires modification. The close proximity of the two step discontinuities and the presence of the probes modify the propagation characteristics within this section. However, an improved design for the

section can be derived by comparing it with a coaxial waveguide of similar dimensions. In a waveguide whose conductors are of the same diameters as those in the transition section, the TEM mode can propagate freely but the TE_{11} mode is evanescent, being just beyond cutoff. Since the outer conductor diameter is constrained to be a half a wavelength (by the array compatibility condition), the diameter of the inner conductor must be increased to allow the TE_{11} mode to propagate. From the expressions for the cutoff wavelengths of the modes, with an outer conductor of this diameter, the ratio of the radii of the conductors must be reduced to at least 3:1, which gives an inner conductor diameter of a sixth of a wavelength. By choosing the diameter of the outer conductor of the tuning section to be a third of a wavelength, the characteristic impedance of this section is the same as that associated with the TEM mode in the main section, and the impedance effects of the waveguide step discontinuities are predominantly capacitive[144] as in the original design. Consequently, by redesigning the transition section so that its outer conductor diameter is a half a wavelength and its inner conductor diameter is a sixth of a wavelength, the coaxial antenna is likely to be less sensitive to small fluctuations in frequency, because of the changes in the TE_{11} mode propagation characteristics.

A secondary design constraint considered in the development of the coaxial antenna is the overall physical length of the antenna. For certain applications, notably the mounting of a single antenna on a vehicle or aircraft, the effective physical length of the optimum design from Chapter 8 is too long, with the waveguide sections of the antenna occupying valuable space within the vehicle. To reduce the length, the tuning section is folded back into the inner conductor of the main section, as shown in Figure 9.2. This modification does not affect the performance of the antenna apart from altering the optimum design of the loop probes, due to the change in their immediate waveguide environment. All the remaining characteristics of the waveguide sections are exactly the same as in the previous design. The main disadvantage of this folded design is the difficulty of varying the tuning section dimensions in a simple manner.

Changes to the probe design follow inevitably from the suggested modifications to the waveguide design, if the optimum performance of the antenna is to be achieved. The new optimum probe design is determined experimentally in conjunction with the optimisation of the lengths of the modified waveguide sections. Moreover, these changes to the waveguide and probe designs alter the effective input impedance of the antenna, necessitating the redesigning of the compensation networks. These are designed following the procedures outlined in Chapter 8.

9.4 Suggested further experimental studies.

The performance of the coaxial antenna can be specified completely in terms of its radiation and input port characteristics. The input port parameters relating to impedance and bandwidth have been determined by experimentation (see Chapter 8), but the radiation patterns and the polarization diversity of the antenna were discussed qualitatively upon the basis of the modal radiation patterns derived in Section 6.2. Since these modal patterns represent the actual radiation patterns of the coaxial antenna to a first approximation only, it will be necessary to measure the actual patterns in order to complete the performance specification. By applying the N.F.T., as formulated in Section 6.3, the far-field radiation patterns associated with the excitation of each dominant mode in the antenna can be evaluated. Moreover, since these patterns will be expressed in terms of the field components in the far-field, this technique will also complete the specification of the polarization characteristics of the antenna.

Although an optimum geometry was derived in the experimental development of the optimum design for the antenna, the effects of the probe shape on the input properties of the antenna were not studied in sufficient depth, to enable a full appreciation of the operation of the probes. To complete this understanding of the probes it is suggested that an experimental study be conducted on the effects of the

probe shape on the input impedance and bandwidth of the antenna, in particular. It is further suggested that to facilitate this study, a time domain technique[154,155], involving the measurement of the response of the probe to an impulse or step function signal and the subsequent Fourier analysis of this response, should be employed. By this technique the input properties of the probes over the entire frequency band of operation can be computed from a single measurement, as compared with the tedious and time consuming experimental effort required for the equivalent frequency domain measurements. Furthermore, a more detailed study of the effects of varying the thickness of the probes could also be attempted, using time domain techniques than was practicable with frequency domain measurements.

Before completing the evaluation of the performance of the coaxial antenna in an array, an investigation of mutual coupling, which modifies both the radiation and the impedance properties of the array, is necessary. An array of coaxial antennas can be considered as a general N-port network, and because the input ports to the dominant modes are fully independent, each mode port will correspond to a single network port. The parameters describing the network are self and mutual impedances representing the radiation and mutual interaction effects of the modes. From this equivalent circuit representation, the total complex power applied to the array ports can be expressed in terms of

the port voltages and an impedance matrix derived from the network parameters. This complex power must equal the complex power associated with the array, which can be evaluated from the fields of the elements. Thus, by equating the two power expressions the mutual impedances may be estimated.

The mutual coupling effects can also be estimated from a complete knowledge of the scattering matrices of the elements of the array, since these matrices fully describe the radiation, scattering, and input characteristics of the elements[82]. The knowledge of the scattering matrix of the coaxial antenna is incomplete due to the difficulty of determining the scattering submatrix $\underset{\sim}{S}_{\beta\beta}$ by analytical methods. The $\underset{\sim}{S}_{\beta\beta}$ can be determined by experiment, but this would require a considerable number of measurements, corresponding to the separation of the radiation effects of each spherical mode considered in the antenna representation, and its interactions with all the remaining modes. However, the mutual coupling effects represented by the $\underset{\sim}{S}_{\beta\beta}$ are second or higher order effects, resulting from the energy that is back scattered from the array to the element, so that the direct path effects, represented by the modal receiving and radiation patterns $\underset{\sim}{S}_{\alpha\beta}$ and $\underset{\sim}{S}_{\beta\alpha}$, will be the predominant coupling effects. Since the application of the N.F.T. to the coaxial antenna determines these two submatrices, an alternative method for estimating the mutual coupling

between coaxial antennas, to the first order, is to follow the procedure formulated in Chapter 3.

To check the accuracies of the two estimations of mutual coupling, and hence, to conclude the experimental study of the coaxial antenna, the infinite array, waveguide simulator technique[53] should be applied. The simulator provides conditions corresponding to certain scan angles of the array, and the impedance of the element in the array at these scan angles can be obtained as a function of frequency, by measuring the input impedance of the simulator at each frequency. A comparison of this with the estimated values would then indicate the accuracies of the two suggested methods. Finally, the most stringent check would be the accurate prediction of the scan angles at which the element pattern nulls appear for a particular configuration of coaxial antennas in an array.

9.5 Conclusion.

The performance of the coaxial antenna, specified in terms of its radiation and input port characteristics, is determined by the antenna itself, and the degree of control exercised by the system circuitry over the antenna. The element design remains substantially the same for all applications, but the design of the control circuitry varies to satisfy differing system conditions. To recapitulate, two basic circuitry systems have been suggested for the coaxial antenna, the simple four-port system and the modified system.

Since the simplicity of the former system was achieved at the cost of reduced control over the operation of the antenna, especially the polarization diversity, this system is most suitable for inclusion in large arrays requiring only restricted control of the radiated polarization states. By greatly increasing the complexity of the circuitry, the modified system provides complete control over the operation of the antenna, so that this system is of most use in applications requiring a single radiator characterised by a wide beam, arbitrarily polarized radiation pattern. For each particular application of the antenna the control circuitry adopted will be based on these two systems, with the final design being determined by the requirements of the application. As examples, two applications of the antenna, other than inclusion in an array system, have been discussed.

Certain refinements to the design of the antenna have been indicated that will improve the performance of the antenna. Because the performance of the control circuitry is merely a function of the system complexity (that is, the required degree of antenna control can always be achieved by the addition of further circuitry), these modifications are to the element design only. Any change to the control circuitry will depend, in practice, upon the requirements of the particular application.

The present study is complete in the sense that the optimum design of the coaxial antenna has been derived to satisfy the design specifications outlined in Chapter 5. However, in some aspects the operation of the antenna is not fully understood. To improve this understanding a further experimental study has been outlined that would include the accurate measurement of the radiation patterns of the antenna by applying the N.F.T., the investigation of the input properties of the loop probes, with relation to the probe shape and thickness, using time domain techniques, and waveguide simulator measurements of mutual coupling effects. The simulator measurements will check the accuracies of the estimates of the mutual coupling between coaxial antennas calculated using the suggested equivalent circuit and scattering matrix methods. The equivalent circuit method is similar to a recently presented technique for analysing coupling in an infinite, planar array [51], based upon the complex power condition and the grating lobe series of the antenna. Consequently, the extended study would permit the specification of the radiation, coupling, and input characteristics of the coaxial antenna to be completed.

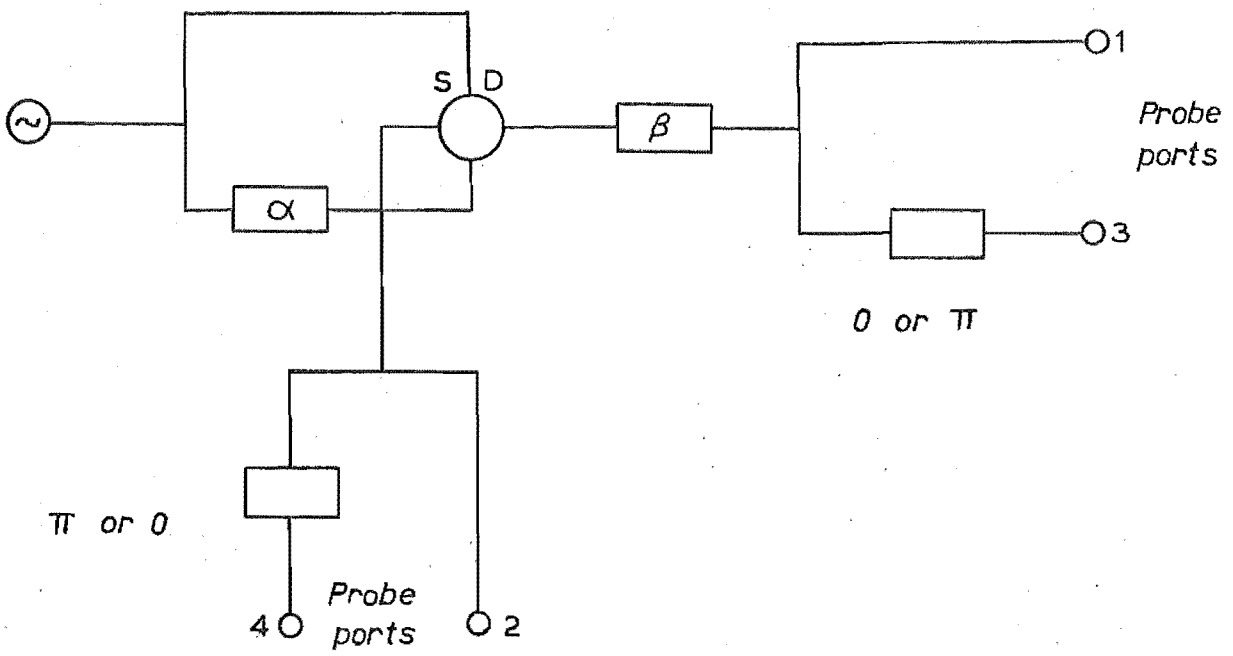

FIGURE 9·1 : SYSTEM CIRCUITRY FOR V.H.F. MOBILE STATION ANTENNA

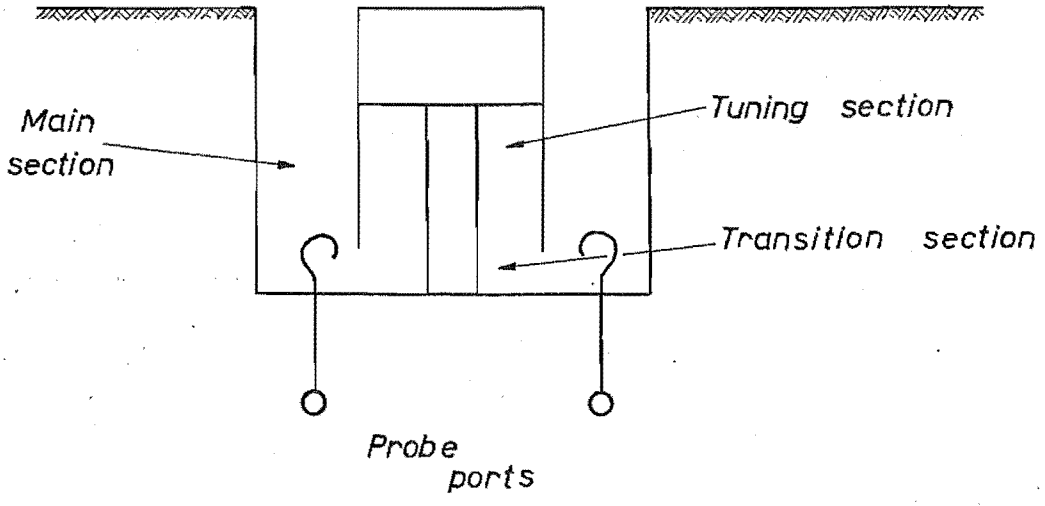

FIGURE 9·2 : FOLDED COAXIAL ANTENNA

Appendix I : Spherical vector modes.

Within a source free region the electric and magnetic fields satisfy the vector Helmholtz equation,

$$\underline{\nabla}\,\underline{\nabla}\cdot\underline{U} - \underline{\nabla}\times\underline{\nabla}\times\underline{U} + k^2\underline{U} = 0, \qquad \text{(I-1)}$$

where the field $\underline{U}$ is assumed to be harmonic with time variations of the form $e^{j\omega t}$ understood. In spherical coordinates independent solutions of this equation are constructed as

$$\underline{\ell}_{mn} = \underline{\nabla}\psi_{mn},$$

$$\underline{m}_{mn} = \underline{\nabla}\psi_{mn}\times\underline{R}, \qquad \text{(I-2)}$$

and $$\underline{n}_{mn} = \frac{1}{k}\underline{\nabla}\times\underline{m}_{mn},$$

where $\underline{R}$ is a position vector from the coordinate origin. The first set of these solutions corresponds to the longitudinal part and the other two sets correspond to the transverse solutions. Thus, since the $\underline{m}_{mn}$ are normal to $\underline{R}$ they constitute the TE partial field, while the $\underline{n}_{mn}$ can be considered as the TM modes. The ψ_{mn} are the solutions of the scalar Helmholtz equation and in spherical coordinates are given by

$$\psi_{mn} = z_n(k\rho)P_n^m(\cos\theta)\,e^{jm\phi}, \qquad \text{(I-3)}$$

where the range of the indices are $-n \leq m \leq n$, and $0 \leq n < \infty$. The associated Legendre functions are defined, following Stratton[25], as

$$P_n^m(x) = \frac{(1-x^2)^{\frac{m}{2}}}{2^n n!} \frac{d^{n+m}}{dx^{n+m}} (x^2-1)^n, \tag{I-4}$$

which is valid for negative m as well as positive m. The negative order functions therefore are defined as

$$P_n^{-m}(x) = \frac{(n-m)!}{(n+m)!} P_n^m(x) \tag{I-5}$$

The $Z_n(k\rho)$ are the spherical radial functions appropriate to the nature of the field. For example, if the mode is to represent an outward travelling wave, the radial function is $Z_n(k\rho) = h_n^{(2)}(k\rho)$.

In many problems it is convenient to express the TE and TM modes in (I-2) as odd and even functions of ϕ. Thus,

$$\underline{m}_{emn} = \frac{1}{2}[\underline{m}_{mn} + \underline{m}_{-mn}],$$

and

$$\underline{m}_{omn} = \frac{1}{2j}[\underline{m}_{mn} - \underline{m}_{-mn}], \tag{I-6}$$

and similarly for $\underline{n}_{emn}$. Combining these odd and even forms with (I-2) and (I-3), the explicit expressions

for the TE and TM vector mode functions for $0 \leq m \leq n$ and $1 \leq n \leq \infty$ are,

$$\underset{o}{\underline{m}}_{emn}(\rho,\theta,\phi) = \mp \frac{m}{\sin\theta} Z_n(k\rho)\, P_n^m(\cos\theta) \begin{matrix}\sin\\\cos\end{matrix} m\phi\ \hat{\underline{\theta}}$$

$$- Z_n(k\rho) \frac{\partial}{\partial\theta} P_n^m(\cos\theta) \begin{matrix}\cos\\\sin\end{matrix} m\phi\ \hat{\underline{\phi}}, \qquad \text{(I-7)}$$

and

$$\underset{o}{\underline{n}}_{emn}(\rho,\theta,\phi) = \frac{n(n+1)}{k\rho} Z_n(k\rho)\, P_n^m(\cos\theta) \begin{matrix}\cos\\\sin\end{matrix} m\phi\ \hat{\underline{\rho}}$$

$$+ \frac{1}{k\rho} \frac{\partial}{\partial\rho} [\rho Z_n(k\rho)] \frac{\partial}{\partial\theta} P_n^m(\cos\theta) \begin{matrix}\cos\\\sin\end{matrix} m\phi\ \hat{\underline{\theta}}$$

$$\mp \frac{m}{k\rho\sin\theta} \frac{\partial}{\partial\rho} [\rho Z_n(k\rho)]\, P_n^m(\cos\phi) \begin{matrix}\sin\\\cos\end{matrix} m\phi\ \hat{\underline{\phi}}.$$

Appendix II : The electric vector potential

The electric vector potential $\underline{F}$ is introduced such that

$$\underline{E} = \nabla \times \underline{F},$$
$$\underline{H} = \frac{j}{\omega\mu} [\nabla\nabla \cdot \underline{F} + k^2 \underline{F}]. \tag{II-1}$$

The two rectangular components of the potential, F_x and F_y, satisfy the scalar Helmholtz equation. Thus, suitable forms for these components are

$$F_x = -\frac{1}{2\pi} \iint_{Ap.} Q(\xi,\eta) \frac{e^{-jkR}}{R} \, d\xi d\eta,$$
$$F_y = +\frac{1}{2\pi} \iint_{Ap.} P(\xi,\eta) \frac{e^{-jkR}}{R} \, d\xi d\eta, \tag{II-2}$$

where $P(\xi,\eta)$ and $Q(\xi,\eta)$ are amplitude factors, $\frac{e^{-jkR}}{R}$ is the free space Green's function, and Ap. denotes that the integrations are performed over the aperture of the antenna. Substituting (II-2) into (II-1), the $\hat{x}$ component of the aperture electric field is given by,

$$E(x,0) = \lim_{z\to 0} E_x = \lim_{z\to 0} \frac{1}{2\pi} \iint_{Ap.} P(\xi,\eta) \left[\frac{jk}{R} + \frac{1}{R^2}\right] e^{-jkr} \cdot \frac{z}{R} \, d\xi d\eta, \tag{II-3}$$

since $R = [z^2 + (x-\xi)^2 + (y-\eta)^2]^{1/2}$.

By changing the variables of integration to

$$\alpha = \xi - x = r\cos\psi, \qquad \beta = \eta - y = r\sin\psi, \tag{II-4}$$

and (II-3) becomes

$$E(x,0) = \lim_{z\to 0} \frac{z}{2\pi} \iint_{Ap.} P(\alpha+x,\beta+y)\, \frac{e^{-jkR}}{z^2+\alpha^2+\beta^2}\left[\frac{1}{\sqrt{z^2+\alpha^2+\beta^2}} + jk\right] d\alpha d\beta. \tag{II-5}$$

In the aperture r is small so that α and β are small and $P(\alpha+x,\beta+y) \to P(x,y)$. Furthermore, since z is small

$$e^{-jkR} = e^{-jk\sqrt{z^2+r^2}} \simeq 1 - jk\sqrt{z^2+r^2}. \tag{II-6}$$

Consequently, from (II-5), changing the variables of integration to the polar coordinates (r,ψ), and performing the ψ integration,

$$E(x,0) = \lim_{z\to 0} zP(x,y) \int_0^a \frac{1}{\sqrt{z^2+r^2}}\left[\frac{1}{\sqrt{z^2+r^2}} + k^2\right] r\,dr, \tag{II-7}$$

where a is the radius of the aperture. Finally, by substituting $R = \sqrt{z^2+r^2}$, (II-7) can be reduced to

$$E(x,0) = \lim_{z\to 0} P(x,y)\left[1 - \frac{z}{\sqrt{z^2+a^2}}\right],$$

$$= P(x,y). \tag{II-8}$$

Hence $P(x,y)$, which appears in (II-2) as an amplitude factor, is the $\hat{x}$ component of the tangential electric field in the aperture. In a similar manner, it can be shown that $Q(x,y)$ is the $\hat{y}$ component of the aperture field.

Appendix III : Addition theorems for spherical vector modes.

The translational addition theorems for spherical vector modes developed by Stein[84] and Cruzan[85] can be summarized as

$$\underline{m}_{\mu\nu} = \sum_{n=0}^{\infty} \sum_{m=-n}^{n} (A_{mn}^{\mu\nu} \underline{m}'_{mn} + B_{mn}^{\mu\nu} \underline{n}'_{mn}), \qquad \text{(III-1)}$$

and

$$\underline{n}_{\mu\nu} = \sum_{n=0}^{\infty} \sum_{m=-n}^{n} (A_{mn}^{\mu\nu} \underline{n}'_{mn} + B_{mn}^{\mu\nu} \underline{m}'_{mn}), \qquad \text{(III-2)}$$

where the modes $\underline{m}_{\mu\nu}$ and $\underline{n}_{\mu\nu}$ are referred to the origin O_1, and the modes $\underline{m}'_{mn}$ and $\underline{n}'_{mn}$ are referred to the origin O_2 whose coordinates with respect to O_1 are (R_o, θ_o, ϕ_o). The vector modes are in the complex form as given in Appendix I.

The coefficients in (III-1) and (III-2) are defined by

$$A_{mn}^{\mu\nu} = (-1)^m \sum_p a(\mu,\nu|-m,n|p,p)\, a(\nu,n,p)\, Z_p(kR_o)\, P_p^{\mu-m}(\cos\theta_o)\, e^{j(\mu-m)\phi_o}, \qquad \text{(III-3)}$$

and

$$B_{mn}^{\mu\nu} = (-1)^{m+1} \sum_p a(\mu,\nu|-m,n|p,p-1)\, b(\nu,n,p)\, Z_p(kR_o)\, P_p^{\mu-m}(\cos\theta_o)\, e^{j(\mu-m)\phi_o}, \qquad \text{(III-4)}$$

where

$$a(\nu,n,p) = j^{n+p-\nu} [2n(n+1)(2n+1)+(n+1)(\nu-n+p+1)(\nu+n-p) - n(n-\nu+p+1)(\nu+n+p+2)]/[2n(n+1)], \qquad \text{(III-5)}$$

and

$$b(\nu,n,p) = j^{n+p-\nu}\left[(\nu+n+p+1)(n-\nu+p)(\nu-n+p)(\nu+n-p+1)\right]^{\frac{1}{2}} \cdot (2n+1)/[2n(n+1)]. \qquad \text{(III-6)}$$

In these expansions the index p assumes the values

$$|\nu-n| \leq p \leq \nu+n, \qquad \text{(III-7)}$$

and the choice of the spherical radial functions $z_p(kR_o)$ is determined by the form of the solution at O_2.

The remaining coefficients are given by

$$a(\mu,\nu|-m,n|p,q) = (-1)^{\mu-m}\left[\frac{(\nu+\mu)!(n-m)!(p+m-\mu)!}{(\nu-\mu)!(n+m)!(p-m+\mu)!}\right]^{\frac{1}{2}} (2p+1) \cdot \begin{bmatrix} \nu & n & p \\ \mu & -m & -\mu+m \end{bmatrix} \begin{bmatrix} \nu & n & q \\ 0 & 0 & 0 \end{bmatrix}, \qquad \text{(III-8)}$$

where

$$\begin{vmatrix} j_1 & j_2 & j_3 \\ m_1 & m_2 & m_3 \end{vmatrix}$$

is the Wigner 3-j symbol[138].

Appendix IV : Proof of stationary nature of aperture admittance expression.

The stationary nature of (4.32) is proved by applying the calculus of variations. Thus, (4.29) and (4.30) are multiplied by $\rho\delta E_\phi$ and $-\rho\delta E_\rho$, respectively, where δ denotes small quantity, integrated over the aperture domain, and summed to give

$$\int_0^{2\pi}\int_0^{a}(\rho\delta E_\phi H_\rho - \rho\delta E_\rho H_\phi)\,d\rho\,d\phi = \frac{-1}{2\pi}\int_0^{2\pi}\int_0^{a}\int_0^{2\pi}\int_0^{a}[(E_r\sin\psi+E_\psi\cos\psi)$$

$$(\delta E_\phi L_1-\delta E_\rho L_3) + (-E_r\cos\psi+E_\psi\sin\psi)(\delta E_\phi L_2-\delta E_\rho L_4)]\frac{e^{-jkR}}{R}$$

$$\cdot r\rho\,dr\,d\psi\,d\rho\,d\phi, \qquad \text{(IV-1)}$$

using (2.6) and (2.7). From the simultaneous equations in Y for H_ρ and H_ϕ derived from the magnetic field continuity equation, the L.H.S. of (IV-1) is also given by

$$-C_{h1}Y\delta I_{h1}I_{h1} + j\sum_{n=1}^{\infty}{}'[C_{hn}\delta I_{hn}I_{hn} - C_{en}\delta I_{en}I_{en}]. \qquad \text{(IV-2)}$$

Similarly, multiplying (4.29) by ρE_ϕ and (4.30) by $-\rho E_\rho$, integrating over the aperture and summing the resultant expressions gives

$$\int_0^{2\pi}\int_0^{a} (\rho E_\phi H_\rho - \rho E_\rho H_\phi)\, d\rho\, d\phi = \frac{-1}{2\pi} \int_0^{2\pi}\int_0^{a}\int_0^{2\pi}\int_0^{a} [(E_r \sin\psi + e_\psi \cos\psi)$$

$$(E_\phi L_1 - E_\rho L_3) + (-E_r \cos\psi + E_\psi \sin\psi)(E_\phi L_2 - E_\rho L_4)]\cdot$$

$$\cdot \frac{e^{-jkR}}{R}\, r\rho\, dr\, d\psi\, d\rho\, d\phi, \qquad \text{(IV-3)}$$

which, from the alternative equations for H_ρ and H_ϕ, is also given by

$$-C_{h1} Y I_{h1}^2 + j \sum_{n=1}^{\infty}{}' [C_{hn} I_{hn}^2 - C_{en} I_{en}^2]. \qquad \text{(IV-4)}$$

From (4.32), by the calculus of variations, the variation of Y due to a small perturbation of the aperture field $\delta\underline{E}$ is

$$\delta Y = \frac{1}{C_{h1} I_{h1}^4} \{ I_{h1}^2 [\frac{1}{2\pi} \int_0^{2\pi}\int_0^{a}\int_0^{2\pi}\int_0^{a} [(\delta E_r \sin\psi + \delta E_\psi \cos\psi)$$

$$(E_\phi L_1 - E_\rho L_3) + (E_r \sin\psi + E_\psi \cos\psi)(\delta E_\phi L_1 - \delta E_\rho L_3)$$

$$+ (-\delta E_r \cos\psi + \delta E_\psi \sin\psi)(E_\phi L_2 - E_\rho L_4) + (-E_r \cos\psi + E_\psi \sin\psi)$$

$$(\delta E_\phi L_2 - \delta E_\rho L_4)] \frac{e^{-jkR}}{R}\, r\rho\, dr\, d\psi\, d\rho\, d\phi + j \sum_{n=1}^{\infty}{}' (2C_{hn} \delta I_{hn} I_{hn}$$

$$- 2C_{en} \delta I_{en} I_{en})] - 2\delta I_{h1} I_{h1} [\frac{1}{2\pi} \int_0^{2\pi}\int_0^{a}\int_0^{2\pi}\int_0^{a} [(E_r \sin\psi + E_\psi \cos\psi)$$

$$(E_\phi L_1 - E\rho L_3) + (-E_r \cos\psi + E_\psi \sin\psi)(E_\phi L_2 - E_\rho L_4)] \frac{e^{-jkR}}{R}\, r\rho\, dr\, d\psi\, d\rho\, d\phi$$

$$+ j \sum_{n=1}^{\infty}{}' (C_{hn}I_{hn}^2 - C_{en}I_{en}^2)]\}. \qquad \text{(IV-5)}$$

By symmetry the first term in (IV-5) is

$$2 \times \frac{1}{2\pi} \int_0^{2\pi} \int_0^{a} \int_0^{2\pi} \int_0^{a} [(E_r \sin\psi + E_\psi \cos\psi)(\delta E_\phi L_1 - \delta E_\rho L_3)$$

$$+ (-E_r \cos\psi + E_\psi \sin\psi)(\delta E_\phi L_2 - \delta E_\rho L_4)] \frac{e^{-jkR}}{R} \rho \, d\rho \, d\psi \, d\rho \, d\phi, \qquad \text{(IV-6)}$$

which is found by equating (IV-1) and (IV-2). Also equating (IV-3) and (IV-4) allows the last term in (IV-5) to be determined. Substituting these expressions into (IV-5) gives

$$\delta Y = \frac{1}{C_{h1}I_{h1}^4} \{I_{h1}^2 [2C_{h1}Y\delta I_{h1}I_{h1} - j2 \sum_{n=1}^{\infty}{}' (C_{hn}\delta I_{hn}I_{hn} - C_{en}\delta I_{en}I_{en})$$

$$+ j2 \sum_{n=1}^{\infty}{}' (C_{hn}\delta I_{hn}I_{hn} - C_{en}\delta I_{en}I_{en})] - 2\delta I_{h1}I_{h1}C_{h1}YI_{h1}^2\}$$

$$= 0. \qquad \text{(IV-7)}$$

Hence, the expression for the aperture admittance of the circular waveguide antenna is stationary with respect to small variations of the aperture field about its correct value.

Appendix V : Reduction of the variational expression for aperture admittance.

(A) By representing the aperture fields by a set of waveguide modes of the forms TE_{1n} and TM_{1n}, the tangential components of the aperture electric field in cylindrical coordinates are

$$E_\rho = \sin\phi \sum_{m=1}^{\infty} \left[A_m \frac{j_1(h'_m\rho)}{\rho} + B_m h_m J'_1(h_m\rho) \right] = \sin\phi e_\rho ,$$

and

$$E_\phi = \cos\phi \sum_{m=1}^{\infty} \left[A_m h'_m J'_1(h'_m\rho) + B_m \frac{J_1(h_m\rho)}{\rho} \right] = \cos\phi e_\phi . \qquad (V\text{-}1)$$

Substituting these forms into (4.25) and (4.27), noting the form of the Lommel integration formulae for cylindrical Bessel functions[133], and performing the integrations over the aperture domain gives

$$I_{hn} = \frac{\pi A_n J_1^2(h'_n a)}{2}(h'^2_n a^2 - 1), \qquad (V\text{-}2)$$

and

$$I_{en} = \frac{\pi B_n h_n^2 a^2 J_o^2(h_n a)}{2}. \qquad (V\text{-}3)$$

(B) The first term in the numerator of (4.32), Y_{num}, is evaluated by introducing the integral representation for the Green's function[156]. Thus,

$$\frac{e^{-jkR}}{R} = \int_0^\infty \frac{\zeta d\zeta}{\sqrt{\zeta^2 - k^2}} J_o(R\zeta), \qquad (V\text{-}4)$$

where the contour of integration is along the positive real ζ axis with an upward indentation at the pole $\zeta = k$, as shown in the figure.

Choice of contour for integral representation of the Green's function.

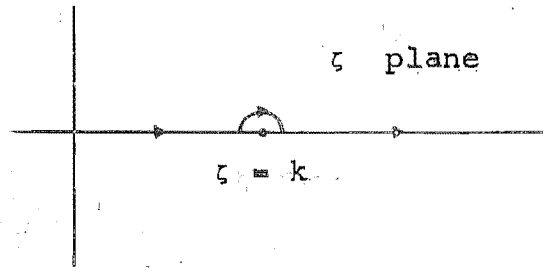

Applying the addition theorem for Bessel functions (V-4) becomes

$$\frac{e^{-jkR}}{R} = \int_0^\infty \frac{\zeta d\zeta}{\sqrt{\zeta^2 - k^2}} \sum_{\ell=0}^{\infty} \varepsilon_\ell J_\ell(p\zeta) J_\ell(r\zeta) \cos\ell(\phi-\psi), \quad \text{(V-5)}$$

where ε_ℓ is the Neumann factor. Substituting (V-1) and (V-5) into (4.32) and performing the integrations over the ϕ and ψ variables gives Y_{num} as

$$Y_{num} = \frac{j\pi}{2\omega\mu} \int_0^a \int_0^a \int_0^\infty \frac{\zeta d\zeta}{\sqrt{\zeta^2 - k^2}} \{(e_r + e_\psi)[e_\phi\{-\zeta^2 J_1'(\zeta\rho) J_0(\zeta r) + k^2 J_0(\zeta\rho) J_0(\zeta r)\} - e_\rho\{\frac{\zeta}{\rho} J_1(\zeta\rho) J_0(\zeta r) - k^2 J_0(\zeta\rho) J_0(\zeta r)\}] + (-e_r + e_\psi)[e_\phi\{\zeta^2 J_1'(\zeta\rho) J_2(\zeta r) + k^2 J_2(\zeta\rho) J_2(\zeta r)\} - e_\rho\{-\frac{\zeta}{\rho} J_1(\zeta\rho) J_2(\zeta r) + k^2 J_2(\zeta\rho) J_2(\zeta r)\}]\} r\rho dr d\rho, \quad \text{(V-6)}$$

where e_r and e_ψ are of the same forms as e_ρ and e_ϕ, respectively, with a different summation index q. Performing the integrations over the radial variables ρ and r,

$$Y_{num} = \frac{j\pi}{2\omega\mu} \int_0^\infty \frac{\zeta d\zeta}{\sqrt{\zeta^2 - k^2}} \sum_{m=1}^{\infty} \sum_{q=1}^{\infty} [\{U_3^m(\zeta)+U_3^m(\zeta)\}V_{00}^q(\zeta)+\zeta U_1^m(\zeta)V_{22}^q(\zeta)$$

$$+\{\zeta U_1^m(\zeta)+U_2^m(\zeta)-U_3^m(\zeta)\}V_{20}^q(\zeta)], \qquad (V-7)$$

where

$$U_1^m(\zeta) = -2A_m \int_0^a \{h_m'\zeta\rho J_0(h_m'\rho)J_0(\zeta\rho) - \frac{\partial}{\partial\rho}[J_1(h_m'\rho)J_1(\zeta\rho)]\}d\rho$$

$$+ \frac{2k^2}{\zeta} \int_0^a [A_m h_m' J_2(h_m'\rho)J_2(\zeta\rho) - B_m h_m J_2(h_m\rho)J_2(\zeta\rho)]\rho d\rho,$$

$$U_2^m(\zeta) = \frac{2A_m k^2 J_1(h_m'a)J_1(\zeta a)}{\zeta} + 2B_m k^2 \int_0^a h_m \rho J_0(h_m\rho)J_0(\zeta\rho)d\rho,$$

$$U_3^m(\zeta) = \frac{2A_m(k^2-\zeta^2)}{\zeta} [\int_0^a h_m'\zeta\rho J_0(h_m'\rho)J_0(\zeta\rho)d\rho - J_1(h_m'a)J_1(\zeta a)],$$

$$V_{00}^q(\zeta) = \int_0^a [A_q h_q' J_0(h_q'r)J_0(\zeta r) + B_q h_q J_0(h_q r)J_0(\zeta r)]rdr, \qquad (V-8)$$

$$V_{22}^q(\zeta) = \int_0^a [A_q h_q' J_2(h_q'r)J_2(\zeta r) - B_q h_q J_2(h_q r)J_2(\zeta r)]rdr,$$

and

$$V_{20}^q(\zeta) = \int_0^a [A_q h_q' J_2(h_q'r)J_0(\zeta r) - B_q h_q J_0(h_q r)J_0(\zeta r)]rdr.$$

The integrations in (V-8), with the exception of the integral in $V^{q}_{20}(\zeta)$ which must be performed numerically, are evaluated by the Lommel integration formulae.

The ζ integration must be considered in three parts; the integrations along the axis up to the pole, around the pole, and from the pole to infinity. That is,

$$\int_0^{\infty} Fn(\zeta)\,d\zeta = \lim_{\zeta' \to k} \int_0^{\zeta'} Fn(\zeta)\,d\zeta + \lim_{b \to 0} \int_{\pi}^{0} Fn(\theta)\,d\theta + \lim_{\zeta' \to k} \int_{\zeta'}^{\infty} Fn(\zeta)\,d\zeta, \qquad \text{(V-9)}$$

where $Fn(\zeta)$ is the functional dependence of Y_{num} on ζ, and b is the radius of the semicircular indentation centred at the pole $\zeta = k$. The contribution from the pole is found by integrating around this indentation. Hence, substituting $\zeta = k + be^{j\theta}$ in (V-7) and taking the limit as b tends towards zero, the contribution from the pole is

$$\lim_{b \to 0} \int_{\pi}^{0} \frac{be^{j\theta} \cdot jbe^{j\theta} d\theta}{\sqrt{2kbe^{j\theta} + b^2 e^{j2\theta}}} \qquad \left[\begin{matrix}\text{Higher order} \\ \text{terms in } k+be^{j\theta}\end{matrix}\right]$$

$$= \lim_{b \to 0} \int_{\pi}^{0} \frac{jbe^{j2\theta} d\theta}{\sqrt{\frac{2ke^{j\theta}}{b} + e^{j2\theta}}} \qquad \left[\begin{matrix}\text{Higher order} \\ \text{terms}\end{matrix}\right]$$

$$= 0.$$

The ζ integration reduces to two parts, for $0 \leq \zeta < k$ and $k < \zeta \leq \infty$. Substituting $\zeta = k\sin\theta$ in (V-7) over the former range and $\zeta = k\cosh\alpha$ over the latter range, Y_{num} is

$$Y_{num} = \lim_{\theta' \to \pi/2} \left[\frac{\pi}{2\omega\mu} \int_0^{\theta'} k\sin\theta d\theta \sum_{m=1}^{\infty} \sum_{q=1}^{\infty} \right.$$

$$\{[U_2^m(k\sin\theta)+U_3^m(k\sin\theta)]V_{00}^q(k\sin\theta)+k\sin\theta U_1^m(k\sin\theta)V_{22}^q(k\sin\theta)$$

$$\left. +[k\sin\theta U_1^m(k\sin\theta)+U_2^m(k\sin\theta)-U_3^m(k\sin\theta)]V_{20}^q(k\sin\theta)\}\right]$$

$$+ \lim_{\alpha' \to 0} \left[\frac{j\pi}{2\omega\mu} \int_{\alpha'}^{\infty} k\cosh\alpha d\alpha \sum_{m=1}^{\infty} \sum_{q=1}^{\infty} \{[U_2^m(k\cosh\alpha)+U_3^m(k\cosh\alpha)]\right.$$

$$V_{00}^q(k\cosh\alpha)+k\cosh\alpha U_1^m(k\cosh\alpha)V_{22}^q(k\cosh\alpha)$$

$$\left. +[k\cosh\alpha U_1^m(k\cosh\alpha)+U_2^m(k\cosh\alpha)-U_3^m(k\cosh\alpha)]V_{20}^q(k\cosh\alpha)\}\right]. \qquad (V-11)$$

The integrations over θ and α must be performed numerically.

REFERENCES

1. Brown, J., and Jull, E.V.: "The prediction of aerial radiation patterns from near-field measurements", Proc. IEE., 1961, 108B, pp 635-644.
2. Blakey, J.R.: "Near-field measurements and the determination of aerial patterns", Radio Electronic Engr. (G.B.), 1964, 28, pp 295-303.
3. Jensen, F.: "Electromagnetic near-field - far-field correlations", Technical Univ. of Denmark, Report LD15, July 1970.
4. Allen, J.L.: "Array antennas: new applications for an old technique", IEEE Spectrum, 1964, 1, pp 115-130.
5. Hansen, R.C.: "Microwave scanning antennas", Academic Press, 1966, VOLS. II and III.
6. Special publications: Radio Science, 1968, 3, n5
   Proc. IEEE., 1968, 56, n11.
7. Silver, S.: "Microwave antenna theory and design", McGraw-Hill, 1949, Chap. 6.
8. Cutler, C.C., King, A.P., and Kock, W.E.: "Microwave antenna measurements", Proc. IRE., 1947, 35, p 1462.
9. Levy, G.S., Bathker, D.A., Ludwig, A.C., Neff, D.E., and Seidel, B.L.: "Lunar range radiation patterns of a 210-foot antenna at S-band", IEEE. Trans., 1967, AP-15, pp 311-313.
10. Smith, P.G.: "Far-field pattern measurements by radio star sources", IEEE. Trans., 1966, AP-14, n1.

11. Bates, R.H.T., and Elliot, J.: "The determination of the true side-lobe level of long broadside arrays from radiation-pattern measurements made in the Fresnel region", Proc. IEE., 1956, Monograph 169R (103, C, p 307).

12. Booker, H.G. and Clemmow, P.C.: "The concept of an angular spectrum of plane waves, and its relation to that of polar diagram and aperture distribution", Journal IEE., 1950, 97, Pt. III, pp 11-17.

13. Brown, J.: "A theoretical analysis of some errors in aerial measurements", Proc. IEE., 1958, Monograph 285R (105, C, pp 343-351).

14. Bickmore, R.W.: "Fraunhofer pattern measurements in the Fresnel zone", Can. J. Phys., 1957, 35, p 1299.

15. Soejima, T.: "Near-field problems of antennas", Elect. Comm. Japan, 1965, 48, pp 56-67.

16. Jull, E.V.: "An investigation of near-field radiation patterns measured with large antennas", IRE. Trans., 1962, AP-10, pp 363-368.

17. Jull, E.V.: "The estimation of aerial radiation patterns from limited near-field measurements", Proc. IEE., 1963, 110, pp 501-506.

18. Blakey, J.R.: "Errors in near-field measurements and their effect on computed radiation patterns", Electronics Letters, 1966, 2, pp 299-300.

19. Martin, W.W.: "Computation of antenna radiation patterns from near-field measurements", IEEE. Trans. 1967, AP-15, pp 316-318.

20. James, J.R., and Longdon, L.W.: "Prediction of arbitrary electromagnetic fields from measured data", Alta Frequenza, 1969, 38, Numero Speciale, pp 286-290.

21. Hansen, R.C.: op. cit., Volume I, Chap. 1.

22. Hamid, M.A.K.: "The radiation pattern of an antenna from near-field correlation methods", IEEE. Trans., 1968, AP-16, pp 351-353.

23. Stratton, J.: "Electromagnetic theory", McGraw-Hill, 1941, Chap. 9.

24. Morse, P.M., and Feshbach, H.: "Methods of theoretical physics", McGraw-Hill, 1953, Chap. 6.

25. Stratton, J.: op. cit., Chap. 7.

26. Fox, L., and Mayers, D.F.: "Computing methods for scientists and engineers", Clarendon Press, 1968.

27. Jones, D.S.: "The theory of electromagnetism", Pergamon Press, 1964, Chap. 1.

28. Harrington, R.F.: "Time-harmonic electromagnetic fields", McGraw-Hill, 1961.

29. Jahnke, E., and Emde, F.: "Tables of functions with formulae and curves", reprint by Dover, 1943.

30. Jordan, E.C., and Balmain, K.G.: "Electromagnetic waves and radiating systems", Prentice-Hall, 1968, Chap. 12.

31. Woodward, P.M., and Lawson, J.D.: "The theoretical precision with which an arbitrary radiation pattern may be obtained from a source of finite size", Journal IEE., 1948, 95, Pt. III, pp 363-370.

32. Andrews, C.L.: "Microwave probes for electric fields near metal surfaces", IEEE. Trans., 1968, AP-16, pp 441-445.

33. Burgess, R.E.: "The screened loop aerial", Wireless Engineer, 1939, 16, n193, pp 492-499.

34. Whiteside, H., and King, R.W.P.: "The loop antenna as a probe", IEEE. Trans., 1964, AP-12, pp 291-297.

35. Watt, A.D.: "VLF radio engineering", Pergamon Press, 1967.

36. Carter, P.S.: "Circuit relations in radiating systems and applications to antenna problems", Proc. IRE., 1932, 20, p 1004.

37. Wheeler, H.A.: "The radiation resistance of an antenna in an infinite array or waveguide", Proc. IRE., 1948, 36, pp 478-487.

38. King, R.W.P.: "Theory of linear antennas", Harvard Univ. Press, 1956.

39. Allen, J.L.: "The theory of array antennas", Lincoln Lab., 1963, Report 323.

40. Stark, L.: "Radiation impedance of a dipole in an infinite planar phased array", Radio Science, 1966, 1, pp 361-377.

41. Allen, J.L.: "A simple model for mutual coupling effects on patterns of unequally spaced arrays", IEEE. Trans., 1967, AP-15, pp 530-533.

42. Chang, V.W.H.: "Infinite phased dipole array", Proc. IEEE, 1968, 56, pp 1892-1900.

43. Edelberg, S., and Oliner, A.A.: "Mutual coupling effects in large antenna arrays", IRE. Trans, 1960, AP-8, p 286.

44. Galindo, V. and Wu, C.P.: "Numerical solutions for an infinite phased array of rectangular waveguides with thick walls", IEEE. Trans., 1966, AP-14, pp 149-158.

45. Galindo, V., and Wu, C.P.: "Properties of a phased array of rectangular waveguides with thin walls", IEEE. Trans., 1966, AP-14, pp 163-173.

46. Wheeler, H.A.: "The grating lobe series for the impedance variation of an antenna in a planar phased-array", IEEE. Trans., 1966, AP-14, pp 707-714.

47. Rhodes, D.R.: "On a fundamental principle in the theory of planar antennas", Proc. IEEE., 1964, 52, pp 1013-1021.

48. Farrell, G.F., and Kuhn, D.H.: "Mutual coupling in infinite planar arrays of rectangular waveguide horns", IEEE. Trans., 1968, AP-16, pp 405-414.

49. Borgiotti, G.V.: "Modal analysis of periodic planar phased arrays of apertures", Proc. IEEE., 1968, 56, pp 1881-1892.

50. Borgiotti, G.V.: "Radiation and reactive energy of aperture antennas", IEEE. Trans., 1963, AP-11, pp 94-95.

51. Diamond, B.L.: "A generalized approach to the analysis of infinite planar array antennas", Proc. IEEE., 1968, 56, pp 1837-1851.

52. Brown, C.R., and Carberry, T.F.: "A technique to simulate the self and mutual impedances of an array", IEEE. Trans., 1963, AP-11, pp 377-378.

53. Hannan, P.W., Meier, P.J., and Balfour, M.A.: "Simulation of phased array antenna impedance in waveguide", IEEE. Trans., 1963, AP-11, pp 715-716.

54. Hannan, P.W., and Balfour, M.A." "Simulation of a phased-array antenna in waveguide", IEEE. Trans., 1965, AP-13, pp 342-353.

55. Keller, J.B.: "Geometrical theory of diffraction", J. Opt. Soc. Am., 1962, 52, pp 116-130.

56. Dybdal, R.B., Rudduck, R.C., and Tsai, L.L.: "Mutual coupling between TEM and TE_{01} parallel-plate waveguide apertures", IEEE. Trans., 1966, AP-14, pp 574-580.

57. Hamid, M.A.K.: "Mutual coupling between sectoral horns side by side", IEEE. Trans., 1967, AP-15, pp 475-477.

58. Bates, R.H.T.: "Mode theory approach to arrays", IEEE. Trans., 1965, AP-13, pp 321-322.

59. Lechtreck, L.W.: "Effects of coupling accumulation in antenna arrays", IEEE. Trans., 1968, AP-16, pp 31-37.

60. Hannan, P.W.: "Discovery of an array surface wave in a simulator", IEEE. Trans., 1967, AP-15, pp 574-576.

61. Allen, J.L.: "On surface-wave coupling between elements of large arrays", IEEE. Trans., 1965, AP-13, p 638.

62. Wu, C.P., and Galindo, V.: "Surface-wave effects on dielectric sheathed phased arrays of rectangular waveguides", BSTJ., 1968, 47, pp 117-142.

63. Knittel, G.H., Hessel, A., and Oliner, A.A.: "Element pattern nulls in phased arrays and relation to guided waves", Proc. IEEE., 1968, 56, pp 1822-1837.

64. Amitay, N., and Galindo, V.: "Characteristics of dielectric loaded and covered circular waveguide phased arrays", IEEE. Trans., 1969, AP-17, pp 722-729.

65. Wu, C.P.: "Characteristics of coupling between parallel-plate waveguides with and without dielectric plugs", IEEE. Trans., 1970, AP-18, pp 188-194.

66. Wu, C.P.: "Analysis of finite parallel-plate waveguide arrays", IEEE. Trans., 1970, AP-18.

67. Montgomery, C.G., Dicke, R.H., and Purcell, E.M.: "Principles of microwave circuits", McGraw-Hill, 1948, Chap. 5 and Chap. 9.

68. Raschke, R.R., and Heidrich, A.J.: "Application of scattering matrix method to antenna coupling problems", IEEE Electromagnetic Compatibility Symp. Rec., 1967, pp 126-144.

69. DuFort, E.C.: "A scattering matrix method for solving waveguide array impedance problems", Radio Science, 1968, 3, pp 475-485.

70. Mailloux, R.J.: "First order solutions for mutual coupling between waveguides which propagate two orthogonal modes", IEEE. Trans., 1969, AP-17, pp 740-746.

71. Wasylkiwskj, W., and Kahn, W.K.: "Mutual coupling and element efficiency for infinite linear arrays", Proc. IEEE., 1968, 56, pp 1901-1907.

72. Wasylkiwskj, W., and Kahn, W.K.: "Theory of mutual coupling among minimum-scattering antennas", IEEE. Trans., 1970, AP-18, pp 204-216.

73. Gately, A.C., Stock, D.J.R., and Ru-Shao Cheo, B.: "A network description for antenna problems", Proc. IEEE., 1968, 56, pp 1181-1193.

74. Hannan, P.W.: "The element-gain paradox for a phased-array antenna", IEEE. Trans., 1964, AP-12, pp 423-433.

75. Hannan, P.W., Lerner, D.S., and Knittel, G.H.: "Impedance matching phased-array antenna over wide scan angles by connecting circuits", IEEE. Trans. 1965, AP-13, pp 28-34.

76. Amitay, N.: "Improvement of planar array match by compensation through contiguous element coupling", IEEE. Trans., 1966, AP-14, pp 580-586.

77. Hannan, P.W.: "Proof that a phased-array antenna can be impedance matched for all scan angles", Radio Science, 1967, 2, pp 361-369.

78. Varon, D., and Zysman, G.I.: "On the mismatch of electronically steerable phased-array antennas", Radio Science, 1968, 3, pp 487-489.

79. King, D.D., and Peters, H.J.: "Element interaction in steerable arrays", Microwave J., 1963, 6, pp 73-77.

80. Kyle, R.H.: "Mutual coupling between log-periodic antennas", IEEE. Trans., 1970, AP-18, pp 15-22.

81. Kahn, W.K., and Kurss, H.: "Minimum-scattering antennas", IEEE. Trans., 1965, AP-13, pp 671-675.

82. Harrington, R.F.: "Matrix methods for field problems", Proc. IEEE., 1967, 55, pp 136-149.

83. Morse, P.M., and Feshbach, H.: op.cit., Chap. 13.

84. Stein, S.: "Addition theorems for spherical wave functions", Quart. Appl. Math., 1961, 19, pp 15-24.

85. Cruzan, O.R.: "Translational addition theorems for spherical vector wave functions", Quart. Appl. Math., 1961, 20, pp 33-40.

86. Iijima, T.: "Theory of radiation from an open-ended waveguide", Elect. Comm. Japan, 1965, 48, pp 533-540.

87. Weinstein, L.A.: "Theory of symmetrical waves in a circular waveguide with open end", J. Tech. Phys. USSR., 1948, 18, pp 1543-1564.

88. Pearson, J.D.: "Diffraction of electromagnetic wave by a semi-infinite circular waveguide", Proc. Camb. Phil. Soc., 1953, 49, p 659.

89. Levine, H., and Schwinger, J.: "On the theory of electromagnetic wave diffraction by an aperture in an infinite plane conducting screen", Comm. Pure and Appl. Math., 1950, 3, pp 355-391.

90. Miles, J.W.: "The coupling of a cylindrical tube to a half-infinite space", J. Acoustical Soc. Am., 1948, 20, pp 652-664.

91. Samaddar, S.N.: "Theory of radiation from open end of circular waveguide flush mounted to a flat ground plane", J. Engineering Math., 1967, 1, pp 251-272.

92. Mishustin, B.A.: "Radiation from the aperture of a circular waveguide with an infinite flange", Soviet Radiophys. (U.S.A.), 1965, 8, pp 852-858.

93. Silver, S.: op.cit., Chap. 10.

94. Chu, L.J.: "Calculation of the radiation properties of hollow pipes and horns", J. Appl. Phys., 1940, 11, pp 603-610.

95. Potter, P.D.: "A new horn antenna with suppressed sidelobes and equal beamwidths", Microwave J., 1963, 6, pp 71-78.

96. Jones, D.S.: op.cit., Chap. 9.

97. Cole, W.J., Nagelberg, E.R., and Nagel, C.M.: "Iterative solution of waveguide discontinuity problems", BSTJ., 1967, 66, p 649.

98. Marcuvitz, N.: "Waveguide handbook", McGraw-Hill, 1951, Chap. 2.

99. Lewin, L.: "Advanced theory of waveguides", Iliffe, 1951, Chap. 7.

100. King, A.P.: "The radiation characteristics of conical horn antennas", Proc. IRE., 1950, 38, pp 249-251.

101. Bickel, S.H., and Bates, R.H.T.: "Effects of magneto-ionic propagation on the polarization scattering matrix", Proc. IEEE., 1965, 53, pp 1089-1091.

102. Jordan, E.C., and Balmain, K.G.: op.cit., Chap. 11.

103. Wheeler, H.A.: "A systematic approach to the design of a radiator element for a phased-array antenna", Proc. IEEE., 1968, 56, pp 1940-1951.

104. Jasik, H.: "Antenna engineering handbook", McGraw-Hill, 1961, Chap. 1.

105. Rumsey, V.H.: "Part I - transmission between elliptically polarized antennas", Proc. IRE., 1951, 39, pp 535-540.

106. Schelkunoff, S.A.: "Some equivalence theorems of electromagnetics and their application to radiation problems", BSTJ., 1936, 15, pp 92-112.

107. Levine, H., and Papas, C.H.: "Theory of the circular diffraction antenna", J. Appl. Phys., 1951, 22, pp 29-43.

108. Marcuvitz, N.: op.cit., Chap. 4.

109. Jasik, H.: op.cit., Chap. 27.

110. Pistolkors, A.A.: "Theory of circular diffraction antenna", Proc. IRE., 1948, 36, p 56.

111. Rhodes, D.R.: "Flush mounted antenna for mobile application", Electronics, March 1949, 22, pp 115-117.

112. Cumming, W.A., and Cormier, M.: "Design data for small annular slot antennas", IRE. Trans., 1958, AP-6, pp 210-211.

113. Wait, J.R.: "A low frequency annular-slot antenna", J. Nat. Bur. Stds., 1958, 60, pp 59-64.

114. Galejs, J., and Thompson, T.W.: "Admittance of a cavity-backed annular slot antenna", IRE. Trans., 1962, AP-10, pp 671-678.

115. Cohn, G.I., and Flesher, G.T.: "Theoretical radiation pattern and impedance of a flush-mounted coaxial aperture", Proc. Nat. Elect. Conf., 1958, 14, pp 150-168.

116. Samaddar, S.N.: "Radiation from open end of a coaxial waveguide with an infinite conducting flange covered by a plasma layer", Int. J. Elect., 1968, 24, pp 217-230.

117. Yeh, Y.S., and Wait, J.R.: "On the theory of radiation from an annular slot in a compressible plasma", Radio Science, 1968, 3, pp 171-180.

118. Ling, C., Lefferts, E., Lee, D., and Potenza, J.: "Radiation pattern of planar antennas with optimum and arbitrary illumination", IEEE. Int. Conv. Rec., 1964, 12, Pt. 2, pp 112-124.

119. Scheffer, H.: "The radiation of the open coaxial line when excited by H-modes", Arch. Elekt. Ubertragung (German), 1968, 22, pp 514-518 (In German).

120. Plonsey, R.: "Aperture fields", IRE. Trans., 1962, AP-10, pp 342-343.

121. Jamieson, A.R., and Bates, R.H.T.: "An aerial capable of radiating any polarization", Paper presented at NELCON II conf. Auckland N.Z., 1968.

122. Koch, G.F., and Scheffer, H.: "Coaxial radiator as feed for low noise paraboloid antennas", Nachrichtentechn. Z., 1969, 22, pp 166-172.

123. Malowicki, E.: "Coaxial cavity radiator", IEEE. Trans., 1969, AP-17, pp 637-640.

124. Silver, S.: op. cit., Chap. 7.

125. Jones, D.S.: op. cit., Chap. 5.

126. Medhurst, R.G.: "Dipole aerials in close proximity", Wireless Engineer, 1951, 28, pp 356-358.

127. Marcuvitz, N.: op. cit., Chap. 1.

128. Kraus, J.D.: "Antennas", McGraw-Hill, 1950, Chap. 11.

129. Allen, J.L., et. al.: "Phased array studies", Lincoln Lab., 1965, Report 381, Part III.

130. Lewin, L.: op.cit., Chap. 1.

131. Watson, G.N.: "Theory of bessel functions", Cambridge, 1966 Edition, Chap. 2.

132. Abramowitz, M., and Stegun, I.A.: "Handbook of mathematical functions", reprint by Dover, 1965.

133. Watson, G.N.: op.cit., Chap. 5.

134. Abramowitz, M., and Stegun, I.A.: op.cit., Chap. 10.

135. Carter, P.S.: "Antenna arrays around cylinders", Proc. IRE., 1943, 31, pp 671-693.

136. Leitner, A., and Spence, R.D.: "Effect of a circular ground plane on antenna radiation", J. Appl. Phys., 1950, 21, pp 1001-1006.

137. Morse, P.M., and Feshbach, H.: op.cit., Chap. 1.

138. Edmonds, A.R.: "Angular momentum in quantum mechanics", Princeton Univ. Press, 1957.

139. Ramo, S., Whinnery, J.R., and Van Duzer, T.: "Fields and waves in communication electronics", Wiley, 1965, Chap. 8.

140. Tyrrell, W.A.: "Hybrid circuits for microwaves", Proc. IRE., 1947, 35, pp 1294-1306.

141. Deschamps, G.A.: "Part II - Geometrical representation of the polarization of a plane electromagnetic wave", Proc. IRE., 1951, 39, pp 540-544.

142. Kaplan, L.J., Ormsby, J.F.A., Fowle, E.N., Johnson, K.R., Bates, R.H.T., and Bickel, S.H.: "Radar calibration test satellite", IEEE. Trans., 1969, AES-5, July.

143. Bates, R.H.T., and Jamieson, A.R.: "Towards reducing errors in radar measurement of Faraday rotation", Electronics Letters, 1968, 4, n.8.

144. Whinnery, J.R., and Jamieson, H.W.: "Equivalent circuits for discontinuities in transmission lines", Proc. IRE., 1944, 32, pp 98-114.

145. Whinnery, J.R., Jamieson, H.W., and Robbins, T.E.: "Coaxial line discontinuities", Proc. IRE., 1944, 32, pp 695-709.

146. Somlo, P.I.: "The computation of coaxial line step capacitances", IEEE. Trans., 1967, MTT-15, pp 48-53.

147. Ragan, G.L.: "Microwave transmission circuits", McGraw-Hill, 1948, Chap. 8.

148. Collin, R.E.: "Field theory of guided waves", McGraw-Hill, 1960, Chap. 7.

149. Kraus, J.D.: op.cit., Chap. 6.

150. Jordan, E.C., and Balmain, K.G.: op.cit., Chap. 14.

151. Jasik, H.: op.cit., Chap. 31.

152. Radio Research Lab. Harvard Univ.: "Very high-frequency techniques - Volume I", 1946, Chap. 3.

153. Bates, R.H.T.: "The characteristic impedance of the shielded slab line", IEEE. Trans., 1956, MTT-4, pp 28-33.

154. Nicolson, A.M.: "Broad-band microwave transmission characteristics from a single measurement of the transient response", IEEE. Trans., 1968, IM-17, pp 395-402.

155. Bates, R.H.T., and Burrell, G.A.: "Simultaneous display of frequency and pulse responses of antennas", Paper presented at AICA-IFIP conf. Munich, 1970.

156. Watson, G.N.: op.cit., Chap. 13.